Quantifying Dissolved Lignin Phenols in the Albemarle–Pamlico Estuarine System and Coastal North Carolina following the 2018 Hurricane Florence

A thesis by:

Kathleen J. Ferris

July 2022

Director of Thesis: Dr. Eli Hvastkovs

Department of Chemistry

Abstract

The global carbon cycle (GCC) involves the exchange and transformation of carbon across the ocean, atmosphere, and terrestrial reservoirs. It consists of a positive feedback loop involving dissolved organic matter in natural waters, greenhouse gases, and global warming. Extreme weather events such as hurricanes can accelerate this feedback loop by rapidly increasing the flux of organic matter to coastal systems. One of the largest storms of the 2018 hurricane season was Hurricane Florence, which released over 900 mm of precipitation across the state causing runoff, erosion, and flooding of terrestrial organic material (TOM). This study quantified dissolved lignin, a bulky biopolymer that is found within the cell wall of vascular land plants, as a biomarker of TOM influx into the Albemarle–Pamlico Estuarine System (APES) and coastal ocean of North Carolina.

Water samples were collected in October and November of 2018 which represented hurricane–influenced samples. In contrast, water samples collected in July 2019 represented non–storm conditions. A subset of each filtered water sample were sent to the NC State Stable Isotope Laboratory for bulk dissolved organic carbon ($\delta^{13}C_{DOC}$) analysis, to help identify its source. Additionally, an existing method for quantifying dissolved lignin, originally designed for liquid chromatography, was modified to allow low volume quantification of dissolved lignin via gas chromatography–mass spectrometry (GC–MS). Dissolved lignin was quantified in 3 replicates each of standard reference materials (SRM): NIST SRM 1944 (New York/ New Jersey Waterway Sediment), NIST SRM 8704 (Buffalo River Sediment), and Aldrich Humic Acid. Total dissolved lignin was determined to be (160.12 ± 12.84 μg L^{-1}), (129.87 ± 6.30 μg L^{-1}) , and (1,124.34 ± 33.21 μg L^{-1}), in SRM 1944, 8704, and Aldrich Humic Acid, respectively. There are no existing measurements of dissolved lignin in these reference materials in the literature. Thus, the low standard deviation and high precision across replicates suggested that the method that was developed was precise, and thus applicable to natural water samples.

Water samples collected from the APES and coastal ocean system in 2018 yielded overall higher concentrations of total dissolved lignin (2.84 ± 1.84 μg L^{-1}) than those collected during 2019 (0.67 ± 0.67 μg L^{-1}). The estuary had, on average, higher dissolved lignin concentrations in both 2018 and 2019 than that of the coastal ocean waters. Lignin interclass ratios of syringyl to vanillyl monomers (S/V; angiosperm vs gymnosperm) and C/V (cinnamyl to vanillyl; grasses versus woods) were calculated and used to provide insight on TOM sources. Average S/V values were 1.96 ± 2.71 and 2.10 ± 2.86, in 2018 and 2019 respectively. Average C/V were 1.54 ± 1.80 and 2.33 ± 2.94, in 2018 and 2019 respectively. Degradation of TOM was determined using acid to aldehyde ratio of vanillyl and syringyl monomers; $[Ad/Al]_V$ and $[Ad/Al]_S$. Ratios of $[Ad/Al]_V$

were 8.11 ± 15.93 and 3.69 ± 4.58, in 2018 and 2019 respectively. Similarly, ratios of $[Ad/Al]_S$ were 11.11 ± 26.18 and 8.26 ± 10.98, in 2018 and 2019 respectively. These ratios in conjunction with $\delta^{13}C_{DOC}$ which was –27.9 ± 1.7 and –26.6 ± 0.9 % for 2018 and 2019 respectively, suggested that the dissolved lignin samples of 2018 were generally derived from fresh angiosperm and gymnosperm tissues, while 2019 samples were much more degraded in comparison but had similar plant tissue sources.

The overarching results from this study indicate that Hurricane Florence directly increased the concentration of terrestrially derived dissolved lignin to the APES and coastal North Carolina by approximately 76.4 % via erosion, flooding, and runoff. Such rapid pulses of TOM have been shown in other coastal ecosystems to increase regional concentrations of $CO_2(g)$, a greenhouse gas. Although not directly quantified in this study, a similar effect likely occurred in coastal NC because of the 2018 hurricane season.

Quantifying Dissolved Lignin Phenols in the Albemarle–Pamlico Estuarine System and Coastal North Carolina following the 2018 Hurricane Florence

A thesis

Presented to the Faculty of the Department of Chemistry

East Carolina University

In Partial Fulfillment of the Requirements for the Degree

Master of Science in Chemistry

By

Kathleen J. Ferris

July 2022

Quantifying Dissolved Lignin Phenols in the Albemarle–Pamlico Estuarine System and Coastal North Carolina following the 2018 Hurricane Florence

By

Kathleen J. Ferris

APPROVED BY:

DIRECTOR OF THESIS_____
Eli Hvastkovs, Ph.D.

COMMITTEE MEMBER_____
Siddhartha Mitra, Ph.D.

COMMITTEE MEMBER_____
Anne Spuches, Ph.D.

CHAIR OF THE DEPARTMENT
OF CHEMISTRY_____
Andrew Morehead, Ph.D.

INTERIM DEAN OF THE
GRADUATE SCHOOL_____
Kathleen T Cox, Ph.D.

ACKNOWLEDGMENTS

I would like to express my deepest gratitude to my thesis advisor and chair of my committee, Dr. Siddhartha Mitra for his invaluable patience and guidance. I would also not have been able to journey through this process without my chemistry advisor Dr. Eli Hvastkovs and my thesis committee member Dr. Anne Spuches who generously led me to success with their extensive knowledge and expertise. Additionally, this research would not have been possible without the funding from the National Science Foundation. The method developed in this study would not have been feasible without the generous scholarship awarded to me by the East Carolina University Water Resources Center which allowed for the purchase of equipment critical to complete this research.

Special thanks to my lab members for their help in research, editing, practice, feedback and moral support which I could not have finished without. I am also grateful to the crew of the Research Vessel *Blackbeard* and Research Vessel *Neil Armstrong* without whom this research would not have been possible. I would like to thank Dr. Chris Osburn from the Department of Marine, Earth, and Atmospheric Sciences at North Carolina State for analyzing dissolved organic carbon samples for their stable isotopes, which was influential in this study. Thanks, should also be given to members of the ECU College of Engineering & Technology which fabricated equipment that was critical to complete this research.

TABLE OF CONTENTS

LIST OF TABLES

LIST OF FIGURES

LIST OF SYMBOLS AND ABBREVIATIONS

APES	Albemarle Pamlico – Estuarine System
DOC	Dissolved Organic Carbon
DOM	Dissolved Organic Material
EWE	Extreme Weather Event
GCC	Global Carbon Cycle
GFF	Glass Fiber Filters
LDOC	Labile dissolved organic carbon
OC	Organic Carbon
OM	Organic Matter
OMT	O – methyl transferase
POC	Particulate Organic Carbon
RDOC	Refractory components of dissolved organic carbon
SRM	Standard Reference Material
TOM	Terrestrial Organic Material
$\delta^{13}C$–DOC	Stable carbon isotopic composition in terms of DOC
Σ_8	Sigma – 8: The sum of all phenol yields
Λ_8	Lambda – 8: The sum of all phenol yields scaled to DOC amount

I. Introduction

Over the past century, with temperatures rising and climate change progressing, oceanic storm frequency and intensity have risen. Specifically, North Carolina has been affected by 387 storms, including tropical storms and hurricanes, between 1851 and 2020. Eighty–four of those storms have made landfall, directly impacting coastal North Carolina ("Hurricane Statistics". *North Carolina State Climate Office*, n.d., https://products.climate.ncsu.edu/weather/hurricanes/statistics). An increase in tropical storms and hurricanes will naturally lead to increased erosion and runoff in the coastal areas of North Carolina. For example, it was estimated that since 1970 large scale flood events accounted for 80–90% of particulate organic carbon (POC) eroded from mountainous regions (Hilton et. al 2008). Similarly, storm and flooding events have been shown to increase terrestrial dissolved organic carbon (DOC) loading into coastal areas (e.g., Bianchi et al. 2013, Rudolph et al. 2020).

Greater storm frequency increases the rate of terrestrial material introduced into estuarine systems like those in coastal North Carolina. A study by Yoon and Raymond in 2012 reported that one singular tropical storm event accounted for 40% of the annual DOC export in Esopus Creek, Allaben, New York, which drains into the tidal Hudson River, NY. Such introduction of terrestrial organic matter (TOM) can alter the system's hydrologic, ecological, and biogeochemical characteristics (Paerl et al. 2001). As an example, flooding of the Atchafalaya River and Bay by the 2011 Mississippi River flooding event caused the coastal Gulf of Mexico to transform from a net sink of CO_2 (autotrophic) to a net source of CO_2 (heterotrophic) (Bianchi et al. 2013). Similarly, the passage of Hurricane Irene (2011) across the Neuse River estuary and Pamlico Sound led to the system switching from autotrophic to heterotrophic (Crosswell et al. 2014). Thus, event–driven

terrigenous organic matter loading changes the overall DOC composition while also changing the overall bioreactivity of coastal waters.

During the 2018 hurricane season, Hurricane Florence made landfall in eastern North Carolina in mid–September bringing approximately 900 mm rainfall over the four–day period and high wind speeds (top speed of 160 knots) to the coastal region (Stewart et al. 2019). This rainfall affected the Albemarle–Pamlico Estuary System (APES) which is connected to the Atlantic Ocean by route of three inlets: the Oregon, Ocracoke, and Hatteras inlets (***Figure 1***).

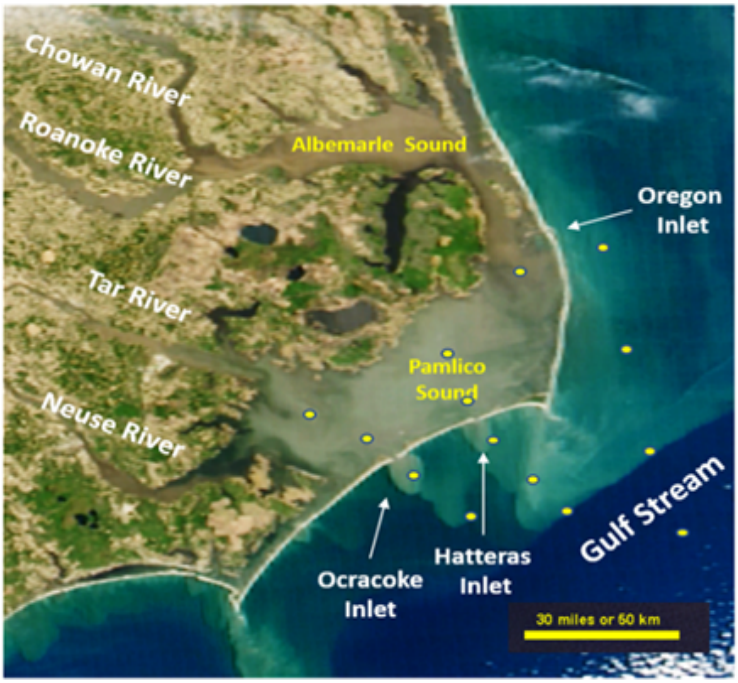

Figure 1: A map of the Albemarle–Pamlico Estuary System including the Oregon, Ocracoke, and Hatteras Inlets.

In addition to Hurricane Florence, the 2018 hurricane season included a total of fifteen storms in the Atlantic Ocean. Only three directly influenced coastal North Carolina; Tropical Storm Chris, Hurricane Florence and Hurricane Michael. These storms in addition to those affecting other areas across the Atlantic Ocean, resulted in a record–breaking season in terms of precipitation and damage, costing approximately $50 billion in damages and 172 fatalities. Extreme weather events (EWE), such as these, not only influence land masses on a monetary and personal level, but also may promote excess flood–water discharge and increase loading of POC and DOC concentrations into estuaries.

One component of TOM is an organic polymer called lignin. Lignin is a complex phenolic polymer which is found tightly cross–linked within the cell wall polysaccharides of vascular land plants (Hedges & Ertel 1982). Lignin is the second most abundant aromatic polymer, following cellulose, that is found in terrestrial ecosystems lending to its influence on organic carbon found in the biosphere (Ayyachamy et al. 2013). Lignin is an important factor to a plant's rigidity and hydrophobic properties and is an integral part of the global carbon cycle (e.g., Goñi & Hedges 1992). Due to its abundance in soil, lignin can be used as a biogeochemical tracer for the introduction of TOM into the ocean (e.g., Hedges & Ertel 1982). Using surface water samples collected following Hurricane Florence, a high precipitation event, and samples taken the following year during a time of no storm influenced precipitation, dissolved lignin was quantified to measure the amount of TOM introduced into the APES. Quantifying dissolved lignin in a coastal system after a major storm yields insight into how the carbon cycle is regionally altered by EWE, which are expected to increase in the future.

II. Background & Theory

a. Hurricane Florence, 2018

Hurricane Florence lingered over eastern North Carolina and northeastern South Carolina for two days. In this time, it deposited a record–breaking amount of precipitation (***Figure 2, Table 1***) that caused flooding, erosion, a total of 52 fatalities (NC and SC) and $16.7 billion worth of damages in North Carolina and $607 million in damages in South Carolina (https://www.weather.gov/ilm/HurricaneFlorence; Stewart & Berg, 2019)). As a result of Hurricane Florence, nine rivers in North Carolina experienced an excess of their "1–in–500 year expected return intervals" (https://www.weather.gov/ilm/HurricaneFlorence; Stewart & Berg, 2019; Callaghan, 2020).

The hurricane started forming about 90 nautical miles (nmi) (167 km) southeast of Santiago Island (Cabo Verde Islands) as a tropical depression the evening of August 31st (Stewart & Berg, 2019). Over the next several days, Florence intensified to a tropical storm and strengthened over 48 hours to a hurricane with 65 knot (kt) winds (120 km h^{-1}) and a 30 nmi (56 km) diameter eye (Stewart & Berg, 2019). Florence then amplified to Category IV hurricane, on the Saffir–Simpson

Table 1: Precipitation records for North Carolina storms represented in millimeters of rain, inches of rain and which storm caused it.

** H. represents storms that are Hurricanes whereas T.S. stands for tropical storms*

Rank	Precipitation		Storm*
	mm	inches	
1	912.6	35.93	H. Florence 2018
2	611.1	24.06	H. Floyd 1999
3	602.7	23.73	Mid–July Hurricane 1916
4	598.7	23.57	H. Frances 2004
5	594.6	23.41	T.S. Fred 2021

https://en.wikipedia.org/wiki/List_of_wettest_tropical_cyclones_in_the_United_States#North_Carolina

Scale, with 115 kt winds (213 km h^{-1}) and located approximately 1200 nmi (2222 km) east–southeast of Bermuda, over the central Atlantic Ocean (Stewart & Berg, 2019). After this increase in size and wind speed, it went through a period of weakening to a tropical storm before a period of rapid increasing to a hurricane once again through outflow jets in the northwestern and southeastern quadrants of the hurricane (Stewart & Berg, 2019). Hurricane Florence reached its peak strength on September 11th with 130 kt (241 km h^{-1}) winds located 725 nmi (1343 km) off the coast of Cape Fear, North Carolina (Stewart & Berg, 2019). As Florence moved closer to shore, it weakened to a slow moving 80 kt (148 km h–1) (based on NOAA WSR–88D Doppler Weather radar) hurricane when it made landfall on September 14th in Wrightsville Beach, North Carolina (Callaghan, 2020; Stewart & Berg, 2019).

Due to Florence's slow–moving nature, it deposited > 254 mm (10 in) in most places across the southern part of North Carolina and northern South Carolina, and 508 mm (20 in) near the eastern NC–SC border (Stewart & Berg, 2019). Florence also deposited record breaking precipitation in Elizabethtown, North Carolina with 912.6 mm (35.93 in) of rain (***Table 1***) (Callaghan, 2020; S & B 2019). The previous record was from Hurricane Floyd in 1999 with 611.1 mm (24.06 in) of rain in Southport, North Carolina (***Table 1***). The record for rain in South Carolina was also broken by Florence with 600.20 mm (23.63 in) at Loris, near the NC border (Callaghan, 2020; S & B 2019) The previous record for precipitation in South Carolina was 443.23 mm (17.45 in) measured near Lake Jocassee, on the Northwestern NC–SC border, caused by Tropical Storm Beryl in 1994 (Callaghan, 2020; S & B 2019).

Storm surges across North Carolina led to damages and fatalities along rivers and tributaries that connect to the Pamlico Sound (Stewart & Berg, 2019). A surge of 2.4 m (8 ft) to 3.4 m (10 ft) above ground level along the Neuse River, in addition to raised water levels of the

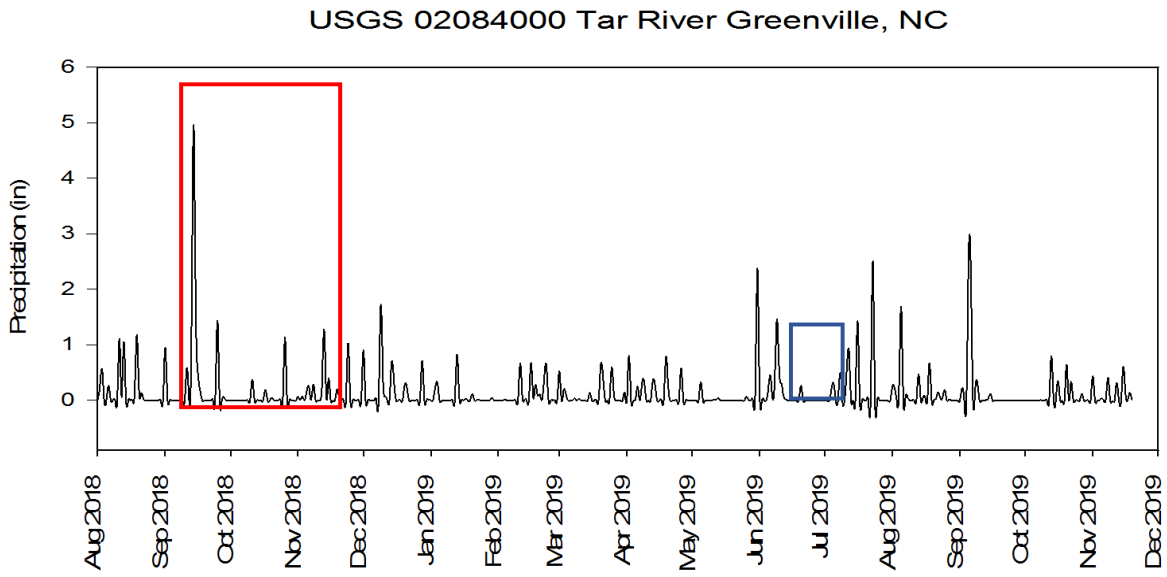

Figure 2: Hydrograph depicting precipitation in inches associated GSPS sampling. The red box shows the precipitation following rainfall from Hurricane Florence (October and November of 2018). The blue box represents the samples taken during a time of minimal or no precipitation in July of 2019.

Pamlico Sound resulted in flooding in Carteret, Craven and Pamlico counties (Stewart & Berg, 2019). The Tar River, which connects to the Pamlico River, in Greenville North Carolina was also subject to flooding of streets, homes and businesses contributing to state–wide damages (https://water.weather.gov/ahps2/hydrograph.php?gage=pgvn7&wfo=mhx). The hydrograph in ***Figure 2*** shows the precipitation measured between August 2018 and December 2019, with sampling time ranges presented. The large peak in mid–September is when Hurricane Florence landed in North Carolina which is almost twice the size of the second largest peak seen in September 2019 caused by Hurricane Dorian.

b. Albemarle–Pamlico Estuary System (APES)

The Albemarle–Pamlico Estuarine System (APES) is the largest lagoonal system in addition to being the second largest estuary in the United States, behind the Chesapeake Bay (Paerl et al 2001). The APES has a basin area of 80,000 km^2 which includes the Pasquotank, Chowan,

Roanoke, Tar–Pamlico, Neuse and White Oak River Basins which stretch across North Carolina and Virginia Coastal Plain and flow into the Pamlico Sound (***Figure 3***) (Harned & Davenport 1990). The APES system is surrounded by a mix of evergreen forest, forested wetlands, cropland, mixed forest, non–forested wetlands, and urbanized areas (Harned & Davenport 1990; Carpenter & Dubbs, 2012).

APES is comprised of two sounds, the Albemarle and the Pamlico, creating the Albemarle–Pamlico Estuary. Neither of the Albemarle or Pamlico Sounds connect directly to the Atlantic Ocean as they are entrapped by a chain of barrier islands called The Outer Banks (Carpenter & Dubbs, 2012). The Albemarle Sound has three open–water estuaries, the freshwater Currituck Sound in the north and the Croatan and Roanoke Sounds in the south that directly connect to the Pamlico Sound (Harned & Davenport, 1990; Carpenter & Dubbs, 2012). The lack of Atlantic Ocean connectivity results in the Albemarle Sound being influenced mostly by freshwater rather than oceanic influence. The Pamlico Sound, connected to the Albemarle Sound in the north, has three inlets that connect to the Atlantic Ocean that are imbedded into the Outer Banks: Oregon, Hatteras and Ocracoke.

The APES is located in the Coastal Plain of North Carolina and Virginia, with an extensive configuration of rivers, wetlands, creeks and the sound (Moorman et al., 2017). The system is a shallow (< 9 m), low salinity lagoonal estuary that has a surface area of 2,330 km^2 with a drainage area of 47,552 km^2 (Giese et al., 1985; Moorman et al., 2017). The annual water budget is 481 m^3 s^{-1} of water entering the Albemarle Sound via the Currituck, Roanoke and Croatan Sounds (Giese et al., 1985; Moorman et al., 2017). Due to the limited interaction with the Atlantic Ocean, the Albemarle Sound has a residence time of 45 days and is mainly circulated by wind–driven tides, except for major storm events (Moorman et al. 2017).

The Pamlico Sound is connected to the southern end of the Albemarle Sound and is a moderate to high salinity, shallow ecosystem (< 7.3 m) that has a surface area of 5,300 km^2 (Giese et al., 1985; Paerl et al., 2001). With an average inflow of 910 $m^3 s^{-1}$ from the Neuse–Trent River system, Tar–Pamlico River system, as well as indirect flow from the Roanoke and Chowan Sounds through the Albemarle Estuarine System (Paerl et al., 2001; Giese et al., 1985). This sound has a residence time of approximately 11 months and the inflowing estuaries serve as a filter for particulate and dissolved materials (Paerl et al., 2001). This filter aspect of the sound, in addition to its long residence time, shallow depth and high productivity serve as the optimal ecosystem for

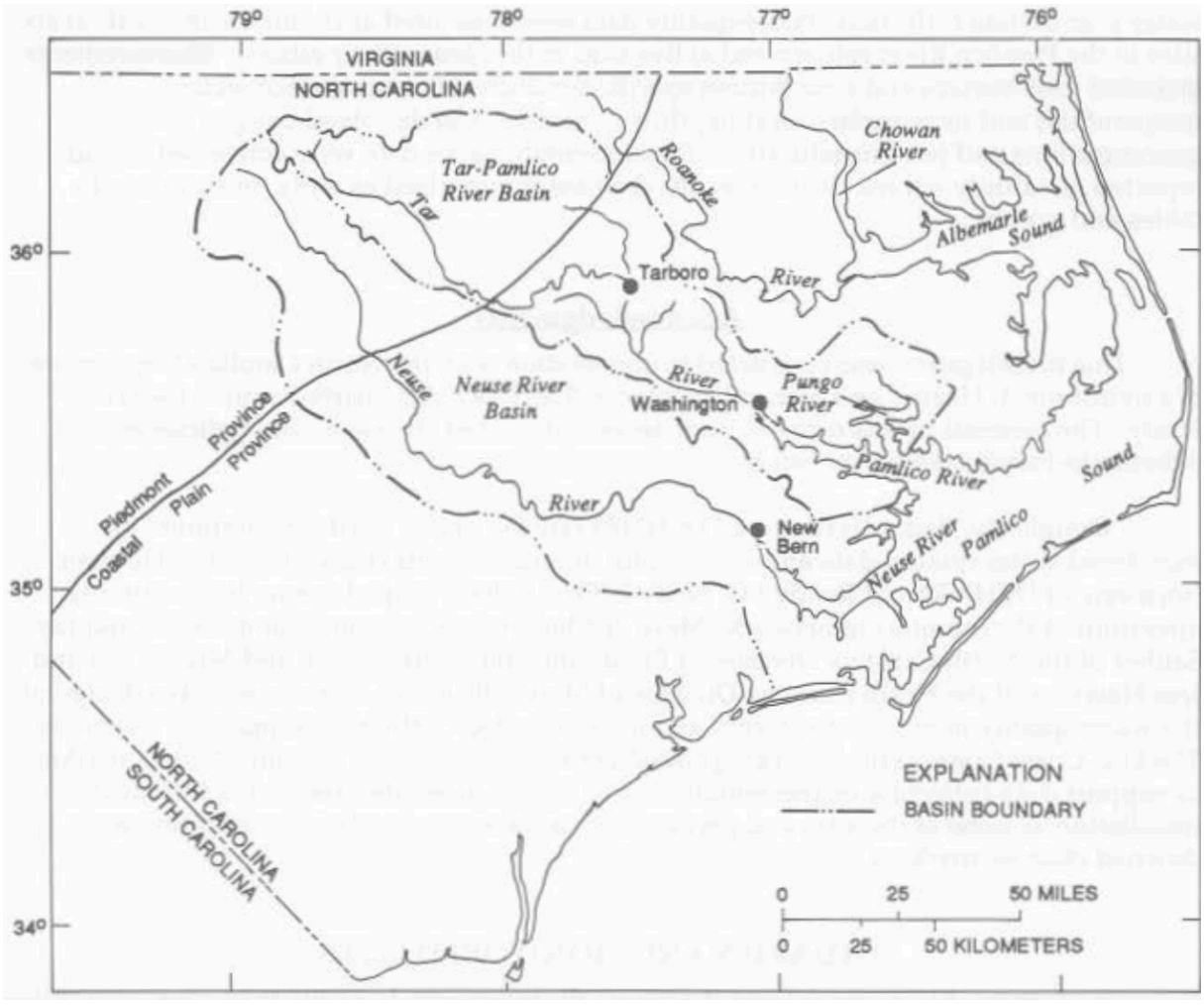

Figure 3: Map of the Albemarle–Pamlico Estuarine System including the Chowan River, Roanoke River, the Albemarle Sound, the Tar River, Pungo River, the Pamlico River, Neuse River and the Pamlico Sound (Garrett, 1994).

various fish populations in addition to inflated freshwater and nutrient loadings (Paerl et al., 2001). It was noted by Giese et al., 1985, that there is an increase in oxidizable organic carbon and material in the bottom sediments near the center of the northern boundary of the Sound as well as the mouths of the Neuse and Pamlico River where fine sediment is more concentrated.

As of 2012, northeastern North Carolina and southeastern Virginia measured approximately 1194 – 1422 mm (47 – 56 inches) of precipitation per year (Carpenter & Dubbs, 2012). The temperature ranges for the system are coldest in January (6 – 8 °C) with hot and humid summers (average of 32 °C) (Carpenter & Dubbs, 2012). The wind that dominates the estuarine system are S–SW with an average velocity of 15 – 16 km h^{-1}, which overall contributes to the circulation of the estuary (Carpenter & Dubbs, 2012). The climate of APES is mostly mild and moist for the most part creating an ideal environment for agriculture, forestry and fisheries.

Due to increasing urbanization around the sound system, anthropogenic nitrogen and phosphorus loadings have doubled in last 40–years (Stow et al., 2001; Paerl et al., 2018). The increase in frequency and intensity of EWEs cause physical influences (erosion, sediment resuspension, flooding and runoff) to water quality of the estuarine system. These environmental perturbations in turn have negative repercussions such as changes in air–water CO_2 exchange, habitat degradation, disease and mortality amongst wildlife and precipitous changes in salinity, pH, dissolved oxygen and re–mineralization of soil organic carbon (Paerl et al., 2018).

c. The Carbon Cycle

The global carbon cycle is a continuous flow of creation, transformation and decomposition of complex carbon compounds with four key reservoirs: terrestrial biosphere, fossil carbon, the atmosphere and the ocean or other water sources (Bolin, 1970; Schimel, 1995; Cole et al. 2007;

Ciais et al., 2013). Climate change and carbon cycling has been an increasingly imminent issue that is difficult to not only quantify but rectify the predicament. The lack of accurate knowledge about the positive and negative feedbacks between the four reservoirs are the limiting factor to credible simulations of the global carbon budget (Schimel, 1995).

c.1. Terrestrial and fossil carbon reservoirs

The terrestrial reservoir begins with primary production by photosynthesis (***Equation A–1*** and ***Equation A–2***) which is what defines Earth from other planets, with its introduction to organic processes to a primitive ecosystem. Plants that conduct photosynthesis take up inorganic carbon, CO_2, in addition to water and sunlight, and produce organic compounds which provide chemical energy to the food chain in the form of glucose, water, free oxygen and energy. Within the terrestrial reservoir, photosynthetic assimilation of atmospheric carbon dioxide, CO_2, is the main source of carbon being introduced from the atmosphere to the biosphere and geosphere (Cole et al 2007). Approximately 120 ± 3 PgC yr^{-1} (petagrams of carbon = 10^{15} grams of carbon; 1 PgC = 1 gigaton of carbon) is removed from the atmosphere by plant photosynthesis, where is it cycled through tissues and the photosynthetic process before being released back into the atmosphere by autotrophic (plants) and heterotrophic (microbial and animal) respiration (***Figure 4***) (Riebeek, 2011; Prentice et al., 2001; Ciais et al., 2013).

The terrestrial biosphere is also a carbon sink, from fossils, plant biomass and soil carbon. Fossil fuels include coal, petroleum and natural gas, which are all produced through the slow (millions of years) transformation of organic carbon into sedimentary rocks, and most of the fossil fuel that is used today is approximately 70 – 100 million years old. The storage of carbon in plant biomass has been speculated to have a wide range of stored carbon, between 450 – 650 PgC

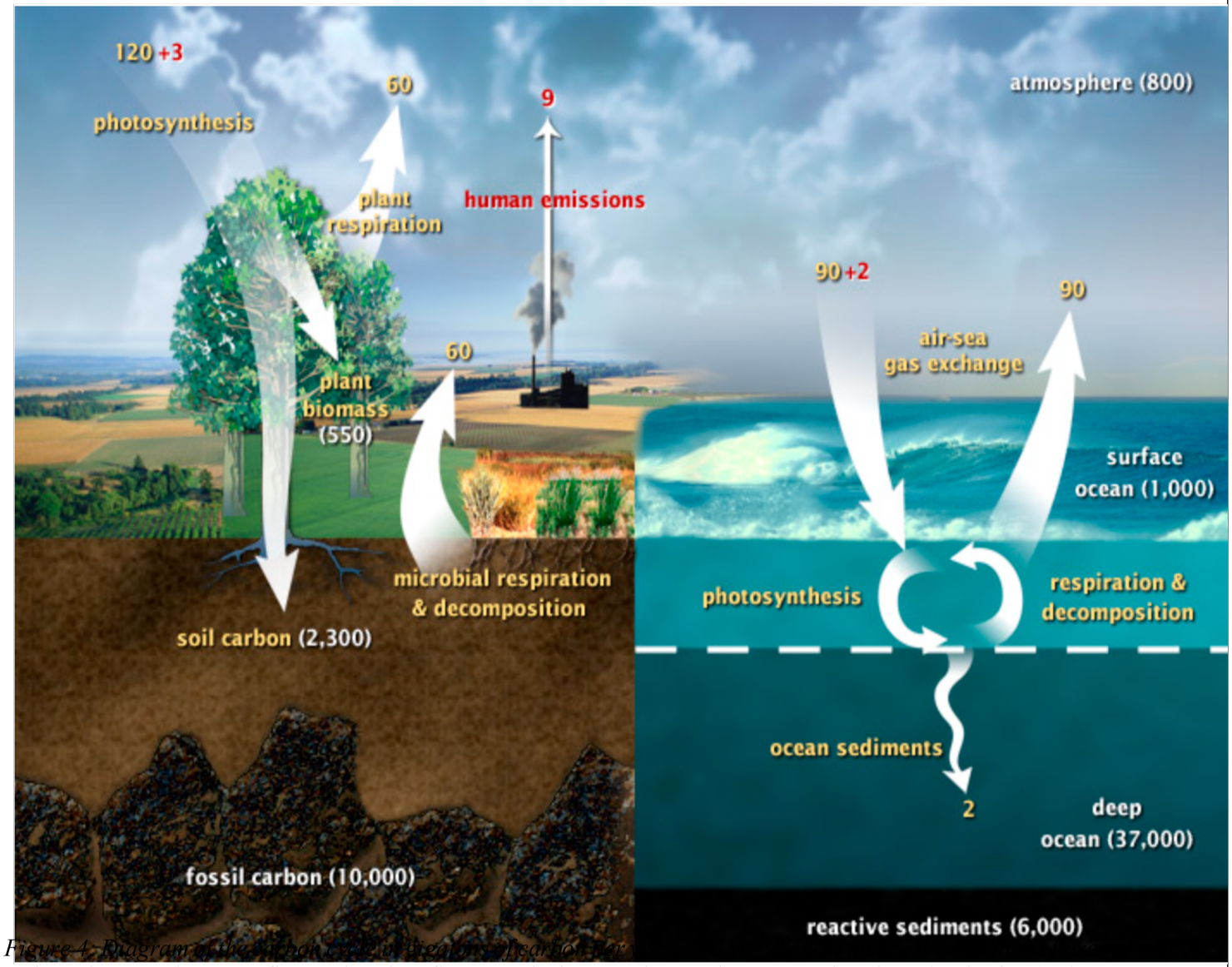

Figure 4: Diagram of the carbon cycle in decades. Carbon per
red numbers are human influenced carbon fluxes, and white numbers indicate stored carbon. (Riebeek, 2011)

(***Figure 4***) and has been difficult to quantify as it is entirely dependent on the method of ecosystem and plant classification, the area of study and the measurement of carbon stocks for each type (Prentice et al., 2001; Post et al., 1990). The carbon found in soil and litter from dead organic material (OM) approximates to 1,500 – 2,400 PgC (Batjes, 1996), an additional amount of old soil carbon in wetland soils, 300 – 700 PgC (Bridgham et al., 2006) and in permafrost soils (permanently frozen soil layer on or under the Earth's surface) at approximately 1,700 PgC (Tarnocai et al., 2009) (***Figure 4***).

Human influence has intensified carbon emissions and in turn negatively influenced the global carbon cycle. A large component of human influence has been from the burning of fossil fuels which has only increased since the emergence of the industrial revolution in the late 18th century (Post et al., 1990). The carbon emissions from fossil fuel combustion and cement production increased more during the years of 2000 – 2011 than the period of 1990 – 1999 with 9.5 ± 0.8 PgC yr^{-1} emitted in 2011 which is 54% greater than in 1999 (***Figure 4***) (Ciais et al., 2013).

Deforestation is a human influence that is also altering the carbon cycle. The overcutting of forests reduces the amount of absorption of CO_2 by trees, lessening the terrestrial carbon sink (Ciais et al., 2013; Al–Ghussain, 2018). The change in land use has actually released an additional 180 ± 80 PgC to the atmosphere estimated from 1750 – 2011 (Ciais et al., 2013). It is noted by Prentice et al., 2001 that deforestation would add 2 – 4 times more CO_2 to the atmosphere.

c.2. Atmospheric reservoir

Prior to 1750, when the Industrial Era began, atmospheric CO_2 was at a concentration of 280 ± 10 ppmv (parts per million volume) for a few thousand years, but since 1750 to 2011 the

CO_2 concentration has increased by 40% (Ciais et al., 2013). This increase didn't occur all at once, yet the increase has notably intensified in recent years; ~ 280 ppmv in 1800, ~ 315 ppmv in 1957, ~ 356 ppmv in 1993 and ~391 ppmv in 2011 (***Figure 4***) (Schimel, 1995; Prentice et al., 2001; Ciais et al., 2013). The concentration of CO_2 has increased at a rate of 2.0 ± 0.1 ppm yr^{-1} between the years of 2002 – 2011 which is the highest rate increase per decade observed since the inception of direct atmospheric measurements in 1958 by Dr. Charles Keeling at the Mauna Loa Observatory in Hawaii (Ciais et al., 2013; Post et al., 1990). The atmospheric CO_2 found in ice cores (last 7,000 years) show a very slow change of only 20 ppmv as opposed to previously discussed increases, leaning researchers to believe that anthropogenic CO_2 increase prior to 1750 to be unlikely (Siegenthaler & Sarmiento, 1993; Ciais et al., 2013).

The increased carbon emissions from the terrestrial biosphere between 1800 to the 1950's is assumed to be due to the expansion of agriculture and forestry in addition to the Industrial Revolution (Schimel, 1995). The current atmospheric CO_2 increased concentration is caused by anthropogenic emissions of CO_2 and has not been surpassed in the last 420,000 years and not likely to have been surpassed in even the last 20 million years, so the increase in CO_2 concentrations is truly unprecedented (Prentice et al., 2001).

The exchange between the atmosphere and the oceans is mostly in equilibrium as the effectiveness of the wind across the ocean's surface exchanges CO_2 rapidly (air – sea gas exchange) (***Figure 4***) (Bolin, 1970; Post et al., 1990; Siegenthaler & Sarmiento, 1993). Air–sea gas exchange is approximated to be 90 PgC yr^{-1} and is caused by the partial pressure difference of CO_2 between the ocean's surface and the atmosphere (Bolin, 1970; Prentice et al., 2001; Siegenthaler & Sarmiento, 1993). The uptake capacity of the ocean is sufficient to integrate 70 – 80% of anthropogenic CO_2 emissions to the atmosphere, but this takes centuries due to ocean

mixing, meaning that even numerous centuries after the occurrence of the emissions, about a quarter of these emissions would still be present in the atmosphere (Prentice et al., 2001; Ciais et al., 2013). If human influence were to cease immediately, it is hypothesized that it would take a few hundred thousand years for the anthropogenic carbon to be alleviated via natural processes (Ciais et al., 2013).

c.3. Oceanic reservoir

The largest reservoir of the carbon cycle is the ocean as it is a carbon sink due to the constant loading of terrestrial organic matter into rivers, estuaries, and other coastal systems. The ocean contains approximately 50 times the carbon that is found in the atmosphere at approximately 38,000 gigatons (Gt) according to NOAA in its deepest depths (Riebeek, 2011; Prentice et al., 2001; Ciais et al., 2013; Post et al., 1990 etc.). Carbon is stored in the ocean in three forms: POC (living organisms or remnants of plants and animals), dissolved inorganic carbon (dissolved CO_2, HCO_3^- and CO_3^{2-}) and DOC (Bolin, 1970; Post et al., 1990). Carbon in the ocean is predominantly comprised of dissolved inorganic carbon (DIC = 38,000 PgC), with a pool of dissolved organic carbon (DOC = 700 PgC) and an additional pool of organic carbon contributed by phytoplankton and other microorganisms (~ 3 PgC) (Hansell et al., 2009; Ciais et al., 2013).

Carbon is mobilized between the ocean surface and the ocean floor through a series of physical process (mixing and circulation), biological processes (production and decomposition of OM) and chemical processes (Bolin, 1970; Post et al., 1990). The biological processes are the backbone of the carbon structure of the ocean by way of surface level dissolved carbon being reduced by photosynthetic biota and then the sinking of the OM that is produced where dissolved inorganic carbon is rich in concentration in the deeper ocean (Hansell & Carlson, 2001; Hansell et

al., 2009 Post et al., 1990). This biological pump of surface level carbon being transported to deeper ocean via the water column where it is remineralized, maintains the robust vertical gradients of the inorganic carbon present in the ocean (Hansell et al., 2009).

Autotrophic production is the primary source of DOC and microbial remineralization is the most prevailing sink, as microbial production in the ocean theoretically generates 50% of primary production with a flux of approximately 30 PgC yr^{-1} (Hansell et al., 2009; Post et al., 1990). The open ocean surface has a DOC concentration of approximately 40 – 80 μmol kg^{-1} with higher values of 70 – 80 μmol kg^{-1} observed in tropical and hotter ecosystems and lower concentrations of 40 – 50 μmol kg^{-1} in subpolar water systems (Hansell & Carlson, 2001; Hansell et al., 2009). The solubility of CO_2 is dependent on temperature which affects the amount of carbon found in the surface waters, as colder waters will influence the solubility of CO_2 to increase and sink, whereas in warmer climates the solubility is lower, and therefore promoting increased air–sea gas exchange (Prentice et al., 2001; Ciais et al., 2013). Warmer water affects the equilibrium of the partial pressure of CO_2 ($pCO2$) as surface water pCO_2 increases by approximately 10 – 20 ppm per °C temperature increase, thus further promoting CO_2 to be released to the atmosphere (Prentice et al., 2001).

The dissolved organic matter in the ocean is roughly the same amount of carbon that is found in the atmosphere (Hansell & Carlson, 2001; Prentice et al., 2001; Ciais et al., 2013 etc.). The DOC found in the ocean are greatly contributed by terrestrial material that is deposited into rivers and estuaries as these are the dominant link between the land biosphere and the ocean that connects over 87% of the Earth's land surface area (Bauer & Bianchi, 2011). This material includes terrestrial plant material, soils and suspended river sediments which all contain carbon, thus influencing the global carbon cycle (Bauer & Bianchi, 2011; Ciais et al., 2013). Of this dissolved

plant material, it is terrestrial vascular plants which contain polymers such as cellulose, hemicellulose and lignin, which can be used as a biogeochemical tracer in the quantification of carbon influences in the oceanic reservoir.

d. Bulk Organic Carbon

d1. Bulk organic carbon and the global carbon cycle

A considerable factor of organic material that is found in rivers, estuaries and the coastal ocean is in the dissolved phase as DOC. The increase in urbanization, soil erosion, fertilizer, and human induced climate change have influenced the dispatch of bulk DOC to the aquatic continuum which connects land to the coastal ocean (Regnier et al., 2013). Carbon is exchanged laterally between terrestrial and oceanic ecosystems where it is then exchanged vertically to the atmosphere by means of greenhouse gases (CO_2, CH_4, N_2O etc.) (e.g., Jiao et al., 2021; Regnier et al., 2013).

A main component of bulk organic carbon is DOC, and it is naturally broken down in an aquatic environment via microbial degradation causing CO_2 release (e.g., Jiao et al., 2021; Hansell, 2013). DOC is categorized into how rapid it is broken down and transformed in the natural environment, either labile DOC (LDOC) or refractory components of DOC (RDOC), with both being considered to be organic pollutants to the environment (e.g., Hansell, 2013; Jiao et al., 2021). LDOC is rapidly degraded and taken up by microbes found in the environment, therefore when a flux of DOC is eroded into the water, detrimental effects ensue (***Figure A–1***). These include oxygen depletion which is caused by the over consumption of oxygen, eutrophication and water acidification and ultimately the release of excess CO_2 to the atmosphere (Cai et al., 2011; Sunda & Cai, 2012; Jiao et al., 2021). These negative repercussions contribute to the conversion of aqueous systems from a carbon sink to a source of carbon emission, ultimately contributing to the

greenhouse gas effect (e.g., Paerl et al., 2018; Jiao et al., 2021). In contrast to this, RDOC is not readily broken down and metabolized by microbes meaning it can be conserved in natural water systems and act as a carbon sink.

d2. Stable isotopic signatures to determine composition

While the exchange and transformation of TOM and DOC are influential in the global carbon budget, the natural isotopic ratio of carbon from these sources can be used to confirm origin (Peterson et al., 1994). Due to the pilgrimage of TOM to the open ocean between rivers, streams, reservoirs and estuaries, the source of the OC is difficult not only to track, but also to categorize as a natural oceanic source of carbon or terrestrially derived.

Carbon isotopic ratios reflect the relative abundance of ^{13}C :^{12}C, each of which is transported differently in the C_3 and C_4 pathways of carbon fixation during photosynthesis (Peterson et al., 1994; Hobbie & Werner, 2003). The C_4 pathway was the most recent adaptation (approx. 20 million years ago) to photosynthesis as these plants conserve water and reduce photorespiration when in dry climates (Lloyd & Farquhar, 1994; Hobbie & Werner, 2003). Furthermore, C_3 plants have a greater ability to acclimate to a broad range temperature and climates to photosynthesize (began approx. 500 million years ago) (Lloyd & Farquhar, 1994; Hobbie & Werner, 2003). C_3 plants are more depleted in ^{13}C than C_4 plants, and literature ranges of isotopic ratios vary, however C_3 plants have an approximate isotopic ratio of –24 to –34 ‰, while C_4 plants have an isotopic range of approximately –6 to –19 ‰ (Lloyd & Farquhar, 1994; Peterson et al., 1994).

e. Lignin

Vascular land plants consist of structural polysaccharides, cellulose, hemicellulose and lignin which provide shape, rigidity and elasticity which give plants their structural integrity (Parthasarathi et al., 2011; Argyropoulos & Menachem, 1998 etc.). These polysaccharides make up a majority (> 75%) of the biomass found in terrestrial vascular plants with lignin being the second most abundant biopolymer in the biosphere (30% of the organic carbon content) (Hedges & Ertel, 1982; Ayyachamy et al., 2013; Liu et al., 2018 etc.). Although vascular plants contain lignin, primitive plants such as algae and fungi lack this biopolymer due to their absence of a vascular system or mechanical reinforcement (Argyropoulos & Menachem, 1998). Lignin is synthesized through the process of polymerization of the phenylpropanoid units in the cell wall of vascular land plants (Zeikus, 1981; Bianchi & Canuel, 2011; Ayyachamy et al. 2018 etc.).The lignin structure is thought to be comprised of three–dimensional phenylpropanoid units which are bound together by irregular carbon–carbon and diaryl–ether linkages (e.g., Sarkanen and Ludwig, 1971; De Leeuw and Largeau, 1993).

Chemically, lignins are a group of macromolecular heteropolymers (600–1000kDa) (Bianchi and Canuel, 2011) with a high molecular weight, a complex composition and varying structure (***Figure 5***). Due to lignins' diverse structure based on tissue source and age of lignocellulosic biomass, the dry weight percentage in plants ranges from 24 – 33% in gymnosperms, 19 – 28% in angiosperm plants and 15 – 25% in grasses (Perez–Pimienta et al., 2021, Zeikus, 1981; Katahira et al., 2018). Lignin found in gymnosperm plants are proposed to have a highly branched structure because of the presence of *p*–coumaryl and coniferyl alcohols whereas angiosperm plants incorporate sinapyl alcohols with a doubly methoxylated aromatic ring (***Figure 5***) which is presumed to limit the branching of its lignin structure (Perez–Pimienta et al.,

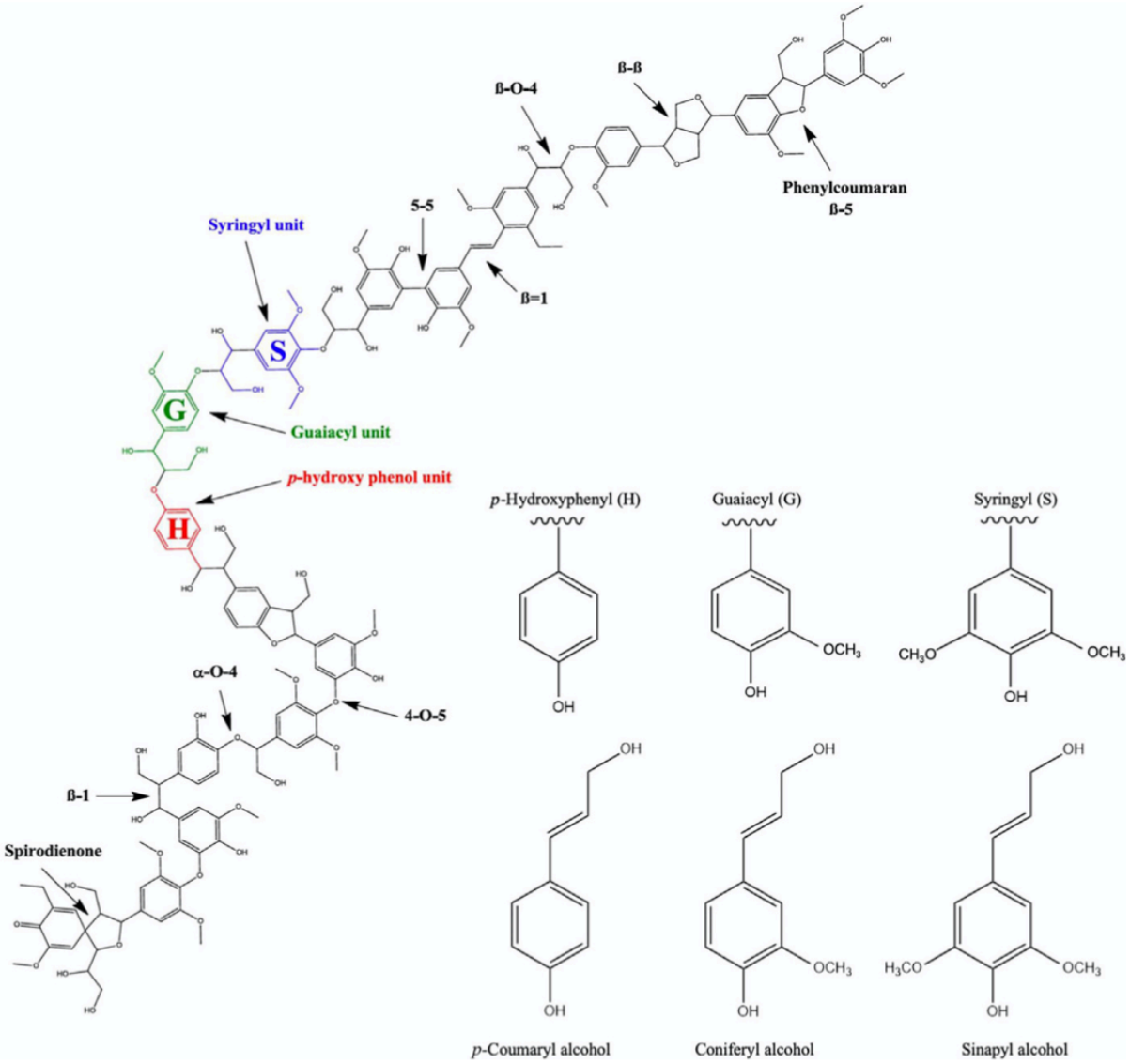

Figure 5: Schematic representation of a lignin structure including the elemental monomers and respective monolignols; sinapyl alcohol (syringyl (S, blue)), coniferyl alcohol (guaiacyl (G, green)) and p–coumaryl alcohol (p–hydroxyphenyl (H, red)) (Lupoi et al., 2015; Perez–Pimienta et al., 2021).

2021). The building blocks for the structure of lignin are predominantly synthesized through the Shikimic acid pathway, which is common in plants as well as fungi and bacteria (Hermann and Weaver, 1999). This pathway utilizes aromatic amino acids to provide the precursors, phenyl alanine and tyrosine, that are used in the biosynthesis of phenylpropanoids compounds necessary to generate the monolignol constituents of lignin which are then used to produce the primary building blocks for lignin (***Figure 6***) (Hermann & Weaver, 1999; Bianchi & Canuel, 2011).

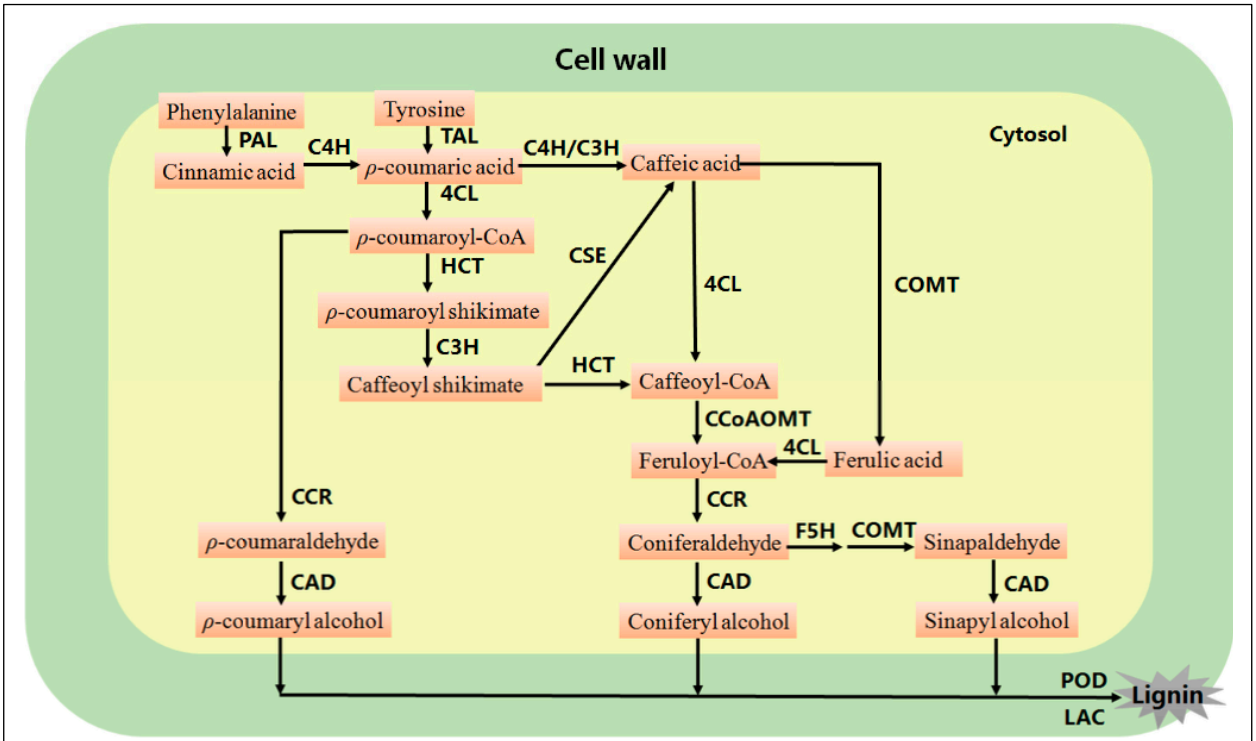

Figure 6: The simplified pathway for the synthesis of the building blocks of lignin which occurs in the cell wall of vascular plants: sinapyl alcohol, coniferyl alcohol and p–coumaryl alcohol (Liu et al., 2018).

The lignin polymer is comprised of the three monomeric units syringyl (S), guaiacyl (G) and *p*–hydroxyphenyl (H), which are linked through ester bonds of the three monolignol units sinapyl, coniferyl and *p*–coumaryl alcohols (***Figures 5, 6***) (Hedges & Ertel, 1982; Liu et al., 2018; Parthasarathi et al., 2011 etc.). These building blocks are cross–linked primarily by carbon–carbon bonds (C – C), aryl ether (*β*–O–4), resinol unit (*β*– *β*), phenylcoumaran unit (*β*–5), biphenyl unit (5–5'), along with less common linkages such as dibenzodioxocin (5–5'/*β*–O–4) and spirodienone units (*β*–1/α–O–α), with *β*–O–4 representing 50% of the linkages to create a three dimensional stable compound (***Figures 5,6***) (Katahira et al., 2018 Bianchi and Canuel, 2011; Du et al., 2019). The degree of oxidative copolymerization of the lignin building block alcohols depends entirely on the macromolecular arrangement present within the plants, based upon plant type and species (Ayyachamy et al., 2013).

Lignin synthesis, or lignification, occurs within the primary and secondary cell walls where the lignin precursors, *l*–phenylalanine and cinnamic acids, are derived from carbohydrates though the shikimic and cinnamic pathways (Argyropoulos & Menachem, 1998). The biosynthetic pathways for both angiosperms and gymnosperms are similar to a certain point at which they diverge. *L*–phenylalanine is converted to *trans*–cinnamic via catalyzation by the enzyme *l*–phenylalanine ammonia lyase (PAL) (Argyropoulos & Menachem, 1998). In addition, in grasses, the enzyme tyrosine ammonia lyase (TAL) is responsible for the formation of *p*–coumaric acid derived from *l*–tyrosine (Argyropoulos & Menachem, 1998). Cinnamic acid is then hydroxylated to p–coumaric acid in addition to caffeic acid which is methylated to ferulic acid by means of O–methyl transferase (OMT) (Argyropoulos & Menachem, 1998).

Due to angiosperms characteristically possessing guaiacyl units when gymnosperms do not, the synthetic pathways of the two deviates. This is due to the OMT enzyme being inhibited by caffeic acid in angiosperms, whereas in gymnosperms, OMT is inhibited by 5–hydroxyferulic acid which limits the production of ferulic acid thus inhibiting syringyl products (Argyropoulos & Menachem, 1998). Finally, the reduction of ferulic acid and sinapic acid occurs through the reductase system producing coniferyl and sinapyl alcohols (Argyropoulos & Menachem, 1998).

The linkages that are seen in ***Figure 5*** are known to influence lignin properties and reactivity for mechanical, chemical and thermal treatments (Elder et al., 2017; Katahira et al., 2018). The cleavage of these bonds is fundamental when analyzing the depolymerization of lignin into its monomer counterparts. It has not been confirmed exactly how oxidative lignin depolymerization occurs on a molecular level, as the aryl ether and C–C linkage patterns greatly varies amongst species with different types of substitutions (Parthasarathi et al., 2011). The cleavage of the aryl ether bond (*β*–O–4) is readily fragmented into water–soluble compounds

which contain phenolic hydroxyl groups, while the α–O–4 linkage leads to the branching of the lignin polymer (Parthasarathi et al., 2011; Liu et al., 2013). The *β*–O–4 bond has been confirmed to be the primary interunit linkage and thus is critical for depolymerization (Katahira et al., 2018; Liu et al., 2013). The other less common linkages, i.e. (5–5'/*β*–O–4), (*β*–1/α–O–α) and (5–5'), have been noted to be species specific and therefore difficult to analyze for molecular cleavage (Parthasarathi et al., 2011; Katahira et al., 2018).

Through oxidation processes, lignin breaks down to four phenolic monomer families: p–hydroxyl (P), vanillyl (V), syringyl (S) and cinnamyl (C) (***Figure 7***). These groups are comprised of one aldehyde, one ketone and one carboxylic acid each, except for the cinnamyl group which is exclusively carboxylic acids (e.g., Hedges and Ertel, 1982). The individual monomers are as follows; *p*–hydroxybenzaldehyde (PAL), *p*–hydroxyacetophenone (PON) and *p*–hydroxybenzoic acid (PAD) comprise the *p*–coumaryl group; vanillin (VAL), acetovanillone (VON) and vanillic acid (VAD) comprise the vanillin group; syringaldehyde (SAL), acetosyringone (SON) and syringic acid (SAD) comprise the syringyl group; and finally, *p*–Coumaric acid (CAD) and ferulic acid (FAD) comprise the cinnamyl group (***Figure 7***) (Hedges & Ertel, 1982).

The distribution of these phenolic monomers in an environmental sample varies depending on the plant group and tissue type (***Figure 7***). Through lignin oxidation, samples produce specific monomers based on their species and whether they are flowering (angiosperm) or non–flowering (gymnosperm) as well as being woody (deciduous and evergreen plants) or non–woody (herbaceous) plants. All land plants exhibit vanillyl monomers, but each group of plants have specific monomer yields following oxidation. Woody gymnosperm tissues exhibit P and V monomers while woody angiosperm tissues exhibit P, V and C but not S monomers. Woody angiosperm tissues, however, break down into V and S monomers, while non–woody angiosperm

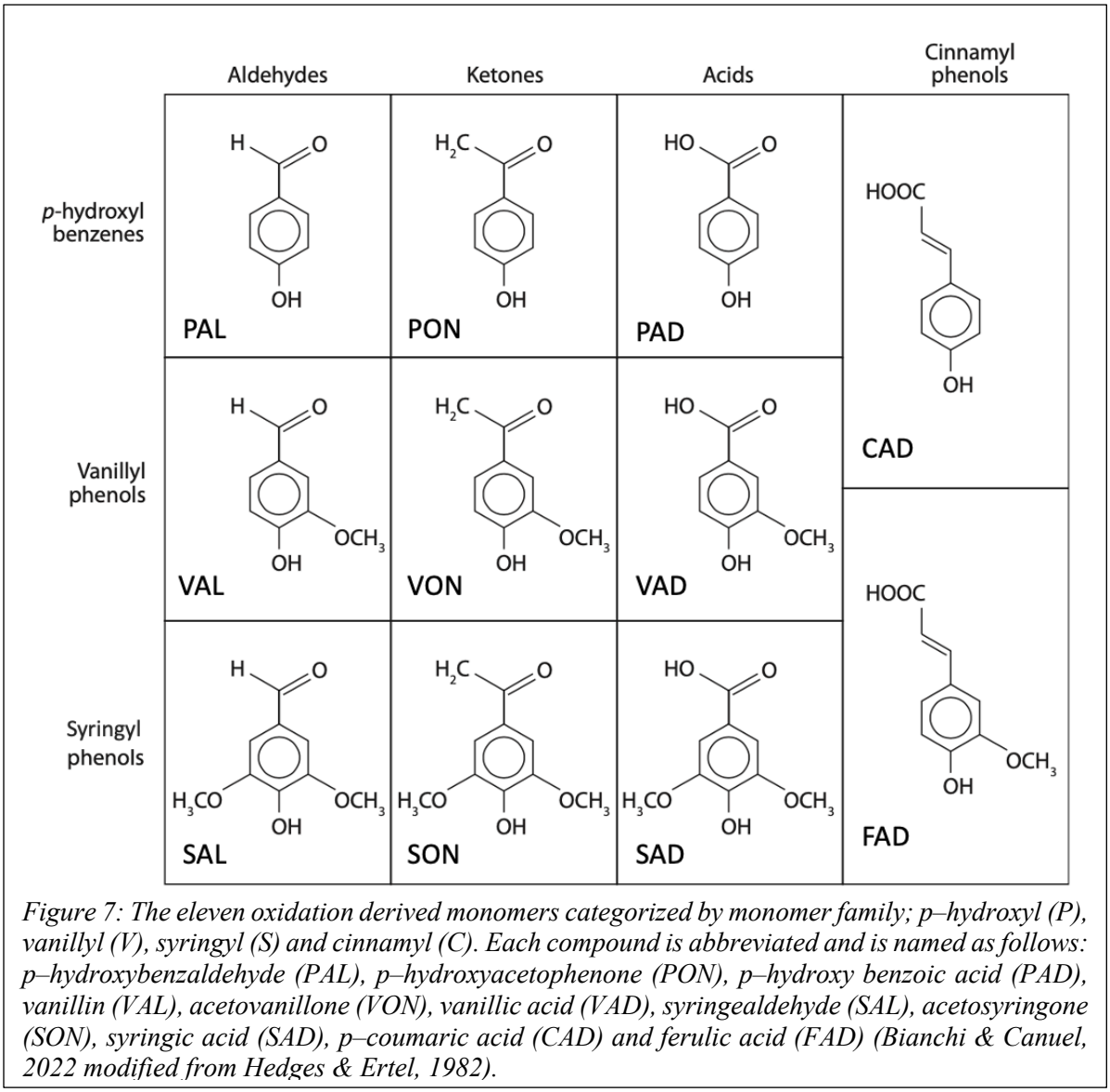

Figure 7: The eleven oxidation derived monomers categorized by monomer family; p–hydroxyl (P), vanillyl (V), syringyl (S) and cinnamyl (C). Each compound is abbreviated and is named as follows: p–hydroxybenzaldehyde (PAL), p–hydroxyacetophenone (PON), p–hydroxy benzoic acid (PAD), vanillin (VAL), acetovanillone (VON), vanillic acid (VAD), syringealdehyde (SAL), acetosyringone (SON), syringic acid (SAD), p–coumaric acid (CAD) and ferulic acid (FAD) (Bianchi & Canuel, 2022 modified from Hedges & Ertel, 1982).

tissues exhibit all four monomer groups. Analyzing the monomer classes aid in determining the specific type of vascular plant source in unknown environmental samples (Hedges & Ertel, 1982).

The ratios of syringyl:vanillyl (S:V) and cinnamyl:vanillyl (C:V) have been used as indicators of plant matter source, as all vascular plants contain vanillyl phenols (especially gymnosperms – seed or cone bearing), syringyl phenols predominate in angiosperms (flowering), and cinnamyl phenols derive primarily from non-woody plant tissues (e.g., grasses) (Hedges and Ertel, 1982; Hedges et al. 1986; Goni et al. 2003). Additionally, the acid:aldehyde phenol ratio

([Ad/Al]) has been utilized as an indicator of the relative degradation of the plant matter contribution, as the abundance of oxidized (acid) phenols increases with degradation (Hedges et al. 1986; Hernes et al. 2007).

f. Previous methods for dissolved lignin

The initial method for lignin isolation from environmental samples was developed by Hedges and Ertel (1982). Soil and sediment samples were oxidized in 10mL Monel minibombs (***Figure 8)*** with cupric oxide as an oxidizing agent, ferrous ammonium sulfate ($Fe(NH_4)_2(SO_4)_2 \bullet 6H_2O$) as an oxygen scavenger, NaOH and a steel agitator and heated to an external temperature of 170 °C for three hours to allow for oxidation to thoroughly occur (***Figure 8***) (Hedges & Ertel 1982). The oxidation products were exchanged into an organic solvent and liquid–liquid extraction was used to concentrate the lignin prior to gas chromatographic analysis with a flame ionization detector. Ethyl vanillin was used as an internal standard to quantify the monomers of interest. The oxidation temperature was later modified from 170°C to an optimal temperature of 155°C (Goñi & Hedges, 1992). Goni and Montgomery (2000) further advanced the field by developing a microwave assisted solvent extraction method (MASE) for lignin isolation, using ethyl acetate as the organic solvent (Goñi & Montgomery, 2000).

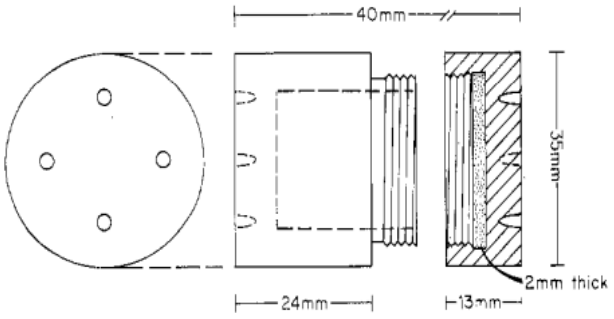

Figure 8: Diagram of 10–mL Monel minibomb used for oxidation (Hedges & Ertel, 1982).

The first group to isolate lignin in the dissolved or colloidal phase was Opsahl & Benner, in 1998. At the time however, the general approach involved concentrating the dissolved carbon

(and associated lignin) using ultrafiltration. Unfortunately, these approaches did not allow adequate isolation of the low molecular weight portion of the dissolved lignin. Thus, there needed to be some way of concentration total dissolved lignin, which evolved when solid phase cartridges became more popular in the field of analytical chemistry.

The first attempt at using solid phase cartridges for lignin isolation was done using C18 pre–packed columns for sample concentration after oxidation (Kögel & Bochter, 1985). The C18 columns Kögel & Bochter used allowed optimal quantification of dissolved lignin phenols. The first person to further evolve the method for isolating lignin using solid phase cartridges was Louchouarn et al., (2000). His method using C–18 cartridges was applied to oceanic and estuarine samples and was able to isolate dissolved lignin in samples as low as 4–8L in volume. Louchouarn also modified the method by adding glucose to the reaction vessels as "sacrificial" carbon in the oxidation.

Kaiser and Benner (2011) were the next major contributors to quantifying dissolved lignin by creating a faster method implementing solid phase extraction. Use of Oasis HLB cartridges was determined to recover 87–90% of all lignin phenols. Other polymers were investigated by Arellano et al. (2018) (e.g., C18, HLB and PPL). Soon thereafter, Yan and Kaiser (2018a) optimized isolation of dissolved lignin using $CuSO_4$ instead of CuO and applying them to very small sample sizes of water (~50 mL). The Yan and Kaiser method was the starting point for the dissolved lignin method development conducted in this study. The challenge faced with the samples collected as part of this research, were the fact that they varied greatly in salinity, DOC abundance, and potential sources of lignin.

III. Methods

a. Sample Collection

The surface water samples used in this study were collected across 20 different locations in the APES, along a transect across the Oregon Inlet, coastal North Carolina outside the OBX and along the western edge of the Gulf Stream (***Figure 9***). Foul weather (e.g., excessive winds) restricted the collection to specific dates. Thus, these samples were collected on 10/25 and 10/26; 11/19–11/24 and 11/30 in 2018. These storm season samples encompassed 41 to 77 days following Hurricane Florence's landfall in coastal North Carolina. In contrast, "non–storm" condition samples were collected on 07/02 and 07/03 of 2019 at 11 different stations.

It must be noted that during the 2018 hurricane season, there was a total of fifteen storms that occurred in the Atlantic Ocean, with three hitting coastal North Carolina; Tropical Storm Chris (July 6th – July 12th), category four Hurricane Florence (August 31st – September 17th), and category five Hurricane Michael (October 7th – October 11th). Samples were collected using R/V *Blackbeard* (10/25, 10/26 and 11/30) as well as R/V *Neil Armstrong* (11/19–11/24 and 11/30) (***Figure 9***). Each sample was collected just below the surface of the water using nitrile gloves in addition to pre–cleaned Nalgene 1L and 4L high density polyethylene (HDPE) bottles. Bottles were cleaned using a dilute solution of distilled deionized (DDI) water and dilute Alconox© to rinse each bottle and followed with triple rinsing using DDI water. All sample bottles were conditioned at the site prior to collection of each sample by rinsing with sample water and discarding in a direction away from sample collection area, prior to collection of the actual sample. Bottles were then placed in insulated coolers with ice after collection.

Upon return to the lab, each sample was filtered using a pre–cleaned and pre–weighed 1.5µm and 0.7 µm pore sized glass fiber filters (GFF) (2018 samples) and 0.7 µm pore size GFF

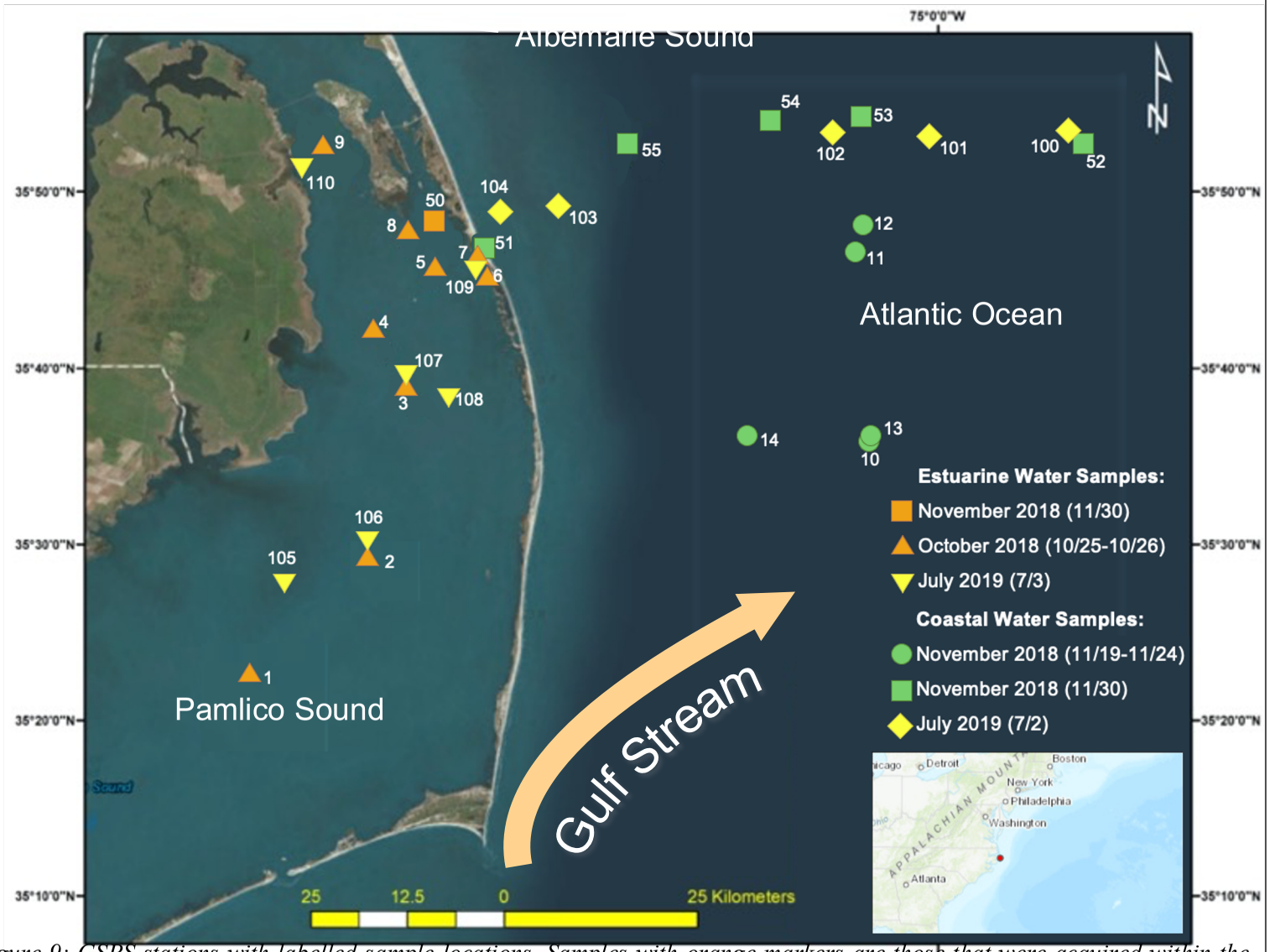

Figure 9: GSPS stations with labelled sample locations. Samples with orange markers are those that were acquired within the sound while those that are green were taken offshore in the Gulf Stream. Reference figure key for shape representations

(2019 only) to filter out any suspended sediments that were present. These filters were saved for analysis by another student in the lab. The water saved from filtering was saved in pre–cleaned Nalgene bottles, similar to those described above, and stored at 4°C until further filtration using Sterivex© polysulfone syringe filters (0.2 μm pore size), to isolate the truly dissolved phase. All glassware, filters and various instruments used in this study were pre–cleaned via combustion at 450º for 4 hours and sealed with aluminum foil before storage.

b. Dissolved carbon and lignin analyses

DOC abundance and stable isotopic composition were isolated in a subset of the sample filtrate. Sample DOC (mg L^{-1}) was determined using a Shimadzu TOC–V_{CPN} equipped with autosampler Shimadzu ASI–V. This model of Shimadzu total organic carbon (TOC) analyzer has a detection limit of 50 (μg L^{-1}). Two calibration curves, a lower concentration six–point calibration curve (ranging 0.000 – 8.500 μg L^{-1}) and a second higher concentration three–point calibration curve (ranging 8.500 – 80.500 μg L^{-1}), were generated using KHP prior to analysis.

A subsample of each station was sent to North Carolina State University's stable isotope laboratory for organic carbon isotopic signatures ($\delta^{13}C$–DOC). The samples were analyzed following the method laid out by Lalonde et al. (2014) with an OI 1030C TOC analyzer. Ultrapure oxygen was used as the carrier gas. The CO_2 that resulted from DOC thermal oxidation process was collected on a purge–and–trap device. The sample gas was then streamed to a Thermo Conflo IV interface device connected to a Thermo Delta V Plus isotope ratio mass spectrometer (IRMS) in continuous flow mode. The TOC–IRMS system was calibrated with IAEA (International Atomic Energy Agency) caffeine standards prior to analysis in addition to Hansell Deep Sea Reference (DSR) samples concurrent with sample analysis for accurate instrument performance

assessment. The Delta V IRMS was modified with ohmic resistors to provide reliable quantitative measurements of $\delta^{13}C$ values of the dissolved samples.

b.1. Development of the method

In order to isolate dissolved lignin in these estuarine and coastal water samples, the method for isolating aqueous phase dissolved lignin as noted in Yan and Kaiser (2018b) was modified. The original procedure (Yan & Kaiser, 2018b) utilized either Bond Elut PPL cartridges (5 g) or octadecyl–bonded (C18, 10 g) cartridges for the isolation of large volumes (>1 L) of water samples containing dissolved lignin. Then cupric sulfate ($CuSO_4$), 0.2 mol L^{-1} *L*–ascorbic acid and 1.1 mol L^{-1} argon sparged sodium hydroxide (NaOH) was used for the oxidation of dissolved lignin samples (150°C for 2 hours). This was followed with a spike of a pre–mixed surrogate standard (*p*–hydroxybenzoic acid–$^{13}C_7$, vanillin–$^{13}C_6$, and syringealdehyde–$^{13}C_6$) prior to purification by HLB cartridges (30 mg, 1 mL). These samples were then washed with methanol/water (20/80 v/v%) and eluted with methanol/methyl acetate (30/70 v/v%) before analysis. Lignin in the eluates was quantified via LC–MS.

Using the same Yan & Kaiser (2018b) method for GC–MS analysis resulted in not being able to detect any lignin monomers, suggesting that analytical modifications needed to be made. The original Yan & Kaiser (2018b) method was used to analyze a mixture of standard materials (caffeine and lignin monomer VAL) to confirm that this method was not viable for GC–MS analysis. To troubleshoot the lack of detectable quantities of lignin, the method was deconstructed into subsections. Each subsection involved use of dissolved monomer standard solutions and iterative modifications.

b.2. Isolation of lignin polymer

A vacuum manifold (***Figure A–2***) was equipped with a 1g C18 Agilent extraction column which was conditioned with 3 mL of methanol twice sequentially, followed by two elutions of 3 mL of acidified DDI water (pH = 2; acidified using 6M H_2SO_4). Each sample was then added to the conditioned column at a flow rate < 5 mL min^{-1}. The cartridge was then rinsed with 3 mL of acidified DDI water twice to ensure the entire cartridge was acidified and conditioned before the addition of sample. Subsequently, cartridges were eluted with 3 mL of methanol (OmniSolv HPLC grade) into a pre–cleaned 15 mL graduated conical glass tube and stored at 4 °C until further analysis.

b.3. Oxidation of lignin polymer

The eluted sample in methanol was evaporated to dryness using UHP N_2 gas in a heated sand bath. The sample was then reconstituted using 200 μL of methanol and transferred to a Savillex mini tube (***Figure A–3***). The conical glass tube was rinsed with an additional 100 μL of methanol and the rinse was then added to the Savillex mini tube. The Savillex mini tube was placed into the heated sand bath and blown to dryness with UHP N_2 gas. The sample was reconstituted in 200 μL of 1.1 M NaOH that had been pre–sparged with Ar. The residual sample in the Savillex mini tube was then spiked with 10 μL of 10 mM $CuSO_4$ (as an oxidizing agent) and 10 μL of 0.2 M ascorbic acid (sacrificial carbon to compensate for excess oxidizing agent). Both $CuSO_4$ and ascorbic acid were freshly prepared, monthly and sparged with argon before each use.

The Savillex mini tubes were then added in a cyclical manner to a Teflon bomb (reference figure). An additional 5 mL of 1.1 M NaOH (sparged with argon) was added to the bomb prior to sealing it. The Teflon bomb was heated in a programable oven (reference figure) from 30 °C →

150 °C at 24 °C per minute and held for 2 hours. Upon completion of the heating cycle, the bomb was immediately cooled under cold running water to stop any further oxidation.

b.4. Post oxidation extraction

The post–oxidation samples in the Savillex mini tubes were acidified with 6 M H_2SO_4 to a pH < 3 (confirmed with litmus paper). The samples were spiked with approximately 50 μL of ethylvanillin (EVAL) dissolved in 1.0 M NaOH as an internal standard. Aqueous extracts from the oxidation process were filtered through conditioned Oasis HLB© cartridges using gravity flow. The conditioning step consisted of adding 1 mL of methanol (x2) and 1 mL of DDI water (x2), as this is a similar matrix to the sample thus maximizing its elution through the cartridge matrix. The samples were passed through the cartridge under gravity flow, at a flow rate of approximately 0.2 mL min^{-1}. Each cartridge was then rinsed with 300 μL of 20/80 (v/v%) methanol/water twice, to remove impurities.

Following rinsing, the cartridge was eluted using 1 mL of ethyl acetate at a flow rate of 1 mL min^{-1}. The sample was then filtered through an ethyl acetate pre–conditioned Na_2SO_4 drying column and eluted into a precleaned rotovap flask. The drying column was rinsed with ethyl acetate a second time into the rotovap flask with 1 mL of ethyl acetate. The sample was then gently evaporated using the rotovap with the water bath at 60 °C. The sample was concentrated to ~ 0.1 – 0.2 mL using rotoevaporation. The sample was reconstituted with approximately 0.7–0.8 mL of HPLC grade pyridine and transferred to a 2.0 mL gas chromatograph–mass spectrometer (GC–MS) autosampler vial. An additional 100 μL of pyridine was used to rinse the rotovap flask to maximize the efficiency of sample transfer. In order to render the polar lignin–derived monomers amenable to GC–MS analysis, each sample was derivatized by adding 1 mL of N,O–

bis(trimethylsilyl)trifluoroacetamide (BSTFA) to the autosampler vial and heating at 70 °C for one hour in a water bath.

b.5. Gas Chromatography Mass Spectrometry analysis

Each sample was injected into a Shimadzu QP–2010–S GC–MS. A mixed standard containing all phenols (VAL, VON, VAD, SAL, SON, SAD, CAD and FAD) and the internal standard, EVAL (*Figure 10*) was also injected on a daily basis, along with a batch of samples.

The sample was injected (1 μL injection) into the GC in splitless mode with a 1–minute sampling time after which the remaining sample was purged. The column used was 30.0 m in length, 0.25 μm in thickness and 0.25 mm in diameter with a 5% diphenyl/ 95% dimethyl polysiloxane coating. The MS was set to scan mode with a mass range of 50 – 550 m/z. The temperature of the oven was initially set to a temperature of 50 °C with the injection block at 250 °C. The oven was ramped as follows: 50 °C and held for 1.20 minutes, increase to a temperature of 150 °C at 25 °C min^{-1}, then increase from 150 °C to 230 °C at 6 °C min^{-1} and finally increase from 230 °C to 310 °C at 3 °C min^{-1} and held for 4.80 minutes. The carrier gas used was ultra-high purity (UHP) helium at a pressure of 52.8 kPa and column flow of 0.99 mL min^{-1}. The sample was injected at a flowrate of 53.0 mL min^{-1} and analyzed over a 50–minute period. Each chromatogram was individually quantified for each derivatized lignin monomer by comparing to its derivatized monomer counterpart in the mixed standard injection, which was injected daily along with a batch of samples. Each monomer's identity was confirmed using its molecular ion and two qualifier ions, in addition to its retention time (***Table A–1***). Peak areas of monomers in each sample were converted to mass of that monomer using a GC response factor determined from

the mixed standard. Mass of each monomer was then scaled to volume of water sample extracted in order to determine concentration of each monomer for each sample (***Figure 10***).

Dilutions of the mixed lignin standard were analyzed to determine instrument detection limits for each monomer. Instrument detection limits (IDL) were established based on the concentration of each lignin phenol that yielded a signal–to–noise ratio (S/N) between 1.5 and 4. These IDL values were used to distinguish between quantifiable, non–quantifiable and non–detectable sample results. Non–detectable samples had no peak, non–quantifiable peaks were those that were below the S/N ratio for a specific monomer while the quantifiable peaks are above this ratio. Dilutions of the mixed standard were made at a ratio ranging from 1:20 – 1:335 (monomer standard stock:pyridine) (1:19 A stock, 1:255 B stock and 1:333 C stock). Using these stock solutions, injection vials of varying concentrations were used to identify the detection limits via trial and error. The dilutions were done so as to predict and investigate various concentrations of

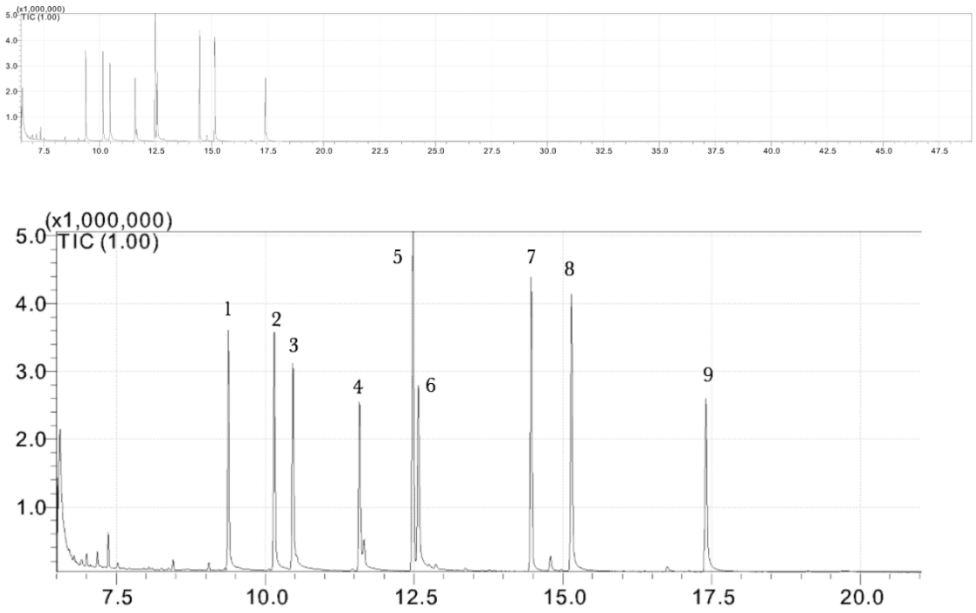

Figure 10: Results of GCMS analysis of lignin phenol standard mixture. Full chromatogram with zoomed peaks of lignin phenols: 1) VAL 2) EVAL 3) VON 4) SAL 5) VAD 6) SON 7) SAD 8) CAD 9) FAD

the mixed standard, which has a pre–calculated concentration of each monomer. It was presumed that each monomer would be detected from varying dilution concentrations as each monomer has a different molecular structure, mass and polarity, suggesting different detection limits.

c. SRM Leaching time series

A time series leaching experiment was conducted with National Institute of Standards and Technology (NIST) Standard Reference Materials (SRM) to determine that the method could be precisely applied to a variety of types of dissolved organic matter. This included the following SRMs: NIST–SRM 1944: New York/New Jersey Waterway Sediment, NIST–SRM 8704: Buffalo River Sediment and Aldrich Humic Acid. These samples were leached for 0 hours, 6 hours, 24 hours and one week (168 hours) and their leachates were subjected to the dissolved lignin procedure described above.

This was done in order to not only ensure that the method worked with a set of samples that most definitely contain lignin, but also to test what time period is optimal for leaching of lignin from sediment samples. An additional reasoning for this experiment was to compare lignin phenol values to those tested previously by Louchouarn et al. (2010). The only SRM that was tested by Louchouarn et al. was NIST–SRM 1944: New York/New Jersey Waterway Sediment. The results determined from this sample set can be compared to those previously quantified, possibly determining a percentile or linear connection between dissolved lignin and sedimentary lignin samples.

Approximately 0.50 grams of each SRM was added to approximately 20.0 mL of DDI water. Each sample was then placed on a shaker table for its predetermined time with three replicates for each time slot, for a total of twelve samples. After the allotted time for each sample,

they were centrifuged and the supernatant was isolated for further analysis, and the pellet was saved and stored in the fridge. The supernatant was then filtered through the same polysulfone filters (0.2 μm pore size) and then analyzed on the TOC–VCPN for DOC concentration (***Figure 11***). These samples were then analyzed for dissolved lignin using the method described above to ensure that the samples would yield quantifiable peaks above a signal to noise ratio (S/N) of 3, for purposes of quantification. These results were also compared to previous dissolved lignin studies done on SRM's to confirm reasonable results.

IV. RESULTS

a. Instrument detection limits/phenol standards

A standard mixture of all the phenols isolated in this study was injected at various concentrations to determine the lowest detectable signal to noise (S/N) ratio. Our lab uses a S/N ratio of 3.00 as a threshold to consider a peak to be detectable and quantifiable. ***Table 2*** lists each phenol, the S/N ratio associated with the minimum detectable quantity of that compound in picograms (pg), the phenol's retention time, as well as the molecular ion and specific ions that are used to qualify the phenol ID. For this class of lignin derived phenols, the instrument detection limit (IDL) varied from 17.7 – 57.9 pg, with the S/N ratio ranging from 1.46 – 3.63. These values of IDL are comparable to other lignin phenol studies (references needed) when taking into consideration the differences in instrumentation, method, and instrument specifications.

Table 2: Instrument detection limit for each lignin phenol and internal standard represented by signal to noise ratio (S/N) and the mass of phenol in picogram (pg). The retention time, molecular ion and qualifier ions used for identification.
[1]First ion in sequence is the molecular ion, followed by its three qualifier ions.

Phenol ID	S/N	Instrument Detection Limit (pg)	Retention time (min)	Ions Monitored[1]
VAL	2.27	17.7	9.090	194, 209, 193, 224
VON	2.08	22.8	10.160	223, 193, 208, 238
VAD	3.63	23.4	12.170	297, 267, 312, 223
SAL	1.95	35.4	11.270	224, 239, 254, 223
SON	2.53	53.2	12.260	238, 223, 253, 268
SAD	1.58	55.2	14.120	327, 312, 297, 342
CAD	2.33	37.8	14.810	293, 219, 249, 308
FAD	1.46	42.1	17.060	338, 323, 308, 249
EVAL	2.55	57.9	9.860	167, 195, 238, 179

b. SRM – Leaching time series

Other than Aldrich Humic Acid, the optimal concentration of DOC was leached from the SRMs at ~ 24 hours (***Figure 11*** and ***Table 3***). Aldrich Humic Acid would theoretically take weeks to reach equilibrium due to its high concentration of organic carbon (***Table 3***), but to keep the

Table 3: DOC (mg L^{-1}) for leaching time series for three standard reference materials; NIST–SRM 1944: New York/New Jersey Waterway Sediment; NIST–SRM 8704: Buffalo River Sediment; Aldrich Humic Acid.

Leaching time (hours):	NIST SRM 1944	NIST SRM 8704	Aldrich Humic Acid
0	12.90 ± 0.09	18.59 ± 0.48	211.03 ± 1.33
6	22.83 ± 0.19	32.50 ± 0.20	732.80 ± 7.46
24	38.25 ± 0.38	34.99 ± 0.34	1520.53 ± 6.36
168	26.97 ± 0.18	35.46 ± 0.34	2224.00 ± 1.57

results comparable, only the 24–hour leached samples were used.

The 24–hour leached SRM samples were subjected to the dissolved lignin method described earlier, as confirmation of the technique, and to provide dissolved lignin values for SRMs previously extracted for solid phase lignin by Louchouarn et al. (2000). The results of these analyses can be seen in ***Figure 12*** and ***Table 4***.

Overall, the lignin phenol abundances of NIST SRM 8704 and NIST SRM 1944 were similar to each other. In contrast, extraction of Aldrich Humic Acid (HA) yielded lignin–derived phenols that were an order–of–magnitude higher than in the SRMs studied (***Table 4***).

Table 4: Average lignin–derived phenol yields and ratios for aqueous leachates of NIST SRM 1944, NIST SRM 8704 and Aldrich Humic Acid. All concentrations are expressed in (μg L^{-1}) unless noted otherwise. All yields are ± their standard deviation of the three replicate samples. Σ_8 is the sum of total lignin phenol yield (Total vanillyl yield + total syringyl yield + total cinnamyl yield) in units of (μg L^{-1}); Λ_8 is the total lignin phenol yield in terms of DOC in units of (mg 100mg DOC^{-1}); The syringyl:vanillyl ratio (S/V); The cinnamyl:vanillyl ratio (C/V); the vanillyl unit acid to aldehyde ratio $[Ad/Al]_V$; and the syringyl unit acid to aldehyde ratio $[Ad/Al]_S$. (n = 3)

Phenol ID	NIST SRM 1944: New York/New Jersey Waterway Sediment	NIST SRM 8704: Buffalo River Sediment	Aldrich Humic Acid
VAL	28.47 ± 1.05	31.67 ± 6.39	66.85 ± 3.09
VON	22.14 ± 9.85	54.43 ± 2.53	54.73 ± 4.66
VAD	56.12 ± 4.62	12.17 ± 2.77	126.99 ± 19.28
SAL	6.50 ± 1.67	7.28 ± 1.69	61.91 ± 7.60
SON	8.54 ± 1.42	2.90 ± 0.31	66.46 ± 3.02
SAD	22.28 ± 6.69	12.05 ± 1.61	234.97 ± 3.34
CAD	8.05 ± 4.87	5.69 ± 0.48	245.94 ± 9.29
FAD	8.02 ± 3.20	3.68 ± 1.27	266.49 ± 6.40
Σ_8	160.12 ± 12.84	129.87 ± 6.30	1124.34 ± 33.21
Λ_8	0.42 ± 0.02	0.37 ± 0.04	0.07 ± 0.00
S/V	0.35 ± 0.08	0.23 ± 0.02	1.47 ± 0.10
C/V	0.15 ± 0.06	0.10 ± 0.01	2.07 ± 0.08
$[Ad/Al]_V$	1.97 ± 0.19	0.40 ± 0.10	1.91 ± 0.36
$[Ad/Al]_S$	3.43 ± 0.40	1.70 ± 0.31	3.84 ± 0.52

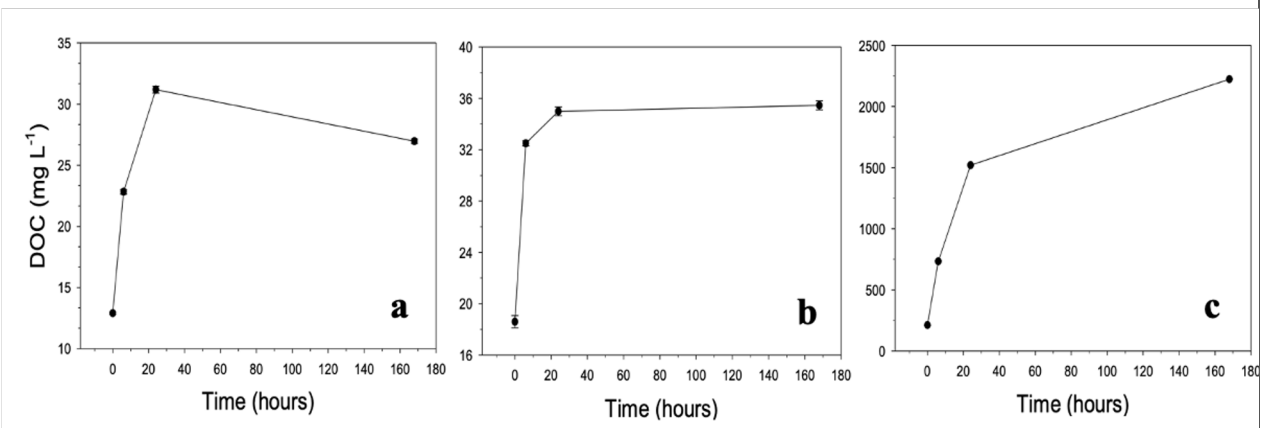

Figure 11: DOC (mg L^{-1}) data collected from the leaching time series experiment samples, each data point is a data sampling time period. a. is NIST–SRM 1944; b. NIST–SRM 8704; c. Aldrich Humic acid.

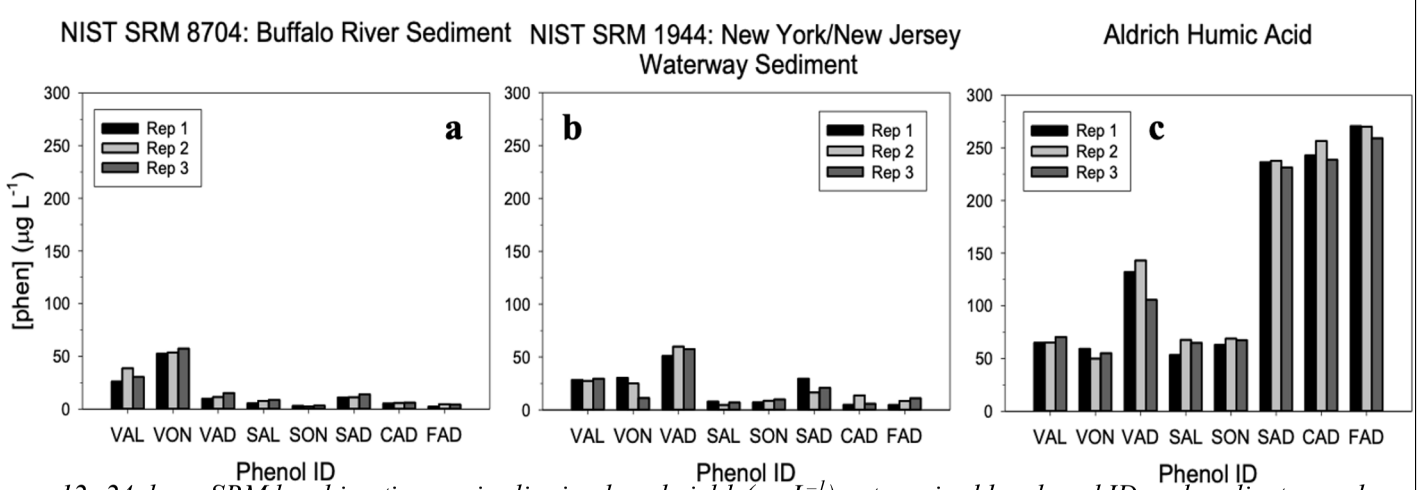

Figure 12: 24–hour SRM leaching time series lignin phenol yields(μg L^{-1}) categorized by phenol ID and replicate number (reps 1–3) . a. NIST SRM 8704; b. NIST SRM 1944; c. Aldrich Humic Acid.

c. Salinity and total suspended sediment (TSS)

The range and average salinity were similar in 2018 and 2019. In 2018, the range in salinity across all stations was 4.2 – 34 (mean ± standard deviation = 23 ± 11 ppt) whereas in 2019, salinity varied from 8.5 to 30 (21 ± 7.6 ppt). The lowest salinity of the GSPS–18 estuarine samples was Stations 50 and 9 (furthest away from Oregon Inlet) with a value of 4.20 and 5.79 ppt respectively. In contrast, the highest GSPS–18 estuarine salinity value was observed at Stations 6 and 7 (29.90 ppt and 29.30 ppt, respectively), with both stations at the mouth of the Oregon Inlet (***Figure 9***).

The lowest GSPS–19 estuarine salinity measurements were taken at Stations 109 and 110, measuring 13.98 and 8.50 ppt respectively. Station 109 is located between where GSPS–18 Stations 6 & 7 were taken, near the Oregon Inlet. Station 110 is located near where GSPS–18 Station 9 was collected, between Roanoke Island and coastal North Carolina. Station 9 (2018) and Station 110 (2019) which were geographically similar locations were similar in salinity across the ~1 year sampling interval.

Coastal ocean samples had the least variation in salinity while estuarine samples had a much wider range in variation for both sampling years (2018 & 2019). This is most likely due to the Outer Banks island chain restricting the mixing of fresh and saline water other than through its inlets which connect the Pamlico Sound to the open ocean. The lack of variation in coastal salinity values in 2018 suggests that Hurricane Florence and associated erosion of freshwater did not impact the salinity measured at coastal ocean samples.

The lowest salinity value of the coastal ocean was observed at Station 51 and the highest at Station 52 with salinity values of 5.40 and 33.51 ppt respectively. This low value measured at Station 51 may have been due to its close proximity to the Oregon Inlet, leading to dilution of the seawater by freshwater exiting from the inlet. An additional observation in support of this is the

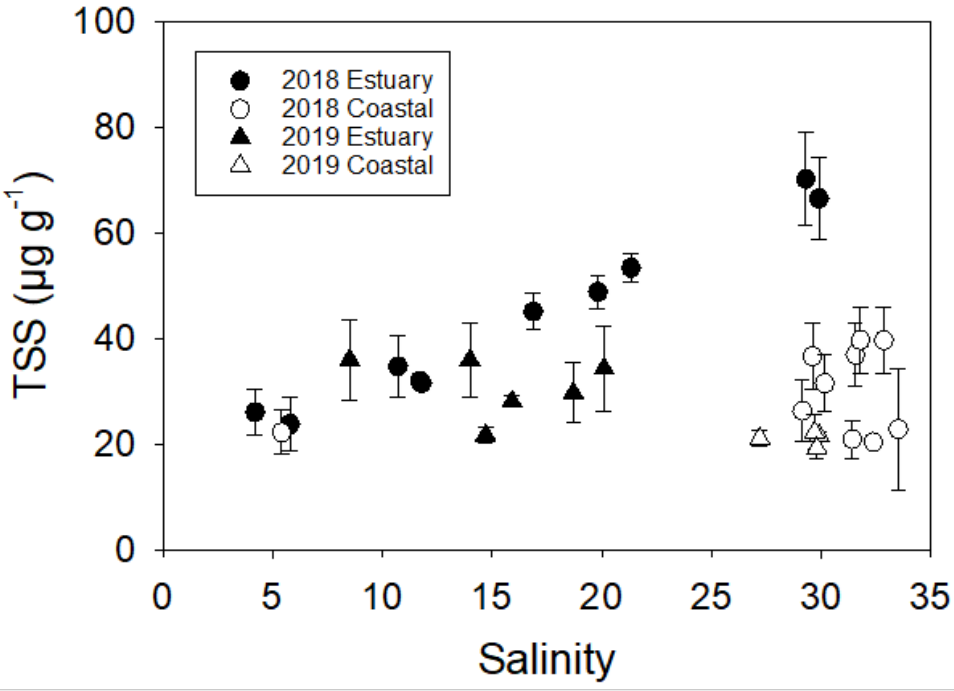

Figure 13: Total suspended sediments (TSS) vs. salinity. Points depicting 2018 and 2019 samples in the estuary as well as further offshore along the NC coast.

fact that higher salinity Station 52 is most distal from the inlet and likely influenced minimally by freshwater dilution from riverine influence. The same trend is observed with 2019 coastal samples with the lowest being close to inlet at Station 104 (27.2 ppt) and the highest being further from the inlet to the estuary at Station 100 (29.2 ppt).

The relationship between salinity and TSS is depicted in ***Figure 13***. Estuarine samples are generally higher in suspended sediments in both 2018 and 2019, compared to coastal and offshore samples. Moreover, both estuarine and coastal water samples collected in 2018 have a broader range in both TSS and salinity and a slight trend of increasing TSS as a function of salinity. In contrast, samples collected in 2019 have predominantly high salinity values and an overall smaller range of TSS and salinity values.

Table 5: Mean total suspended sediment and salinity for GSPS–18 stations. Categorized by station ID, the location of the sample taken, the date and which collection vessel was utilized for sample collection.

Station ID	Location	Date	Collection vessel	Salinity	Avg. TSS ($\mu g\ g^{-1}$)
GSPS–18 Station 1	Estuary	10/25/2018	R/V Blackbeard	21.33	(53.36 ± 2.81)
GSPS–18 Station 2	Estuary	10/25/2018	R/V Blackbeard	16.87	(45.06 ± 3.47)
GSPS–18 Station 3	Estuary	10/25/2018	R/V Blackbeard	11.70	(31.97 ± 1.39)
GSPS–18 Station 4	Estuary	10/26/2018	R/V Blackbeard	11.80	(31.54 ± 0.75)
GSPS–18 Station 5	Estuary	10/26/2018	R/V Blackbeard	19.83	(48.80 ± 3.18)
GSPS–18 Station 6	Estuary	10/26/2018	R/V Blackbeard	29.90	(66.50 ± 7.71)
GSPS–18 Station 7	Estuary	10/26/2018	R/V Blackbeard	29.30	(70.16 ± 8.73)
GSPS–18 Station 8	Estuary	10/26/2018	R/V Blackbeard	10.70	(34.71 ± 5.87)
GSPS–18 Station 9	Estuary	10/26/2018	R/V Blackbeard	5.79	(23.75 ± 5.10)
GSPS–18 Station 10	Coastal	11/19/2018	R/V Neil Armstrong	31.57	(36.90 ± 5.95)
GSPS–18 Station 11	Coastal	11/20/2018	R/V Neil Armstrong	32.85	(39.61 ± 6.26)
GSPS–18 Station 12	Coastal	11/20/2018	R/V Neil Armstrong	31.79	(39.64 ± 6.36)
GSPS–18 Station 13	Coastal	11/23/2018	R/V Neil Armstrong	29.60	(36.59 ± 6.19)
GSPS–18 Station 14	Coastal	11/24/2018	R/V Neil Armstrong	29.14	(26.25 ± 5.85)
GSPS–18 Station 50	Estuary	11/30/2018	R/V Blackbeard	4.20	(26.02 ± 4.29)
GSPS–18 Station 51	Coastal	11/30/2018	R/V Blackbeard	5.40	(22.20 ± 4.16)
GSPS–18 Station 52	Coastal	11/30/2018	R/V Blackbeard	33.51	(22.82 ± 11.45)
GSPS–18 Station 53	Coastal	11/30/2018	R/V Blackbeard	32.38	(20.37 ± 0.42)
GSPS–18 Station 54	Coastal	11/30/2018	R/V Blackbeard	31.42	(20.86 ± 3.64)
GSPS–18 Station 55	Coastal	11/30/2018	R/V Blackbeard	30.16	(31.49 ± 5.34)

Table 6: Total suspended sediment and salinity for GSPS–19 stations.

Station ID	Location	Date	Collection Vessel	Salinity	Avg TSS ($\mu g\ g^{-1}$)
GSPS–19 Station 100	Coastal	7/2/2019	R/V Blackbeard	29.90	(21.68 ± 0.64)
GSPS–19 Station 101	Coastal	7/2/2019	R/V Blackbeard	29.70	(22.21 ± 3.33)
GSPS–19 Station 102	Coastal	7/2/2019	R/V Blackbeard	29.80	(19.26 ± 1.99)
GSPS–19 Station 103*	Coastal	7/2/2019	R/V Blackbeard	26.70	–
GSPS–19 Station 104	Coastal	7/2/2019	R/V Blackbeard	27.20	(21.07 ± 1.45)
GSPS–19 Station 105	Estuary	7/3/2019	R/V Blackbeard	20.10	(34.10 ± 8.06)
GSPS–19 Station 106	Estuary	7/3/2019	R/V Blackbeard	18.70	(29.65 ± 5.68)
GSPS–19 Station 107	Estuary	7/3/2019	R/V Blackbeard	15.90	(28.02 ± 1.02)
GSPS–19 Station 108	Estuary	7/3/2019	R/V Blackbeard	14.70	(21.66 ± 1.41)
GSPS–19 Station 109	Estuary	7/3/2019	R/V Blackbeard	13.98	(35.89 ± 7.06)
GSPS–19 Station 110	Estuary	7/3/2019	R/V Blackbeard	8.50	(35.96 ± 7.59)

The TSS in estuarine samples from 2018 were the highest across all the samples across both years, with the highest being at Station 7 with an average of 70.16 ($\mu g\ g^{-1}$). This value is almost twice the highest TSS value in estuarine samples collected in 2019 [Station 110: 35.96 ($\mu g\ g^{-1}$)]. Station 7 is located at the mouth of the Oregon Inlet, while Station 110 was the station closest to the coastline of the Inner Banks of coastal NC (***Figure 9***). In 2018, Station 7 had one of the highest salinity values, while Station 110 was one of the lowest salinity values of 2019.

The highest TSS coastal water sample of 2018 measured was at Station 12 at 39.64 ($\mu g\ g^{-1}$) while the highest of 2019 was measured at Station 101 with a value of 22.21 ($\mu g\ g^{-1}$). Station 102 is located far off the shore, somewhat close to the sampling location of Station 101 (***Figure 9***). This discrepancy in values indicates that Hurricane Florence influenced the TSS deposited in the estuary as well as the coastal ocean due to runoff and erosion promoting resuspension caused by the storm than that from the non–storm period of 2019.

d. Bulk organic carbon

Water was first filtered at 0.7 µm and then at 0.2 µm (see Methods) and analyzed for bulk carbon, to yield the operationally defined pool of DOC. ***Table 7*** and ***Table 8*** contains DOC concentrations measured in the 0.2 µm filtrate. Compositional analysis of the dissolved phase consisted of analyzing $\delta^{13}C_{DOC}$ and dissolved lignin in the filtrates, both of which are discussed below. GSPS–18 estuarine DOC data (***Table 7***) varied from 1.43 – 7.11 mg L^{-1} with a mean of 4.82 ± 2.0 mg L^{-1} (Stations 1–9, 50; n=10). The GSPS–18 coastal water DOC concentrations varied from 1.10 – 6.48 mg L^{-1} with a mean of 1.97 ± 1.61 mg L^{-1} (Stations 10–14, 51–55; n=10). GSPS–19 (***Table 8***) estuarine DOC data varied from 3.91 – 5.75 mg L^{-1} with a mean of 1.56 ± 0.42 mg L^{-1} (Stations 105–110; n=6). GSPS–19 coastal water DOC varied from 1.32 – 2.19 mg L^{-1} with a mean of 4.63 ± 0.66 mg L^{-1} (Stations 100–102, 104; n=4).

Table 7: Dissolved organic carbon (DOC) for GSPS–18 stations.

Station ID	Location	DOC (mg L^{-1})	δ13C (‰)
Station 1	Estuary	6.14	–27.6
Station 2	Estuary	4.83	–26.2
Station 3	Estuary	5.63	–29.8
Station 4	Estuary	5.54	–29.2
Station 5	Estuary	3.72	–27.2
Station 6	Estuary	1.43	–29.8
Station 7	Estuary	1.50	–27.9
Station 8	Estuary	5.76	–26.1
Station 9	Estuary	6.57	–26.4
Station 10	Coastal	1.27	–30.1
Station 11	Coastal	2.04	–30.2
Station 12	Coastal	1.26	–26.8
Station 13	Coastal	1.53	–31.1
Station 14	Coastal	1.35	–25.0
Station 50	Estuary	7.11	–27.0
Station 51	Coastal	6.48	–28.0
Station 52	Coastal	1.89	–26.8
Station 53	Coastal	1.10	–28.7
Station 54	Coastal	1.25	–26.8
Station 55	Coastal	1.56	–26.2

The $\delta^{13}C_{DOC}$ values for 2018 and 2019 are in ***Table 7*** and ***Table 8***. The GSPS–18 estuarine samples had an average of –27.7 % (Stations 1–9, 50; n = 10), and the coastal water samples from

2018 had an average of –28.0 % (Stations 10–14, 51–55; n = 10). This indicates that the DOC in both the estuary and the coastal waters was largely derived from C3 plant–derived material (***Table 7***). The $\delta^{13}C_{DOC}$ values for the 2019 estuarine samples were more enriched, with an average of –26.6 % (Stations 105–110; n = 6). The coastal water samples from 2019 had an average of –26.6 % (Stations 100–102, 104; n = 4). This indicates that similar to 2018, the DOC was largely derived from C3 plants and soil products (***Table 8*).**

Table 8: Dissolved organic carbon (DOC) for GSPS–19 stations.

Station ID	Location	DOC (mg L^{-1})	δ13C (‰)
Station 100	Coastal	1.34	–26.1
Station 101	Coastal	1.32	–27.0
Station 102	Coastal	1.39	–27.0
Station 103*	Coastal	–	–
Station 104	Coastal	2.19	–26.1
Station 105	Estuary	3.91	–26.1
Station 106	Estuary	4.14	–26.0
Station 107	Estuary	4.57	–25.9
Station 108	Estuary	4.45	–26.0
Station 109	Estuary	4.98	–28.7
Station 110	Estuary	5.75	–26.7

*Insufficient water at GSPS–19 Station 103 due to leaking container.

e. Lignin phenols

The annual total dissolved lignin phenol yields for estuarine and coastal waters in 2018 and 2019 are depicted in ***Figures 15 & 16*** and listed in ***Table 9***. Although DOC decreases in a linear manner as a function of salinity (***Figure 14***), total terrestrial organic matter (lambda–8, Λ_8), does not (***Figure 15 and Figure A–4***). This observation suggests that total DOC is derived from non–lignin sources of dissolved organic carbon, such as marine organic matter. Overall, the phenol yield is higher for all estuarine samples compared to coastal samples. The average phenol yield within the estuary for 2018 was 3.55 ± 2.07 (μg L^{-1}), while the coastal water samples average phenol yield was 2.13 ± 1.34 (μg L^{-1}) (***Table 9***). This variation in average phenol yield between

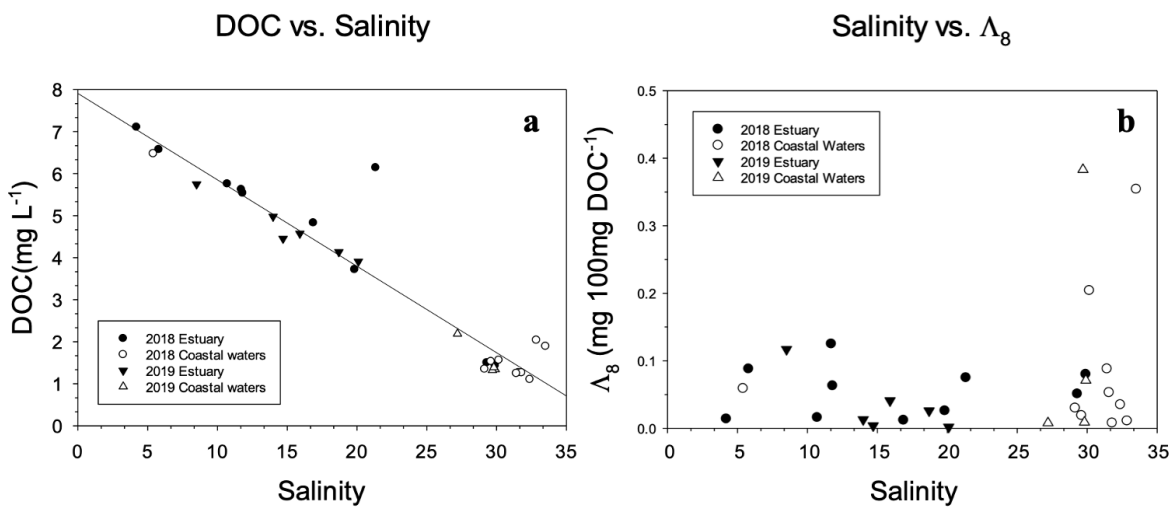

Figure 14: a. Dissolved organic carbon (DOC) in (mg L^{-1}) versus Salinity for GSPS–18 and GSPS–19 samples. Trendline has an r^2 value of 0.9164. b. Lambda 8 (Λ_8) (µg L^{-1}) versus salinity for GSPS–18 and GSPS–19 samples. Data is categorized by sampling area with a solid black circle being 2018 estuarine samples, white circles being 2018 coastal water samples, a solid black triangle being 2019 estuarine samples and white triangles being 2019 coastal water samples.

the estuary and the coastal ocean indicates that the influx of TOM following Hurricane Florence reached the ocean, but primarily stayed within the estuary possibly due to the Outer Banks entrapping the material, water flow, or the minimal interaction with the open ocean as there are only three inlets (Oregon, Hatteras and Ocracoke; ***Figure 9***). Similar concentration trends in lignin are observed in 2018 estuary and coastal water samples (***Figure 15***), with carboxylic acids (VAD, SAD and FAD) consistently being high in concentration at both locations.

The average dissolved phenol yields in 2019 are shown in ***Figure 16.*** There was a clear decrease in lignin–derived phenol yield in the dissolved phase of organic matter between 2018 and 2019. Dissolved lignin phenol yields in 2019 were substantially lower than in 2018 samples (***Figure 15 & 16***). The average phenol yield in the estuary of 2019 was 0.86 ± 0.66 (µg L^{-1}), while the coastal water samples yielded an average of 0.48 ± 0.66 (µg L^{-1}) (***Table 9***). Dissolved lignin–

derived ketones (SON, VON) and carboxylic acids (CAD, FAD) were either not quantifiable or not detectable in estuarine samples in 2019

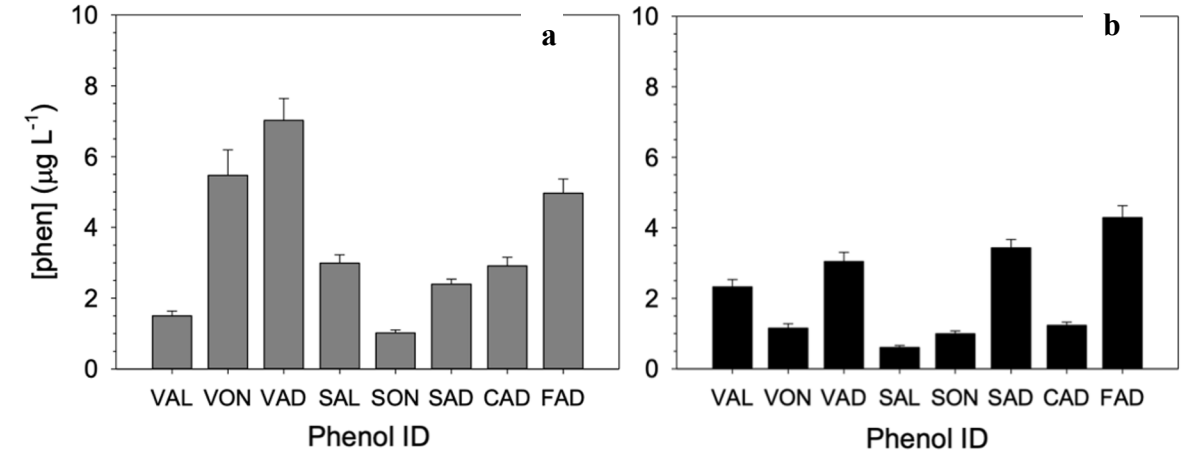

Figure 15: Total phenol yields for GSPS–18 samples. Phenol yields are expressed in (µg L^{-1}) and arranged by individual phenol ID for a. estuarine samples and b. coastal water samples.

.

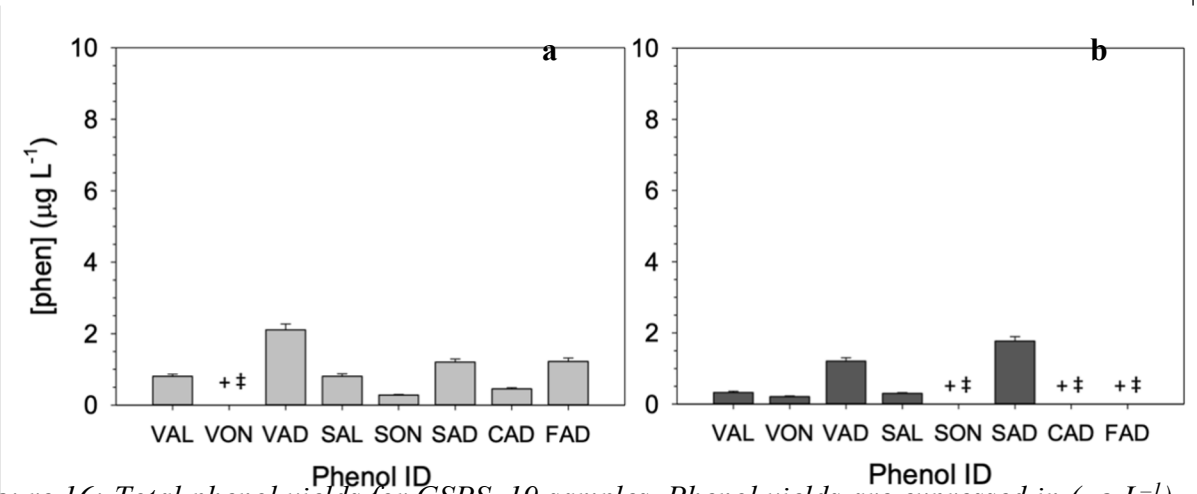

Figure 16: Total phenol yields for GSPS–19 samples. Phenol yields are expressed in (µg L^{-1}) and arranged by individual phenol ID for a. estuarine samples and b. coastal water samples. Phenols with + represent non–quantifiable data and ‡ represented non–detectable data. Phenols with both + ‡ have samples with both results.

Table 9: Total monomer concentrations for 2018 and 2019 estuarine and coastal water samples categorized by phenol ID. Phenol IDs with a (–) has yields that were not quantifiable or not detectable. All concentrations are in (μg L^{-1}). All yields are ± the sum of their instrumental precision.

Phenol ID	2018		2019	
	Estuary	Coastal	Estuary	Coastal
VAL	1.50 ± 0.14	2.32 ± 0.21	0.80 ± 0.06	0.32 ± 0.39
VON	5.48 ± 0.72	1.15 ± 0.13	–	0.21 ± 0.02
VAD	7.02 ± 0.57	3.04 ± 0.26	2.10 ± 0.17	1.20 ± 0.10
SAL	2.99 ± 0.22	0.60 ± 0.06	0.81 ± 0.07	0.30 ± 0.02
SON	1.11 ± 0.07	0.99 ± 0.08	0.28 ± 0.02	–
SAD	2.40 ± 0.14	3.43 ± 0.24	1.20 ± 0.08	1.77 ± 0.13
CAD	2.91 ± 0.24	1.23 ± 0.10	0.45 ± 0.03	–
FAD	4.97 ± 0.40	4.29 ± 0.34	1.22 ± 0.10	–

The Σ_8 values of each station signifies the sum of all phenol monomer volumetric concentrations at that station (***Equation A–3***) (μg L^{-1}) (***Tables 10 & 11).*** Lambda–8, Λ_8, is defined as that total sum of phenols normalized to DOC in that sample and expressed per 100 mg of DOC (e.g., Hedges & Parker, 1976; Ouellet et al., 2009). Thus, both Σ_8 and Λ_8 represent the relative amount of terrestrial vascular plant derived material present in a sample. The average Σ_8 for 2018 estuarine samples was 2.63 ± 2.41 (μg L^{-1}) (Stations 1–9, 50; n=10), while the 2018 coastal water samples had an average of 1.69 ± 2.19 (μg L^{-1}) (Stations 10 – 14, 51 – 55; n = 10). The average Σ_8 for 2019 estuarine samples was 1.77 ± 2.52 (μg L^{-1}) (Stations 105 – 110; n = 6), while the 2019 coastal water samples had an average of 1.58 ± 2.35 (μg L^{-1}) (Stations 100 – 102, 104; n = 4).

Compared to other stations in 2019, Stations 101 (coastal waters) and 110 (estuary) had anomalously high (5x) values of Σ_8. Station 110 is located along the shore of North Carolina (***Figure 9***), which would likely account for the high Σ_8 (6.73 (μg L^{-1})). Due to the location of Station 101 (***Figure 9***) in addition to its high salinity and low DOC value, the lignin–derived phenols may either be an artifact or could possibly be due to a current of water enriched in

terrestrial organic matter. When excluding these uncharacteristically high Σ_8 values, the average Σ_8 for the estuary drops to 0.77 ± 0.73 (μg L^{-1}) (Stations 105 – 109; n = 5), and the coastal waters average drops to 0.42 ± 0.46 (μg L^{-1}) (Stations 100, 102, 104; n = 3). The new averages are more like those seen by average phenol yield discussed earlier and are a better representation of the yields exhibited by these samples.

In 2018, Λ_8 for estuarine samples was 0.06 ± 0.04 (mg 100mg DOC^{-1}) (Stations 1–9, 50; n=10), while the coastal water samples had an average Λ_8 of 0.08 ± 0.11 (mg 100 mg DOC^{-1}) (Stations 10 – 14, 51 – 55; n = 10) ***Tables 10 & 11***. The Λ_8 for 2019 estuarine samples had an average value of 0.02 ± 0.03 (mg 100 mg DOC^{-1}) (Stations 105 – 110; n = 6), while the coastal water samples had an average value of 0.07 ± 0.09 (mg 100 mg DOC^{-1}) (Stations 100 – 102, 104; n = 4). In 2019 (after excluding GSPS–19 Stations 101 and 110), the adjusted Λ_8 averages are 0.01 ± 0.02 (mg 100 mg DOC^{-1}) (Stations 105–109; n = 5) for estuarine samples, and 0.03 ± 0.04 (mg 100 mg DOC^{-1}) (Stations 100, 102, 104; n = 3) for coastal water samples.

e.1. Vanillyl phenols

When comparing the vanillyl monomer group yields from the 2018 sampling period versus the 2019 sampling period, there is a significantly greater yield in 2018 than in 2019. There were multiple samples from each category that did not have detectable levels of vanillyl group monomers. Thus, for comparative purposes only the non–zero values are noted below (***Figure 17)***. Vanillin (VAL) yielded an average of 1.50 ± 0.14 μg L^{-1} for estuarine samples and 2.32 ± 0.21 μg L^{-1} and for coastal water samples. The non–zero averages for acetovanillone (VON) are 1.15 ± 0.13 μg L^{-1} for estuarine samples and 5.48 ± 0.72 μg L^{-1} for coastal water samples. Finally, for vanillic acid (VAD) the estuarine non–zero average is 7.02 ± 0.57 μg L^{-1} and 3.04 ± 0.26 μg L^{-1}

for coastal water samples. Overall, VAD resulted in the highest average, and Station 9 being the most concentrated sample (***Figure 17a***).

In general, the non–zero averages of vanillyl group monomers for GSPS–19 samples are lower than that of GSPS–18 samples. Vanillin (VAL) estuarine samples yielded a 46.4% less average of 0.80 ± 0.06 μg L^{-1}, while the coastal samples yielded 86.1% lower average of 0.32 ± 0.39 μg L^{-1}. In addition, acetovanillone (VON) 2019 samples were 81.9% lower in a for estuarine samples of 0.21 ± 0.02 μg L^{-1}, and the coastal water samples contained no VON monomers. These samples were either not quantifiable per the instrument detection limits or were not detected. Moreover, the non – zero averages for 2019 samples for vanillic acid (VAD) were 70.0% less than 2018 with a value of 2.10 ± 0.17 μg L^{-1} for estuarine samples and 60.5% lower for coastal water samples with a value of 1.20 ± 0.10 μg L^{-1}. Similar to 2018, vanillic acid was the most common and highest concentrated monomer among the 2019 samples. Similar to 2018, Station 110 (located in close proximity to Station 9) (***Figure 9***) was the station that was the most concentrated with lignin phenols.

It is interesting however that besides Station 9, Stations 1, 2, 52, 54 and 55 yielded the highest vanillyl monomers. Stations 1 and 2 are located in the middle of the estuary (***Figure 9***) and Stations 52, 54 and 55 are in the open ocean. These stations are not close to any shoreline, suggesting that the lignin found in these samples have been in the estuary and have flowed south or in from the north of South Carolina (Stations 1 & 2), or have flowed through the estuary and out through the Oregon Inlet to the ocean (Stations 52, 54 and 55).

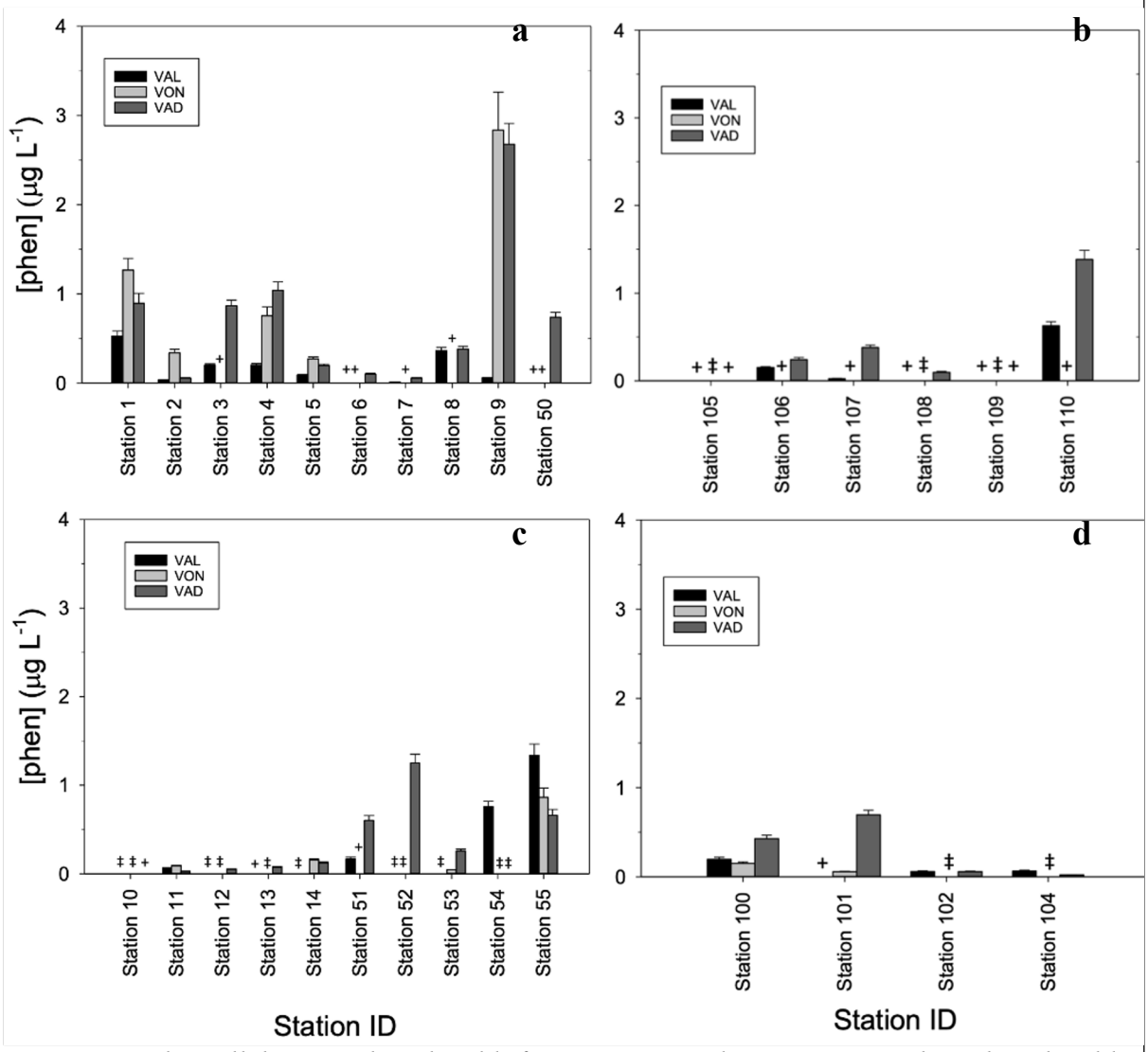

Figure 17: Total vanillyl group phenol yields for GSPS–18 and GSPS–19 samples. Phenol yields are expressed in (μg L^{-1}) and arranged by individual station ID for a. 2018 estuarine samples; b. 2018 coastal water samples; c. 2019 estuarine samples and d. 2019 coastal water samples. Phenols with + represent non–quantifiable data and ‡ represented non–detectable data.

e.2 Syringyl phenols

The non–zero averages were used for mathematical purposes for the same reasons as the vanillyl phenols and the total syringyl group phenol yields can be seen in ***Figure 18***. The GSPS–18 samples average for the monomer, syringaldehyde (SAL) yielded an average of 2.99 ± 0.22 μg L^{-1} for estuarine samples and 0.60 ± 0.06 μg L^{-1} for coastal water samples. The averages for acetosyringone (SON) for estuarine samples is 1.11 ± 0.07 μg L^{-1} and 0.99 ± 0.08 μg L^{-1} for coastal water samples. Finally, for syringic acid (SAD), the estuarine samples yielded an average of 2.40 ± 0.14 μg L^{-1} while the coastal water samples has an average of 3.43 ± 0.24 μg L^{-1}.

As for the GSPS–19 samples, the non–zero average for SAL for estuarine samples decreased from 2018 by 73.1% with a value of 0.81 ± 0.07 μg L^{-1} and a 50.6% decrease for coastal water samples with a value of 0.30 ± 0.02 μg L^{-1}. For SON, the 2019 samples were 74.9% lower than 2018 for estuarine samples with a value of 1.11 ± 0.07 μg L^{-1} and the coastal water samples for 2019 did not contain any acetosyringone monomers. The averages for SAD decreased from 2018 to 2019 by 49.8% with a value of 1.20 ± 0.08 μg L^{-1} for estuarine samples and the coastal water samples were lower by 48.4% with a value of 1.77 ± 0.13 μg L^{-1}. This shows a significant decrease in lignin phenols between 2018 and 2019, further suggesting influence by the hurricane.

Syringyl phenols are not present in all species of terrestrial vascular plants, but expressed predominantly from angiosperm (flowering) plants. The absence of syringyl phenols in both GSPS–18 and GSPS–19 samples is not indicative of the absence of lignin in the sample but rather gymnosperm plant source tissue.

The most concentrated sample of a syringyl group monomer was Station 52, with a SAD yield of 2.09 μg L^{-1}. This station is the furthest east of all coastal sampling sites of GSPS–18

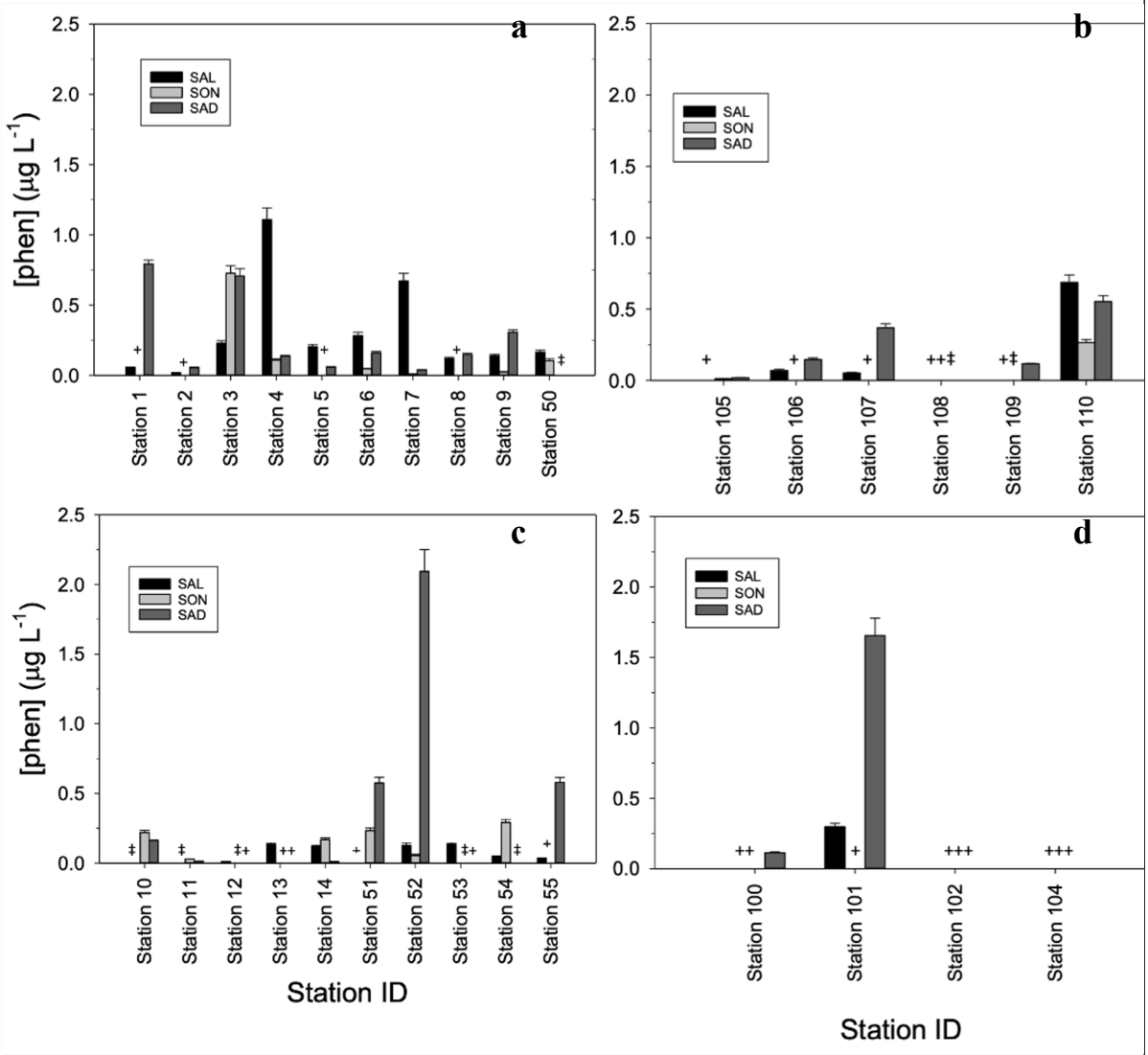

Figure 18: Total syringyl group phenol yields for GSPS–18 and GSPS–19 samples. Phenol yields are expressed in (µg L^{-1}) and arranged by individual station ID for a. 2018 estuarine samples; b. 2018 coastal water samples; c. 2019 estuarine samples and d. 2019 coastal water samples. Phenols with + represent non–quantifiable data and ‡ represented non–detectable data.

(***Figure 9***), and its matching GSPS–19 station, 100, yielded SAD, but was not the most concentrated station sample. However, Station 101 yielded a similar SAD yield of 1.66 µg L^{-1} and this station is close to where samples from Station 52 were collected, but location–based analyses would need to be investigated further to make a concrete connection between those stations.

e.3. Cinnamyl phenols

The cinnamyl phenols, cinnamic acid (CAD) and ferulic acid (FAD) are commonly lower in yield compared to the vanillyl and syringyl groups. They are usually present in samples that are further along in decomposition and are present in non–woody vascular plant tissues. Cinnamyl phenols are predominantly expressed in nonwoody plants can be used to determine whether a plant sample is woody or nonwoody (Hedges & Mann, 1979).

The GSPS–18 estuarine samples have a yield of 2.91 ± 0.24 μg L^{-1} for *p*–coumaric acid (CAD) and 4.97 ± 0.40 μg L^{-1} for ferulic acid (FAD). The 2018 coastal water samples have a non–zero average of 1.23 ± 0.10 μg L^{-1} and an average of 4.29 ± 0.34 μg L^{-1} for FAD. The GSPS – 19 samples yielded a much lower cinnamyl phenol average than that of 2018. For CAD, the 2019 estuarine samples were by lower 84.4% for CAD (0.45 ± 0.03μg L^{-1}) and by 75.4% for FAD (1.22 ± 0.10 μg L^{-1}) compared to 2018. The coastal water samples of 2019 did not contain any detectable cinnamyl phenols.

All three phenol families (vanillyl, syringyl and cinnamyl) have all shown a decrease in phenol yield from 2018 to 2019, indicating that it is highly probable that Hurricane Florence influenced the concentration of lignin in the APES. Further analysis of the monomer yields may reveal possible sources and rate of degeneration.

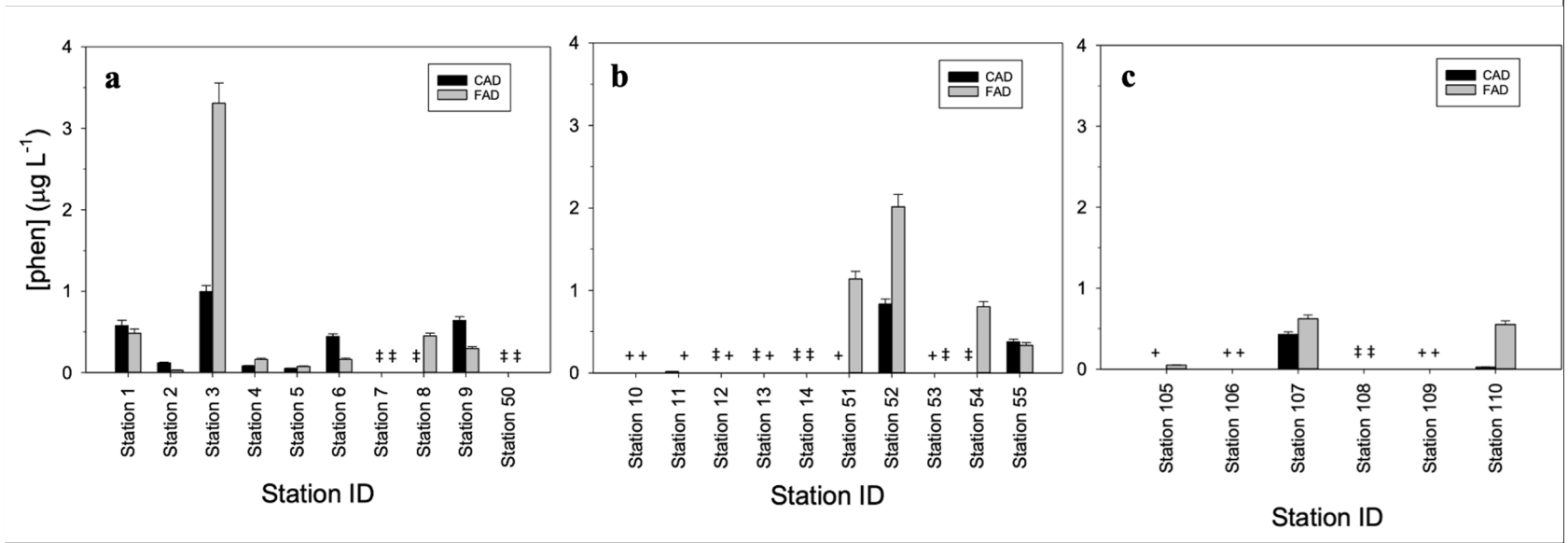

Figure 19: Total syringyl phenol yields for GSPS–18 and GSPS–19 samples. Phenol yields are expressed in (µg L^{-1}) and arranged by individual station ID for a. 2018 estuarine samples; b. 2018 coastal water samples and c. 2019 estuarine samples. There were no detectable nor quantifiable data for samples collected in 2019 in coastal waters. Phenols with + represent non–quantifiable data and ‡ represented non–detectable data. Phenols with both + ‡ have samples with both results.

f. Lignin isomer class ratios for discriminating sources of terrestrial organic matter

f.1. S/V and C/V ratios

In ***Figure 20***, the ratio of the sum of the syringyl group (syringaldehyde, acetosyringone and syringic acid):sum of vanillyl group (vanillin, acetovanillone and vanillic acid) (S/V) is on the y–axis and the sum of the cinnamyl group (*p*–coumaric acid and ferulic acid):the sum of the vanillyl group (C/V) on the x–axis. This relationship provides some insight on sources of vascular plant tissue that yield lignin phenols in the samples that were part of this study (e.g., Hedges & Ertel, 1982; Hedges & Mann, 1979). There are four main classifications of vascular land plants: woody angiosperm, non–woody angiosperm, woody gymnosperm, and non–woody gymnosperm (e.g., Hedges & Ertel, 1982). Using known species of plants and graphing their S/V vs. C/V ratio, a collection of four boxes is used to categorize lignin phenol sources (***Figure 20***).

Known trends of these four categories of plant species have given insight to unknown samples, such as those quantified in this study. The S/V ratio is used primarily for the identification of angiosperm tissues as almost all species of gymnosperms produce vanillyl phenols (V) but characteristically angiosperms produce syringyl phenols (S) in addition to the vanillyl phenols, which results in angiosperm tissues having a ratio greater than zero (Hedges & Mann, 1979).

The C/V ratio is predominantly used to discriminate between woody and non–woody tissues. This is due to the documented research finding that only non–woody vascular plant tissues result in a substantial amount of cinnamyl phenols (C) following oxidation. This means that non–woody angiosperm tissues are found away from both axes when graphing these ratios, as seen in box (b) of ***Figure 20***. Whereas woody angiosperm plant tissues generally produce syringyl and vanillyl phenols, but little to no cinnamyl phenols, resulting in data along the y–axis but away from the origin (box (a) in ***Figure 20***).

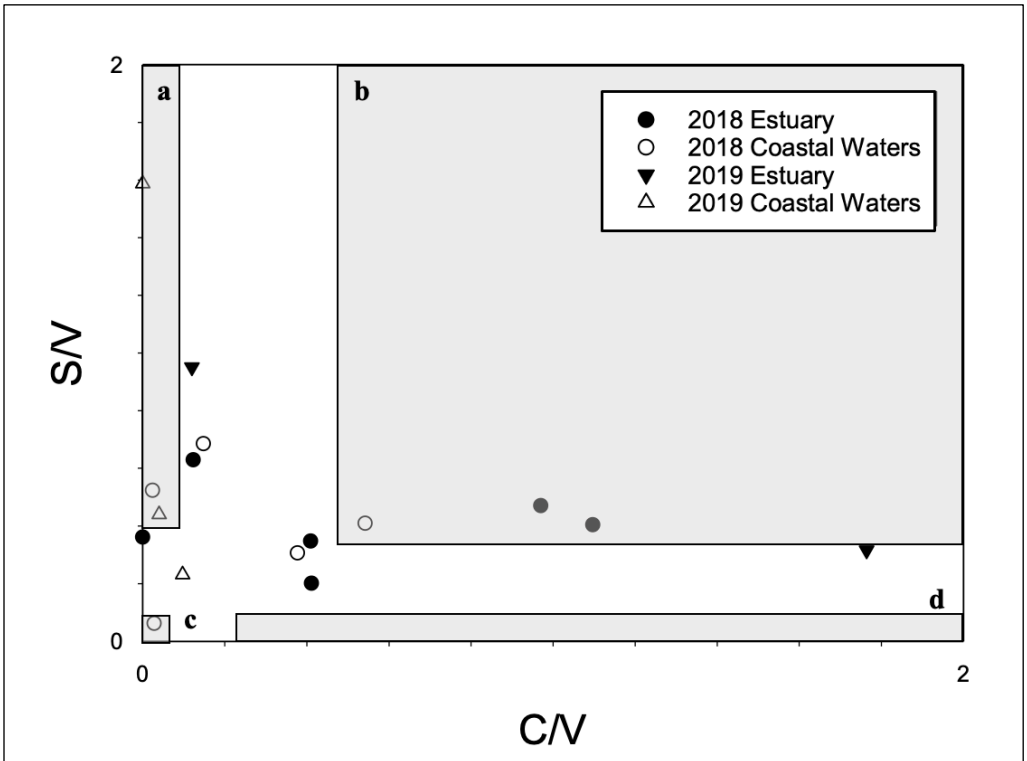

Figure 20: Syringyl:vanillyl (S/V) vs. cinnamyl:vanillyl (C/V) ratios of GSPS–18 and GSPS–19, estuarine and coastal water samples. The boxes shown are typical ranges of the lignin tissue sources are found (e.g., Hedges & Ertel, 1982; Hedges & Mann, 1979; Goñi & Hedges, 1992). (a) woody angiosperm tissues, (b) non–woody angiosperm tissues (e.g., leaves and grasses), (c) woody gymnosperm tissues and (d) non–woody gymnosperm tissues (e.g., needles).

Non–woody gymnosperm tissues customarily do not produce syringyl phenols, while producing vanillyl and cinnamyl phenols, resulting in data along the x–axis, but away from the origin (box (d) in ***Figure 20***). Woody gymnosperm plant tissues produce neither syringyl nor cinnamyl phenols in considerable quantity, which results in data points located at the origin (box (c) in ***Figure 20***). As for the data points that are not categorized in these boxes, it is speculated that these samples derive from a water sample of mixed plant tissue, rather than specific singular plant tissue species.

Data points at the origin are considered woody gymnosperm tissues as they produce neither S or C phenols and between GSPS–18 and GSPS–19 samples, the only station that was graphed at

the origin was Station 54 (box c; ***Figure 20***). Data points that are graphed along the x–axis are non–woody gymnosperm tissues, as they do not yield S phenols but do yield C phenols. While some of the station samples might have contained lignin originating from these tissues, no data points are found within this area (box d; ***Figure 20***). Data points graphed along the y–axis are categorized as woody gymnosperm tissues, as they yield S phenols but do not yield C phenols, Stations 53, 102 and 104 fall within this category (box a; ***Figure 20***). Data points that are not along any axis nor the origin are considered phenols from non–woody angiosperm tissues as they expressed V, S and C phenols, Stations 5, 9 and 12 are present in this category (box b; ***Figure 20***).

f.2. Acid to aldehyde ratios

The use of the acid to aldehyde ratio [Ad/Al] for syringyl ($[Ad/Al]_S$) and vanillyl ($[Ad/Al]_V$) units is utilized to measure the stage of degradation of within the source of lignin (e.g., Ertel & Hedges 1985; Goñi et al., 1993; Kögel 1986). Based on these ratios as well as the S/V and C/V ratios discussed above, the series of sources can be surmised. Syringyl and vanillyl Ad/Al ratios in the range of 0.1 – 0.2, are characteristic of fresh angiosperm and conifer woods, while a range of 0.2 – 1.6 are characteristic of non–woody tissues such as leaves, grasses, and needles (Hedges & Mann, 1979; Otto & Simpson, 2006). Increasing ratio values suggest a higher level of degradation as well as the possible depth of the soil from which the sample was sourced (Ertel & Hedges, 1985). A high ratio coupled with low lignin phenol yields, as seen with Stations 1, 9, 52, 100, 101 and 107, indicates extensive degradation of the lignin tissues in aerobic terrestrial environments (Ertel & Hedges, 1985). There were a few stations for each sample set that were

Table 10: Summary table of GSPS–18 samples by sampling location. Σ_8 is the sum of total lignin phenol yield (Total vanillyl yield + total syringyl yield + total cinnamyl yield) in units of ($\mu g\ L^{-1}$); Λ_8 is the total lignin phenol yield in terms of DOC in units of (mg 100mg DOC^{-1});the syringyl:vanillyl ratio (S/V); cinnamyl:vanillyl ratio (C/V); vanillyl unit acid to aldehyde ratio $[Ad/Al]_V$; and the syringyl unit acid to aldehyde ratio $[Ad/Al]_S$.

Station ID	Σ_8 ($\mu g\ L^{-1}$)	Λ_8 (mg 100mg DOC^{-1})	S/V	C/V	$[Ad/Al]_V$	$[Ad/Al]_S$
GSPS–18 Station 1	4.602	0.075	0.347	0.409	3.424	105.919
GSPS–18 Station 2	0.594	0.012	0.201	0.411	1.523	2.964
GSPS–18 Station 3	7.034	0.125	1.555	4.027	4.303	3.075
GSPS–18 Station 4	3.505	0.063	0.629	0.123	5.215	0.123
GSPS–18 Station 5	0.950	0.026	0.470	0.970	2.160	0.287
GSPS–18 Station 6	1.150	0.080	4.360	5.964	–	0.696
GSPS–18 Station 7	0.761	0.050	11.189	–	5.288	0.726
GSPS–18 Station 8	0.926	0.015	2.645	3.465	1.051	1.225
GSPS–18 Station 9	5.798	0.088	0.404	1.097	59.506	22.040
GSPS–18 Station 10	0.666	0.030	6.265	3.689	–	–
GSPS–18 Station 11	0.219	0.010	0.685	0.148	0.422	–
GSPS–18 Station 12	0.097	0.005	0.409	0.542	–	1.299
GSPS–18 Station 13	0.295	0.001	2.968	0.216	0.182	0.544
GSPS–18 Station 14	0.410	0.031	2.312	–	–	4.373
GSPS–18 Station 50	1.007	0.014	0.361	–	–	–
GSPS–18 Station 51	3.844	0.059	0.977	2.951	5.169	12.888
GSPS–18 Station 52	6.693	0.336	2.469	1.799	15.365	18.357
GSPS–18 Station 53	0.391	0.035	0.523	0.024	–	0.479
GSPS–18 Station 54	1.094	0.088	0.062	0.028	–	–
GSPS–18 Station 55	3.179	0.212	0.306	0.377	1.799	2.824

Table 11: Summary table of GSPS–19 samples by sampling location. Σ_8 is the sum of total lignin phenol yield (Total vanillyl yield + total syringyl yield + total cinnamyl yield) in units of ($\mu g\ L^{-1}$); Λ_8 is the total lignin phenol yield in terms of DOC in units of (mg 100mg DOC^{-1}); the syringyl:vanillyl ratio (S/V); the cinnamyl:vanillyl ratio (C/V); the vanillyl unit acid to aldehyde ratio $[Ad/Al]_V$; and the syringyl unit acid to aldehyde ratio $[Ad/Al]_S$.

Station ID	Σ_8 ($\mu g\ L^{-1}$)	Λ_8 (mg 100mg DOC^{-1})	S/V	C/V	$[Ad/Al]_V$	$[Ad/Al]_S$
GSPS–19 Station 100	0.954	0.070	0.231	0.097	2.168	31.435
GSPS–19 Station 101	5.059	0.202	2.514	2.984	8.229	5.551
GSPS–19 Station 102	0.131	0.008	0.440	0.040	1.203	–
GSPS–19 Station 103*	—	—	—	—	—	–
GSPS–19 Station 104	0.170	0.003	1.587	–	0.597	0.870
GSPS–19 Station 105	0.088	0.001	0.316	1.764	0.735	–
GSPS–19 Station 106	1.092	0.015	0.951	0.120	1.601	2.113
GSPS–19 Station 107	1.858	0.040	9.750	2.593	15.127	12.492
GSPS–19 Station 108	0.163	0.002	3.296	–	3.143	–
GSPS–19 Station 109	0.671	0.013	0.832	2.070	1.844	4.565
GSPS–19 Station 110	6.728	0.071	1.126	8.996	2.210	0.806

*Insufficient water at GSPS 19, Station 103 due to leaking container.

extraordinarily high for both the vanillyl and syringyl acid to aldehyde ratios.

The vanillyl unit acid to aldehyde ratio, $[Ad/Al]_V$ (***Table 10***) for 2018 estuarine samples averaged at 8.25 ± 18.12 and the coastal water samples averaged at 2.29 ± 4.87. These averages are considered high due to Stations 50 and 52. When excluding these outliers, the modified averages are 2.55 ± 2.09 and 0.84 ± 1.72 for estuarine and coastal water stations respectively. The 2019 estuarine samples averaged 4.11 ± 5.45 and the coastal water samples of 2019 averaged 2.9 ± 3.66. These averages are including two stations of high ratios, Stations 107, 108 and 101. When excluding these high ratios, the modified averages are 1.60 ± 0.88 and 1.12 ± 1.09 for estuarine and coastal water stations respectively.

The average of syringyl unit acid to aldehyde ratio, $[Ad/Al]_S$, (Figure ***Table 11***) for 2018 estuarine samples averaged 13.71 ± 33.08 and the coastal water samples averaged 4.08 ± 6.38.

These averages are again, high, due to Stations 1, 9, 51 and 52. When excluding these high ratios, the modified averages are 1.14 ± 1.23 and 1.19 ± 1.60 for estuarine and coastal water samples respectively. The 2019 estuarine samples averaged 3.33 ± 4.81 and the coastal water samples averaged 9.25 ± 15.02. Again, there were stations that had extremely high ratios, Stations 107 and 100. When excluding these values, the modified averages are 1.50 ± 1.92 and 1.85 ± 3.20 for estuarine and coastal water samples respectively.

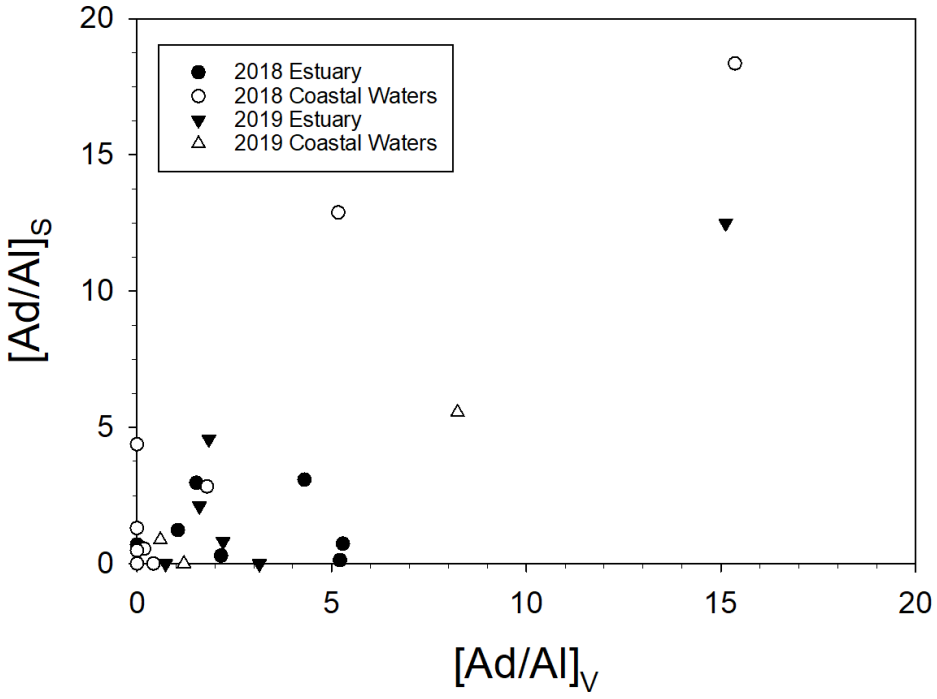

Figure 21:Acid to aldehyde ratio of vanillyl vs. syringyl groups to determine level of degradation. The origin is considered a fresh sample while data points farther away from the origin are considered degraded.

V. Discussion

Over the past century, observations of increased storm intensity and frequency have been accompanied by periods of excessive rainfall and high wind speeds. These have had adverse effects to the environment, such as flooding, runoff, and erosion of terrestrial material into coastal systems. Such event–driven accelerated influx of land–derived OM has disturbed the carbon cycle in coastal areas, with potential impacts to coastal ecosystems.

This study quantified lignin, a chemical marker for terrestrially–derived organic material, in the 2nd largest estuarine system in the United States, the APES and the coastal ocean of North Carolina. Lignin, isolated in particulate matter in coastal systems, has been used in previous studies to shed light on how erosion of TOM varies as a function of coastal storm energy. This study is unique in that it investigated DOC and dissolved phase lignin in water samples collected during the 2018 storm season and compared those to a non–storm period in 2019. This study also introduced a new quantification method of dissolved lignin, adopted from the method introduced by Yan & Kaiser (2018b) utilizing cupric sulfate and GC–MS analysis. The new method was used to quantify dissolved lignin–derived phenols in National Institute of Standards and Technology Standard Reference Materials (SRMs). Dissolved lignin in one of the SRMs was compared to an existing analysis of particulate lignin data in the literature (Louchouarn et al. 2010).

a. SRM – Leaching time series

In this leaching time series experiment, the aqueous dissolved phase lignin in NIST SRM 1944: New York/ New Jersey Waterway Sediment was compared to particulate phase lignin in the same SRM, as described in Louchouarn et al. (2010) **(Figure 21)**. SRM 8704 and Aldrich Humic acid was analyzed for dissolved lignin. However, there are no studies that are available to compare

the dissolved lignin concentrations. Because of their overall hydrophobic polymeric structure, lignin–derived phenol concentrations in particulate phase samples should be elevated compared to lignin in aqueous dissolved phase samples. Louchouarn et al. (2010) used neat samples of SRM 1944 and used a microwave digestion method developed by Goni and Montgomery (2000), which is a modification of the classic cupric–oxide based lignin phenol extraction procedure of Hedges & Ertel (1982) and Goñi & Hedges (1992). This comparison showed no direct correlation between the 24–hour leached dissolved lignin samples the neat particulate standard (***Figure 22)***.

The dissolved lignin phenol yields in this study were substantially lower than solid phase lignin concentrations as reported in Louchouarn et al. (2010), between 49 –97 % less (***Table A–2***). The total lignin parameters, Σ_8 and Λ_8, in this study were a fraction (approx. 1/6 and 1/5 respectively) of that of Louchouarn et al. (2010). The interclass ratios, S/V and C/V, of this study

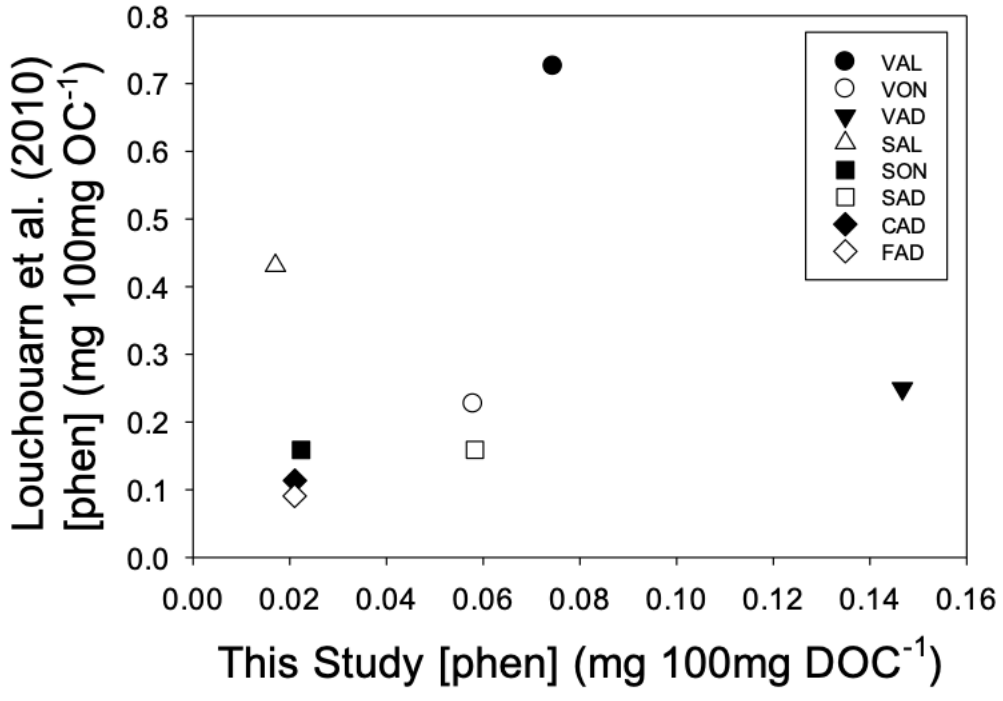

Figure 22: Comparison of analysis of NIST SRM 1944: New York/New Jersey Waterway Sediment from this study versus Louchouarn et al. (2010). r^2 = 0.0551

were approximately half that and equal respectively to the 2010 study. Lastly, the ratios of acid to aldehyde of the V & S groups, were much higher here than that noted in Louchouarn et al 2010. Collectively, these observed differences may be explained by a few reasons. First, NIST SRM 8704: Buffalo River Sediment and Aldrich Humic Acid, were analyzed for lignin phenols which has not been done previously. Although SRM 8704 and SRM 1944 had similar DOC concentrations, their phenol yields were almost completely different (***Table 4***) indicating differing lignin content.

The 24–hour time, though optimal for equilibrating the amount of DOC leached, may not have been the ideal amount of time required to equilibrate lignin between solid and dissolved phases. Alternatively, different chemical reagents are used to extract lignin from the solid versus aqueous phase. Thus, the extraction of lignin from solid and aqueous phases may not be directly comparable. Lastly, Louchouarn et al 2010 quantified lignins using GC–MS with a Varian Ion Trap 3800/4000 system. In contrast, the single quadrupole GC–MS used in this study may have been the reason for the different results observed between solid phase and dissolved phase lignin quantities. Although this was the first attempt at comparing dissolved lignin extraction in SRMs, additional experimental work needs to be done to further investigate the experimental differences in the lignin yields using both techniques. Since that was not the primary goal of this study, these differences will not be discussed further.

b. Bulk DOC and Its Sources

DOC was used a bulk measurement of the organic composition of the water samples collected in 2018 and 2019. In this study, DOC concentrations had an inverse relationship with salinity which increased proceeding seaward (***Figure 14***). Along with DOC, neither TSS nor

salinity varied annually across 2018 and 2019. Thus, collectively, it would seem that Hurricane Florence had little to no impact on these general water quality variables in the APES and coastal North Carolina waters as a result of the 2018 hurricane season.

Similarly, $\delta^{13}C_{DOC}$ of the samples are generally similar between 2018 and 2019. That suggests that the sources of organic matter to the APES and surrounding coastal NC waters did not appreciably change between the 2018 hurricane season and 2019. Most values of $\delta^{13}C_{DOC}$ in both 2018 (estuary and coastal waters) and 2019 (estuary and coastal waters) are between –25 to –28%, which are characteristic of C3 plants (trees and shrubs). There are a few $\delta^{13}C_{DOC}$ values between –30 to –40%, which is characteristic of freshwater phytoplankton (e.g., Rau, 1978; Forsberg et al., 1993, Onstad, 2000).

When comparing the $\delta^{13}C_{DOC}$ data with the graph of S/V vs. C/V data, this data is reasonable as there is a mixture of tissue sources seen in ***Figure 20***. The lack of specific characterization of sources in this figure based on the tissue source boxes, indicate a mixture of sources in the sample. Most of the samples are woody angiosperm and non–woody angiosperm tissues, in agreement with the $\delta^{13}C$–DOC data that indicates terrestrial samples. The $\delta^{13}C_{DOC}$ agree with the general pattern of TOM as determined by lignin interclass ratios (***Figure 20***), in that the sources of TOM were from a mixture of marine and terrestrial material. Though mixing of C3 and phytoplankton are probable based on the data, the majority of the $\delta^{13}C$–DOC values in addition to the S/V and C/V ratios, indicate a mixture dominated by C3 plants. Based on the vegetation found along the eastern coast of North Carolina and Virginia, these plants are most likely to be hardwoods such as Cypress, red maple, green ash, elm, sycamore and sweet gym (https://www.fws.gov/wetlands/data/Water–Summary–Reports/National–Water–Summary–Wetland–Resources–North–Carolina.pdf). Other possible source of lignin in the APES could be

the numerous pocosins located along the watershed. Pocosins are freshwater evergreen shrub wetland, bog, a spongy freshwater wetland consisting of decaying OM, or freshwater marches (same source as above).

c. Lignin yield and its ratios

In contrast to the observations from other bulk water chemistry variables, the hypothesis that Hurricane Florence and the 2018 hurricane season affected the APES and coastal NC waters was supported by lignin–derived phenols. Dissolved lignin across these two time periods are substantially different (***Figures 15*** & ***16***). The Σ_8 values of 2018 are higher in concentration than 2019. Moreover, the Λ_8 of 2018 indicate that a greater amount of the DOC content measured in 2018 are higher in lignin phenol content than that of 2019. Furthermore, VON, SON, CAD and FAD are abundant in 2018, compared to 2019, when they were absent or much lower in concentration than in 2018. Additionally, cinnamyl phenols are absent in the coastal water samples of 2019.

GSPS–18 Station 9 and GSPS–19 Station 110 were the stations that were the most concentrated with VAL, VON and VAD (***Figure 17***), which are located close to shore and where the Albemarle Sound drains into the Pamlico Sound (***Figure 9***). This area is the largest influx of freshwater flow into the Pamlico Sound. This suggests that these stations are highly concentrated due to the flushing of runoff from rivers connected to the Albemarle Sound, which empty to the sound before entering the Pamlico Sound. The similarity between these stations between the years confirm that this area is rich in lignin due to its location. Station 9 is also the second most DOC concentrated sample for the estuarine samples taken in 2018, second only to Station 50. Station 50 however does not yield VAL or VON, and yields a fraction of VAD compared to Station 9. This

indicates that the DOC measured from Station 50, was comprised of differing DOC constituents besides lignin and would require further analyses for confirmation.

The absence of cinnamyl phenols in the coastal water samples of 2019, whether due to the difficulty to quantify these phenols in low concentrations, or the lack of the phenols in the samples altogether impacts the S/V vs. C/V ratios found in ***Figure 20***. The presence of cinnamyl phenols indicate non–woody plant tissues in addition to the difficulty of quantifying these phenols (ex. 2019 samples), exhibits a difficulty in identifying specific source tissues.

Per the research done by Ingrid Kögel (1986), the decomposition of wood and litter material are similar mechanistically. Microbial decomposition of angiosperm tissue occurs at a rapid rate of decomposition caused by the cleaving of the Cα – Cβ positions of the lignin molecule. Such decomposition has been stated to increase the S/V ratio due to the preferential attack of the guaiacyl propane units during the initial stages of decomposition (Kögel, 1986).

The high values of both 2018 and 2019 for the acid to aldehyde ratios of vanillyl and syringyl phenols ($[Ad/Al]_V$, $[ad/Al]_S$ respectively) could be due to a few key factors. A mixture of sample tissue sources, degradation of the lignin and amount of time in the water are all possibly reasons why the data points may not reside within the commonly published tissue areas. Since these samples are taken from open waters of the estuary and the ocean, it is almost impossible to determine the exact source. The origin of the tissues can be inferred using the lignin relative abundances, but it can also be assumed that these tissue samples underwent degradation to some degree which may account for the overly low or overly high ratios. The S/V and C/V ratios may have been caused by the degradation of lignin through fungal, microbial and fractionation (Ouellet et al., 2009; Hedges et al., 1988; Opsahl & Benner, 1995). This is especially true during the months

of July, August and September as the warmer and more humid climate from the summer months, promote microbial–mediated lignin decomposition (Kaiser et al., 2001; Ouellet et al., 2009).

Lastly, this dissolved lignin isolation method is an adaptation of Yan & Kaiser (2018b) and has only been tested on this set of samples, in addition to previously unresearched dissolved lignin SRMs. The reagents and techniques used in this study may specifically result in high acid to aldehyde ratios by design, despite the S/V and C/V ratios being comparable to those isolated in the single SRM.

d. Comparison with other studies

While no studies have investigated dissolved lignin in the APES previously, several studies have quantified dissolved lignin. These are listed in ***Table 12***. When comparing this study to previous dissolved lignin studies, the phenol yields, C/V and S/V ratios are all reasonable. The acid to aldehyde ratios of samples analyzed in this study are elevated and that could be an accurate representation of the level of degradation of the samples analyzed or the degradation of the samples during storage. The other studies did not analyze samples from an estuary or ocean, but either a bay, lake or plant tissue sample.

Table 12: Comparing the ranges of dissolved lignin phenols and interclass ratios from previous studies (Reuter et al. (2017), Arellano et al. (2019) & Yan et al. (2020)) with this study. This includes DOC (mg L^{-1}), salinity (ppt), the total of lignin phenols in terms of sigma–8 (Σ_8) is the sum of total lignin phenol yield (total vanillyl yield + total syringyl yield + total cinnamyl yield) in units of (μg L^{-1}); Λ_8 is the total lignin phenol yield in terms of DOC in units of (mg 100mg DOC^{-1}); the cinnamyl:vanillyl ratio (C/V); the syringyl:vanillyl ratio (S/V); and the syringyl unit acid to aldehyde ratio $[Ad/Al]_S$; and the vanillyl unit acid to aldehyde ratio $[Ad/Al]_V$.*

Study Site	Results								Reference
	DOC	Salinity	Σ_8	Λ_8	C/V	S/V	$[Ad/Al]_S$	$[Ad/Al]_V$	
P. australis leaf leachate	29.6	–	1144.70–1285.5	3.87–4.34	2.35–2.55	0.99–1.00	1.08–1.15	0.84–1.05	Reuter et al. (2017)
Lake Fuchskuhle (southwest)	41.9	–	225.10–469.40	0.54–1.12	0.36	0.41–0.44	0.73–0.87	0.86–0.98	
Lake Fuchskuhle (northeast)	14.7	–	57.83–73.57	0.39–0.50	0.73–0.74	0.57–0.59	0.94–0.97	1.02–1.10	
Apalachicola Bay	1.20–35.80	0.09–35.29	1.49–318.40	0.12–1.55	0.16–1.17	0.35–1.39	0.59–2.05	0.69–2.32	Arellano et al. (2019)
Barataria Bay	2.50–10.70	5.40–28.00	5.72–45.86	0.12–1.15	0.34–2.05	0.87–1.83	0.67–2.23	0.75–1.64	
Galveston Bay (Sept. 4th, 2017)	3.70–6.79	0.00–6.57	341–832*	0.90–1.26	0.06–0.13	0.32–0.48	–	0.77–0.88	Yan et al. (2020)
Galveston Bay (Sept. 28th, 2017)	3.20–4.30	7.84–20.08	118–210*	0.34–0.50	0.09–0.11	0.36–0.42	–	0.66–0.71	
APES 2018	1.43–7.11	4.20–29.90	0.59–7.03	0.01–0.13	0.12–5.96	0.20–11.19	0.12–105.92	1.05–59.51	This Study
Coast of N.C. 2018	1.10–6.48	5.40–33.51	0.10–6.69	0.00–0.34	0.02–3.69	0.06–6.27	0.48–18.36	0.18–15.37	
APES 2019	3.91–5.75	8.50–20.1	0.09–6.73	0.00–0.07	0.12–9.00	0.32–9.75	0.81–12.49	0.74–15.13	
Coast of N.C. 2019	1.32–2.19	26.70–29.90	0.13–5.06	0.00–0.20	0.04–2.98	0.23–2.51	0.87–31.44	0.60–8.23	

* Σ_9 and Λ_8 (sum of total vanillyl, syringyl and p–hydroxyl phenol yields) (n=9) and expressed in (nmol L^{-1}) and in (‰OC) respectively.

VI. CONCLUSION

The Albemarle–Pamlico Estuarine system is the second largest estuarine system in the United States and is home to a vast population of plant and marine species that play a large role in commercial fisheries, tourism and residential communities. As EWEs increase in size and intensity, these influential parts of the ecosystem are adversely impacted by hurricanes and other storms via excess precipitation that causes runoff, erosion and flooding. These consequences affect the ecosystem in more ways than one, as terrestrial material is eroded and deposited into the waterway systems and thus influencing the composition and overall health of the APES and coastal North Carolina Atlantic Ocean. The results from this study suggest that the 2018 hurricane season increased the influx of dissolved TOM into these waters compared to the 2019 mild storm season. Through this understanding of the impact of EWEs, like Hurricane Florence, the concept of the fate of organic matter and nutrients can be further investigated. Along with the increase of storm size, frequency and intensity, climate change continues to accelerate and worsen as the years progress. Further research should be done in order to gain a better understanding of global impacts of storms and their increasingly heavy erosion and flooding and how this impacts waterway systems and its OM composition.

VII. REFERENCES

1. Aiken, G., McKnight, D.M., Thorn, K.A., & Thurman, E.M. (1992). Isolation of hydrophilic organic acids from water using nonionic macroporous resins. *Organic Geochemistry*, 18(4), 567–573.
2. Al–Ghussain, L., (2018). Global Warming: Review on Driving Forces and Mitigation. *Environmental Progress & Sustainable Energy*, 38(1), 13–21. doi: 10.1002/ep.
3. Arellano, A.R., Bianchi, T.S., Hutchings, J.A., Shields, M.R., & Cui, X. (2018). Differential effects of solid-phase extraction resins on the measurement of dissolved lignin-phenols and organic matter composition in natural waters. *Limnology and Oceanography: Methods*, 16(1), 22–34.
4. Argyropoulos, D.S. & Menachem, S.B., (1998). Lignin. *Advances in Biochemical Engineering/Biotechnology*, 57, 127–158.
5. Ayyachamy, M., Cliffe, F.E., Coyne, J.M., Collier, J. & Tuohy, M.G., (2013). Lignin: untapped biopolymers in biomass conversion technologies. *Biomass Conversion and Biorefinery*, 3, 255–269. doi: 10.1007/s13399–013–0084–4
6. Batjes, N.H., (1996). Landmark Papers: Total carbon and nitrogen in the soils of the world. *European Journal of Soil Science*, 47(2), 151–163.
7. Bauer, J.E. & Bianchi, T.S., (2011). Dissolved Organic Carbon Cycling and Transformation. In: Wolanski, E. & McLucky, D. S. (eds.), *Treatise on Estuarine and Coastal Science*, 5, 7–67. Waltham: Academic Press.
8. Benner, R., Biddanda, B., Black, B., & McCarthy, M. (1997). Abundance, size distribution, and stable carbon and nitrogen isotopic compositions of marine organic matter isolated by tangential–flow ultrafiltration. *Marine Chemistry*, 57(3–4), 243–263.
9. Bianchi, T.S., Garcia–Tigreros, F., Yvon–Lewis, S.A., Shields, M., Mills, H.J., Butman, D., Osburn, C., Raymond, P., Shank, G.C., DiMarco, S.F., Walker, N., Reese, B.K., Mullins–Perry, R., Quigg, A., Aiken, G.R. & Grossman, E.L., (2013). Enhanced transfer of terrestrially derived carbon to the atmosphere in a flooding event. *Geophysical Research Letters*, 40, 116–122. doi: 10.1029/2012GL054145
10. Bianchi, T.S. & Canuel, E.A., (2011). *Chemical Biomarkers in Aquatic Ecosystems* (pp. 248–266). Princeton University Press.

11. Bolin, B., (1970). The Carbon Cycle. *Scientific American*, 223(3), 124–135. Scientific American, a division of Nature America, Inc.
12. Bridgham, S.D., Megonigal, J.P., Keller, J.K., Bliss, N.B. & Trettin, C., (2006). The Carbon Balance of North American Wetlands. *Wetlands*, 26(4), 889–916.
13. Cai, W.J., Hu, X., Huang, W.J., Murrell, M.C., Lehrter, J.C., Lohrenz, S.E., Chou, W.C., Zhai, W., Hollibaugh, J.T., Wang, Y., Zhao, P., Guo, X., Gundersen, K., Dai, M & Gong, G.C. (2011). Acidifcation of subsurface coastal waters enhanced by eutrophication. *Nature geoscience*, 4, 766–770.
14. Callaghan, J., (2020). Extreme rainfall and flooding from Hurricane Florence. *Tropical Cyclone Research and Review*, 9, 172–177.
15. Carpenter, D.E. & Dubbs, L., (2012). Albemarle–Pamlico Ecosystem Assessment. *Albemarle–Pamlico National Estuary Partnership*. https://files.nc.gov/apnep/documents/files/publications/EcosystemAssessment2012–PortalSep13.pdf
16. Ciais, P., Sabine, C., Bala, G., Bopp, L., Brovkin, V., Canadell, J., Chhabra, A., DeFries, R., Galloway, J., Heimann, M., Jones, C., Le Quéré, C., Myneni, R.B., Piao, S. and Thornton, P., (2013). Carbon and Other Biogeochemical Cycles. In: Contribution of Working Group I to the Fifth Assessment Report of the Intergovernmental Panel on Climate Change [Stocker, T.F., D. Qin, G.–K. Plattner, M. Tignor, S.K. Allen, J. Boschung, A. Nauels, Y. Xia, V. Bex and P.M. Midgley (eds.)], *Climate Change 2013: The Physical Science Basis*. Cambridge University Press, Cambridge, United Kingdom and New York, NY, USA.
17. Cole, J.J., Prairie, Y.T., Caraco, N.F., McDowell, W.H., Tranvik, L.J., Striegl, R.G., Duarte, C.M., Kortelainen, P., Downing, J.A., Middelburg, J.J. & Melack, J., (2007). Plumbing the Global Carbon Cycle: Integrating Inland Waters into the Terrestrial Carbon Budget. *Ecosystems*, 10, 171–184. doi: 10.1007/s10021–006–9013–8.
18. Crosswell, J.R., Wetz, M.S., Hales, B. & Paerl, H.W., (2014). Extensive CO_2 emissions from shallow coastal waters during passage of Hurricane Irene (August 2011) over the Mid–Atlantic Coast of the U.S.A. *Limnology and Oceanography*, 59(5), 1651–1665.
19. De Leeuw, J.W. & Largeau, C., (1993). A review of macromolecular organic compounds that comprise living organisms and their role in kerogen, coal and petroleum formation. In:

Engel, M.H. & Macko, S.A. (eds.), *Organic Geochemistry*. Topics in Geobiology, 11. Springer, Boston, MA. doi: 10.1007/978–1–4615–2890–6_2.

20. Du, B., Liu, B., Wang, X. & Zhou, J., (2019). A comparison of phenolic monomers produced from different types of lignin by phosphotungstic acid catalysts. *Chemistry Open*, 8, 643–649.
21. Elder, T., Berstis, L., Beckham, G.T. & Crowley, M.F., (2017). Density Functional Theory Study of Spirodienone Stereoisomers in Lignin. *ACS Sustainable Chemistry & Engineering*, 5, 7188–7194.
22. Ertel, J.R. & Hedges, J.I., (1984). The lignin component of humic substances: distribution among soil and sedimentary humic, fulvic, and base–insoluble fractions. *Geochimica et Cosmochimica Acta*, 48, 2065 – 2074.
23. Ertel, J.R. & Hedges, J.I., (1985). Sources of sedimentary humic substances: vascular plant debris. *Geochimica et Cosmochimica acta*, 49, 2097–2107.
24. Forsberg, B.R., Araujo – Lima, C.A.R.M., Martinelli, L.A., Victoria, R.L. & A., B.J. (1993). Autotrophic carbon sources for fish of the central Amazon. *Ecology*, 74, 643–652.
25. Garrett, R.G., (1994). Water–Quality Data from Continuously Monitored Sites in the Pamlico and Neuse River Estuaries, North Carolina, 1991–92. *U.S. Geological Survey: Open–File Report 94–27* (Albemarle–Pamlico Estuarine Study Report No. 94–01). Prepared in cooperation with the Albemarle–Pamlico Estuarine Study of the North Carolina Department of Environment, Health, and Natural Resources.
26. Giese, G.L., Wilder, H.B. & Parker Jr., G.G., (1985). Hydrology of Major Estuaries and Sounds of North Carolina. *United States Geological Survey: Water–Supply Paper 2221*. Prepared in cooperation with the North Carolina Department of Natural Resources and Community Development.
27. Goñi, M.A., Nelson, B., Blanchette, R.A. & Hedges, J.I., (1993). Fungal degradation of wood lignins: Geochemical perspectives from CuO–derived phenolic dimers and monomers. *Geochimica et Cosmochimica Acta*, 57, 3985–4002.
28. Goñi, M.A. & Hedges, J.I., (1992). Lignin dimers: Structures, distribution, and potential geochemical applications. *Geochimica et Cosmochimica Acta*, 56, 4025–4043.
29. Goñi, M.A., & Montgomery, S. (2000). Alkaline CuO oxidation with a microwave digestion system: Lignin analyses of geochemical samples. *Analytical chemistry*, 72(14), 3116–

3121.

30. Hansell, D.A. (2013). Recalcitrant Dissolved Organic Carbon Fractions. *Annual Review of Marine Science*, 5, 421–445.
31. Hansell, D.A., Carlson, C.A., Repeta, D.J. & Schlitzer, R., (2009). Dissolved Organic Matter in the Ocean: A controversy stimulates new insights. *Oceanography*, 22(4), 202–211.
32. Hansell, D.A. & Carlson, C.A., (2001). Marine Dissolved Organic Matter and the Carbon Cycle. *Oceanography*, 14(4), 41–49.
33. Harned, D.A., & Davenport, M.S. (1990). Water Quality Trends and Basin Activites and Characteristics for the Albemarle–Pamlico Estuarine System, North Carolina and Virginia. *U.S. Geological Survey*. https://pubs.usgs.gov/of/1990/0398/report.pdf
34. Hedges, J.I., Blanchette, R.A., Weliky, K., Devol, A.H., (1988). Effects of fungal degradation on the CuO oxidation products of lignin: a controlled laboratory study. *Geochimica et Cosmochimica Acta*, 52, 2717–2726. doi:10.1016/0016–7037(88) 90040–3
35. Hedges, J.I. & Ertel, J.R., (1982). Lignin geochemistry of a Late Quaternary sediment core from Lake Washington. *Geochimica et Cosmochimica Acta*, 46, 1869–1877.
36. Hedges, J.I. & Mann, D.C., (1979). The characterization of plant tissues by their lignin oxidation products. *Geochimica et Cosmochimica Acta*, 43, 1803–1807.
37. Hermann, K.M. & Weaver, L.M., (1999). The Shikimate Pathway. *Annual Review of Plant Physiology and Plant Molecular Biology*, 50, 473–503.
38. Hernes, P.J., & Benner, R. (2003). Photochemical and microbial degradation of dissolved lignin phenols: Implications for the fate of terrigenous dissolved organic matter in marine environments. *Journal of Geophysical Research: Oceans*, 108(C9).
39. Hilton, R.G., Galy, A., Hovius, N., Chen, M.C., Horng, M.J. & Chen, H. (2008). Tropical–cyclone–driven erosion of the terrestrial biosphere from mountains. *Nature Geoscience*, doi: 10.1038/ngeo333
40. Hobbie, E.A. & Werner, R.A. (2003). Intramolecular, compound–specific, and bulk carbon isotope patterns in C3 and C4 plants: a review and synthesis. *New Phytologist*, 161, 371–385.
41. "Hurricane Florence: September 14, 2018". *National Weather Service: NWS Wilmington, NC*, n.d., https://www.weather.gov/ilm/HurricaneFlorence

42. “Hurricane Statistics”. *North Carolina State Climate Office*, n.d., https://products.climate.ncsu.edu/weather/hurricanes/statistics
43. Jiao, N., Liu, J., Edwards, B., Lv, Z., Cai, R., Liu, Y., Xiao, X., Wang, J., Jiao, F., Wang, R., Huang, X., Guo, B., Sun, J., Zhang, R., Zhang, Y., Tang, K., Zheng, Q., Azam, F., Batt, J., Cai, W.J., He, C., Herndl, G.J., Hill, P., Hutchins, D., LaRoche, J., Lewis, M., MacIntyre, H., Polimene, L., Robinson, C., Shi, Q., Suttle, C.A., Thomas, H., Wallace, D. & Legendre, L. (2021). Correcting a major error in assessing organic carbon pollution in natural waters. *Science Advances*, 7: eabc7318.
44. Kaiser, K., Guggenberger, G., Haumaier, L., Zech, W., (2001) Seasonal variations in the chemical composition of dis– solved organic matter in organic forest floor layer leachates of old growth Scots pine (Pinus sylvestris L.) and European beech (Fagus sylvatica L.) stands in northeast– ern Bavaria, Germany. Biogeochemistry 55:103–143. doi: 10.1023/A:1010694032121
45. Kaiser, K., & Benner, R. (2011). Characterization of lignin by gas chromatography and mass spectrometry using a simplified CuO oxidation method. *Analytical chemistry*, 84(1), 459–464.
46. Katahira, R., Elder, T.J. & Beckham, G.T., (2018). A brief introduction to Lignin Structure. *Energy and Environment Series No. 19: Lignin Valorization: Emerging Approaches*. Royal Society of Chemistry, United States. doi: 10.1039/9781788010351.
47. Kögel, I., (1986). Estimation and decomposition pattern of the lignin component in forest humus layers. *Soil Biology and Biochemistry*, 18(6), 589–594.
48. Kögel, I. & Bochter, R., (1985). Characterization of lignin in forest humus layers by high–performance liquid chromatography of cupric oxide oxidation products. *Soil Biology and Biochemistry*, 17(5), 637–640.
49. Lalonde, K., Vähätalo, A.V. & Gélinas, Y., (2014). Revisiting the disappearance of terrestrial dissolved organic matter in the ocean: a δ13C study. *Biogeosciences*, 11, 3707–3719.
50. Liu, Q., Luo, L. & Zheng, L., (2018). Lignins: Biosynthesis and Biological Functions in Plants. *International Journal of Molecular Sciences*, 19(335). doi: 10.3390/ijms19020335
51. Louchouarn, P., Opsahl, S., & Benner, R. (2000). Isolation and quantification of dissolved lignin from natural waters using solid–phase extraction and GC/MS. *Analytical chemistry*, 72(13), 2780–2787.

52. Louchouarn, P., Amon, R.M.W., Duan, S., Pondell, C., Seward, S.M. & White, N., (2010). Analysis of lignin–derived phenols in standard reference materials and ocean dissolved organic matter by gas chromatography/tandem mass spectrometry. *Marine Chemistry*, 118, 85–97.

53. Moorman, M.C., Fitzgerald, S.A., Gurley, L.N., Rhoni–Aref, A. & Loftin, K.A., (2017). Water Quality and Bed Sediment Quality in the Albemarle Sound, North Carolina, 2012–14. *U.S. Department of the Interior: U.S. Geological Survey Open–File Report 2016–1171*, 46 p., https://doi.org/10.3133/ofr20161171.

54. Onstad, G.D., Canfield, D.E., Quay, P.D. & Hedges, J.I. (2000). Sources of particulate organic matter in rivers from the continental USA: Lignin phenol and stable carbon isotope compositions. *Geochimica et Cosmochimica Acta*, 64(20), 3539–3546.

55. Opsahl, S. & Benner, R., (1995). Early diagenesis of vascular plant tissues: lignin and cutin decomposition and biogeochemical implications. *Geochimica et Cosmochimica Acta*, 59, 4889 – 4903. doi: 10.1016/0016–7037(95)00348–7.

56. Opsahl, S. & Benner, R. (1998). Photochemical reactivity of dissolved lignin in river and ocean waters. *Limnology and Oceanography*, 43(6), 1297–1304.

57. Opsahl, S., & Benner, R. (1999). Major flux of terrigenous dissolved organic matter through the Arctic Ocean. *Limnology and Oceanography*, 44(8), 2017–2023.

58. Otto, A. & Simpson, M.J., (2006). Evaluation of CuO oxidation parameters for determining the source and stage of lignin degradation in soil. *Biogeochemistry*, 80, 121–142.

59. Ouellet, J., Lucotte, M., Teisserenc, R., Paquet, S. & Canuel, R., (2009). Lignin biomarkers as tracers of mercury sources in lakes water column. *Biogeochemistry*, 94, 123–140.

60. Paerl, H.W., Bales, J.D., Ausley, L.W., Buzzelli., C.P., Crowder, L.B., Eby, L.A., Fear, J.M. Go, M., Peierls, B.L., Richardson, T.L. & Ramus, J.S.(2001). Ecosystem impacts of three sequential hurricanes (Dennis, Floyd, and Irene) on the United States' largest lagoonal estuary, Pamlico Sound, NC. *Proceedings of the National Academy of Sciences of the United States of America, PNAS*, 98(10), 5655–5660. doi: 10.1073/pnas.101097398

61. Paerl, H.W., Crosswell, J.R., Van Dam, B., Hall, N.S., Rossignol, K.L., Osburn, C.L., Hounshell, A.G., Sloup, R.S. & Harding Jr., L.W., (2018). Two decades of tropical cyclone impacts on North Carolina's estuarine carbon, nutrient and phytoplankton

dynamics: implications for biogeochemical cycling and water quality in a stormier world. *Biogeochemistry*, 141, 307–332.

62. Parthasarathi, R., Romero, R.A., Redondo, A. & Gnanakaran, S., (2011). Theoretical study of the remarkably diverse linkages in lignin. *The Journal of Physical Chemistry Letters*, 2, 2660–2666.
63. Perez–Pimienta, J.A., Rios–Del Toro, E.E., Amezquita–Garcia, H.J. & Escamilla–Alvarado, C., (2021). Advances in biofuels and by–products from lignin. *Sustainable Biofuels*, 101–130. doi:10.1016/B978–0–12–820297–5.00007–4.
64. Prentice, I.C., Farquhar, G.D., Fasham, M.J.R., Goulden, M.L., Heimann, M., Jaramillo, V.J., Kheshgi, H.S., Le Quéré, C., Scholes, R.J., Wallace, D.W.R., …Yool, A., (2001). The Carbon Cycle and Atmospheric Carbon Dioxide. *The Intergovernmental Panel on Climate Change (IPCC), TAR Climate Change 2001: The Scientific Basis*, 183–237.
65. Post, W.M., Peng, T., Emanuel, W.R., King, A.W., Dale, V.H. & DeAngelis, D.L., (1990). The Global Carbon Cycle. *American Scientist*, 78, 310–326.
66. Rau, G. (1978). Carbon–13 depletion in a subalpine lake: Carbon flow implications. *Science*, 201, 901–902.
67. Regnier, P., Friedlingstein, P., Ciais, P., Mackenzie, F.T., Gruber, N., Janssens, I.A., Laruelle, G.G., Lauerwald, R., Luyssaert, S., Andersson, A.J., Arndt, S., Arnosti, C., Borges, A.V., Dale, A.W., Gallego–Sala, A., Goddéris, Y., Goossens, N., Hartmann, J., Heinze, C., Ilyina, T., Joos, F., LaRowe, D.E., Leifeld, J., Meysman, F.J.R., Munhoven, G., Raymond, P.A., Spahni, R., Suntharalingam, P. & Thullner, M. (2013). Anthropogenic perturbation of the carbon fluxes from land to ocean. *Nature geoscience*, 6, 597–607.
68. Reuter, H., Gensel, J., Elvert, M., & Zak, D. (2017). Direct analysis of lignin phenols in freshwater dissolved organic matter. *Analytical chemistry*, 89(24), 13449–13457.
69. Riebeek, H., (2011). The Carbon Cycle. *NASA Earth Observatory.* https://earthobservatory.nasa.gov/features/CarbonCycle
70. Rudolph, J.C., Arendt, C.A., Hounshell, A.G., Paerl, H.W. & Osburn, C.L., (2020). Use of geospatial, hydrologic, and geochemical modeling to determine the influence of wetland–derived organic matter in coastal waters in response to extreme weather events. *Frontiers in Marine Science*, 7(18). doi: 10.3389/fmars.2020.00018.

71. Sarkanen, K.V. & Ludwig, C.H., (1971). *Lignins: Occurrence, formation, structure and reactions*. Wiley Interscience, New York, U.S.A.

72. Schimel, D.S., (1995). Terrestrial ecosystems and the carbon cycle. *Global Change Biology*, 1(1), 77–91. doi: 10.1111/j.1365–2486.1995.tb00008.x.

73. Siegenthaler, U. & Sarmiento, J.L., (1993). Atmospheric carbon dioxide and the ocean. *Nature*, 365, 119–125.

74. Spencer, R.G., Aiken, G.R., Dyda, R.Y., Butler, K.D., Bergamaschi, B.A., & Hernes, P.J. (2010). Comparison of XAD with other dissolved lignin isolation techniques and a compilation of analytical improvements for the analysis of lignin in aquatic settings. *Organic Geochemistry*, 41(5), 445–453.

75. Stewart, S.R., & Berg, R., (2019). National Hurricane Center Tropical Cyclone Report; Hurricane Florence. *National Hurricane Center*. https://www.nhc.noaa.gov/data/tcr/AL062018_Florence.pdf

76. Stow, C.A., Borsuk, M.E. & Stanley, D.W., (2001). Long–term changes in watershed nutrient inputs and riverine exports in the Neuse River, North Carolina. *Water Research*, 35(6), 1489–1499.

77. Sunda, W.G. & Cai, W.J. (2012). Eutrophication induced CO_2 – Acidifcation of subsurface coastal Waters: Imperative effects of temperature, salinity and atmospheric PCO_2. *Environmental Science & Technology*, 46, 10651–10659.

78. Tarnocai, C., Canadell, J.G., Schuur, E.A.G., Kuhry, P. & Mazhitova, G., (2009). Soil organic carbon pools in the northern circumpolar permafrost region. *Global Biogeochemical Cycles*, 23(GB2023). doi: 0886–6236/09/2008GB003327.

79. Verdugo, P., Alldredge, A.L., Azam, F., Kirchman, D.L., Passow, U. & Santschi, P.H., (2004). The oceanic gel phase: a bridge in the DOM–POM continuum. *Marine Chemistry*, 92(1–4), 67–85.

80. Yan, G. & Kaiser, K., (2018a). A rapid and sensitive method for the analysis of lignin phenols in environmental samples using ultra–high performance liquid chromatography–electrospray ionization–tandem mass spectrometry with multiple reaction monitoring. *Analytica Chimica Acta*, 1023, 74–80. doi: 10.1016/j.aca.2018.03.054

81. Yan, G., & Kaiser, K. (2018b). Ultralow Sample Volume Cupric Sulfate Oxidation Method for the Analysis of Dissolved Lignin. *Analytical chemistry*, 90(15), 9289–9295.

82. Yoon, Byungman and Raymond, Peter A. (2012). Dissolved organic matter export from a forested watershed during Hurricane Irene. *Geophysical Research Letters*, 39(L18402). doi: 10.1029/2012GL052785

83. Zeikus, J.G., (1981). Lignin metabolism and the carbon cycle—polymer biosynthesis, biodegradation, and environmental recalcitrance. *Advances in microbial ecology*, 5, 211–243.

VIII. APPENDICES

TABLE OF CONTENTS

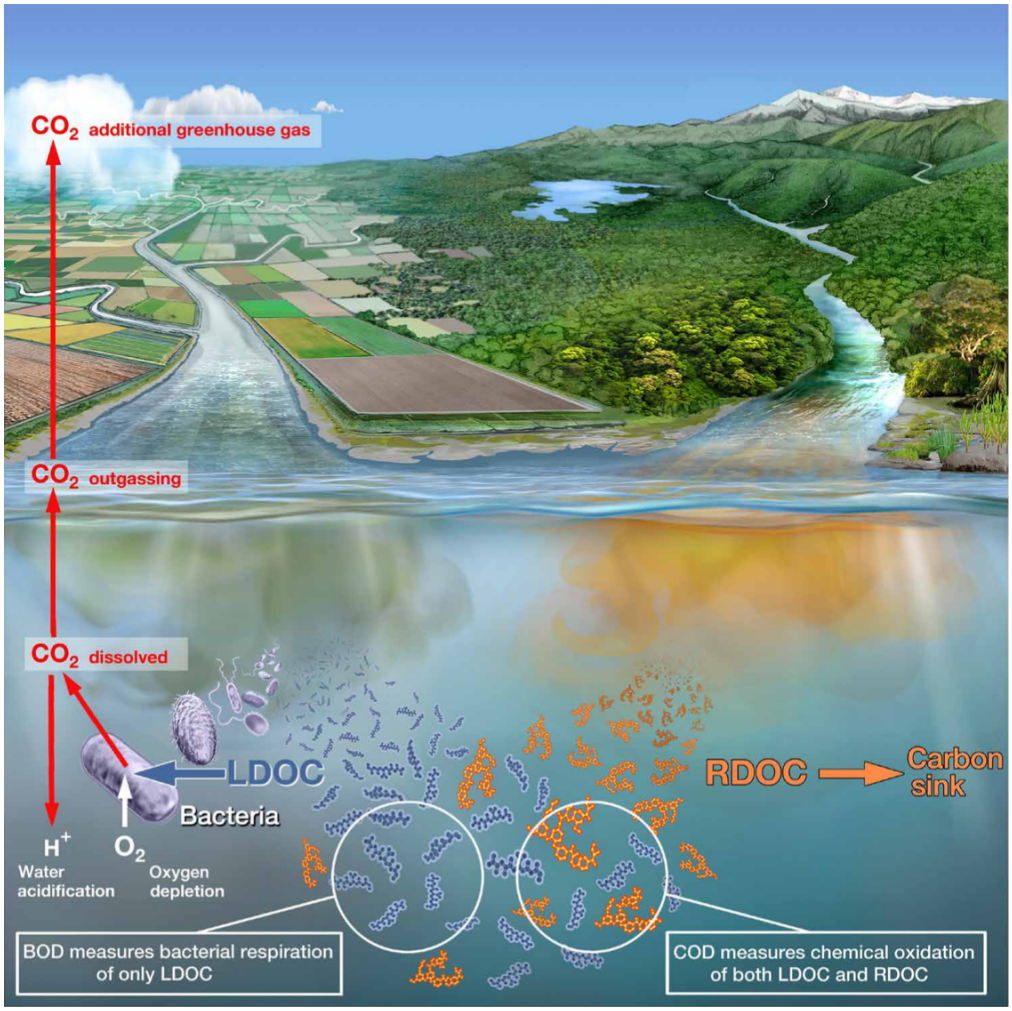

Figure A–1: Schematic representation of LDOC and RDOC in the natural environment.

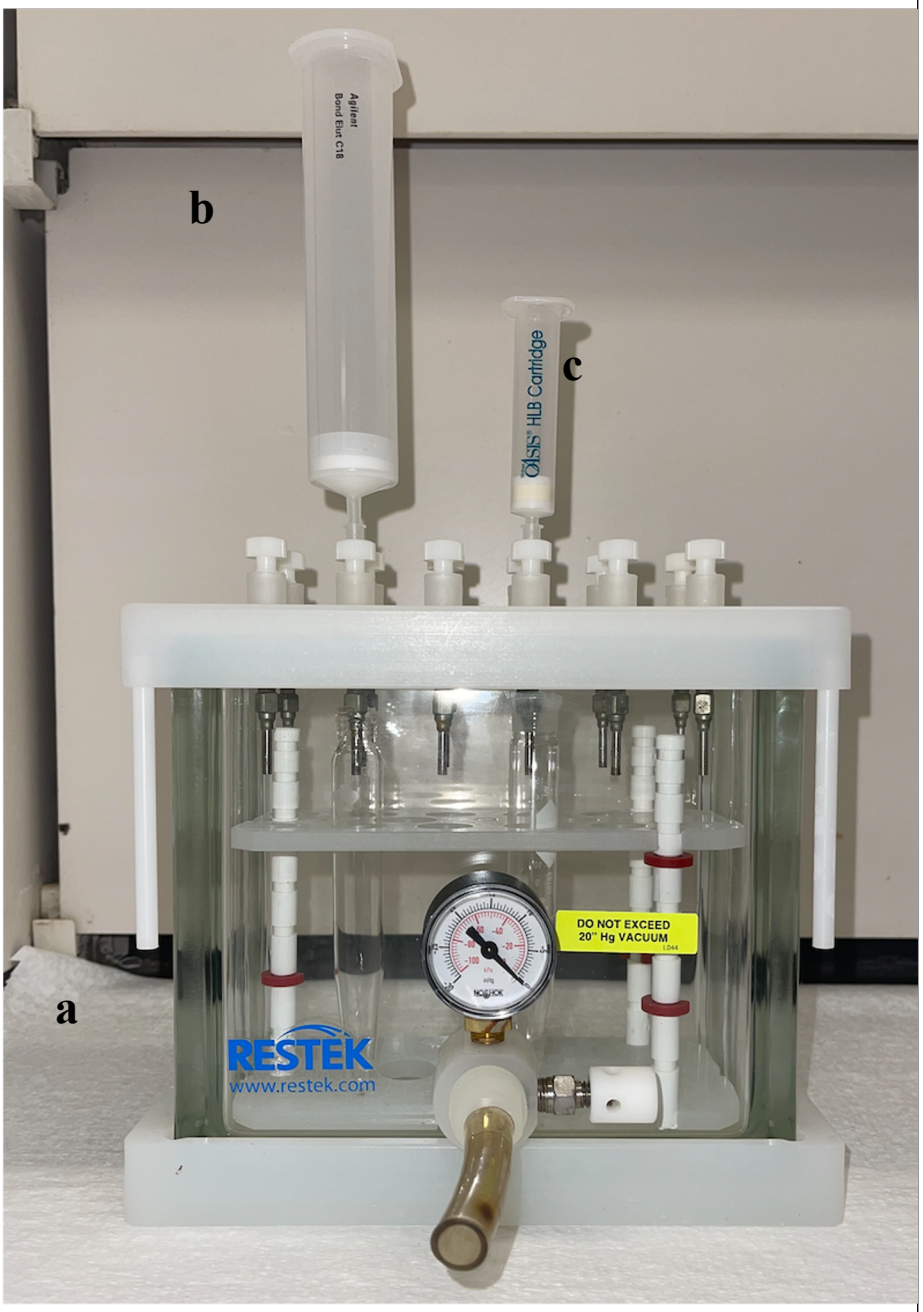

Figure A–2: Restek 12–port vacuum manifold. a. Vacuum manifold with conical tube rack and vacuum port connection tube; b. SPE Agilent Mega Bond Elut C18 (1g, 60 mL) cartridge; c. SPE Oasis HLB cartridge (150 mg, 60 µm)

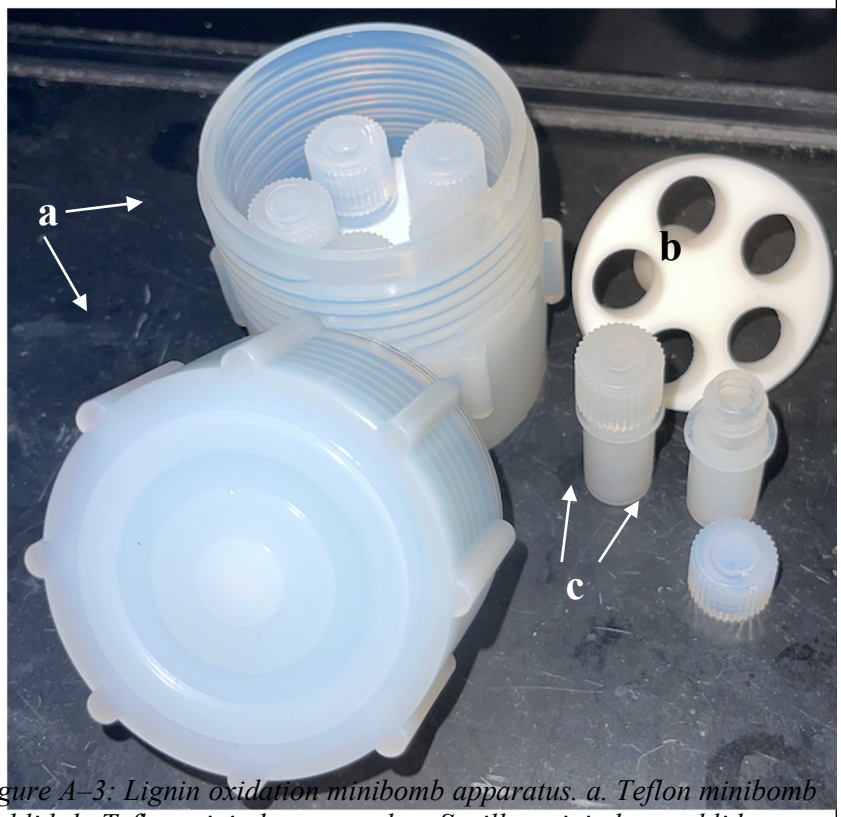

Figure A–3: Lignin oxidation minibomb apparatus. a. Teflon minibomb and lid; b. Teflon minitube carousel; c. Savillex minitubes and lids

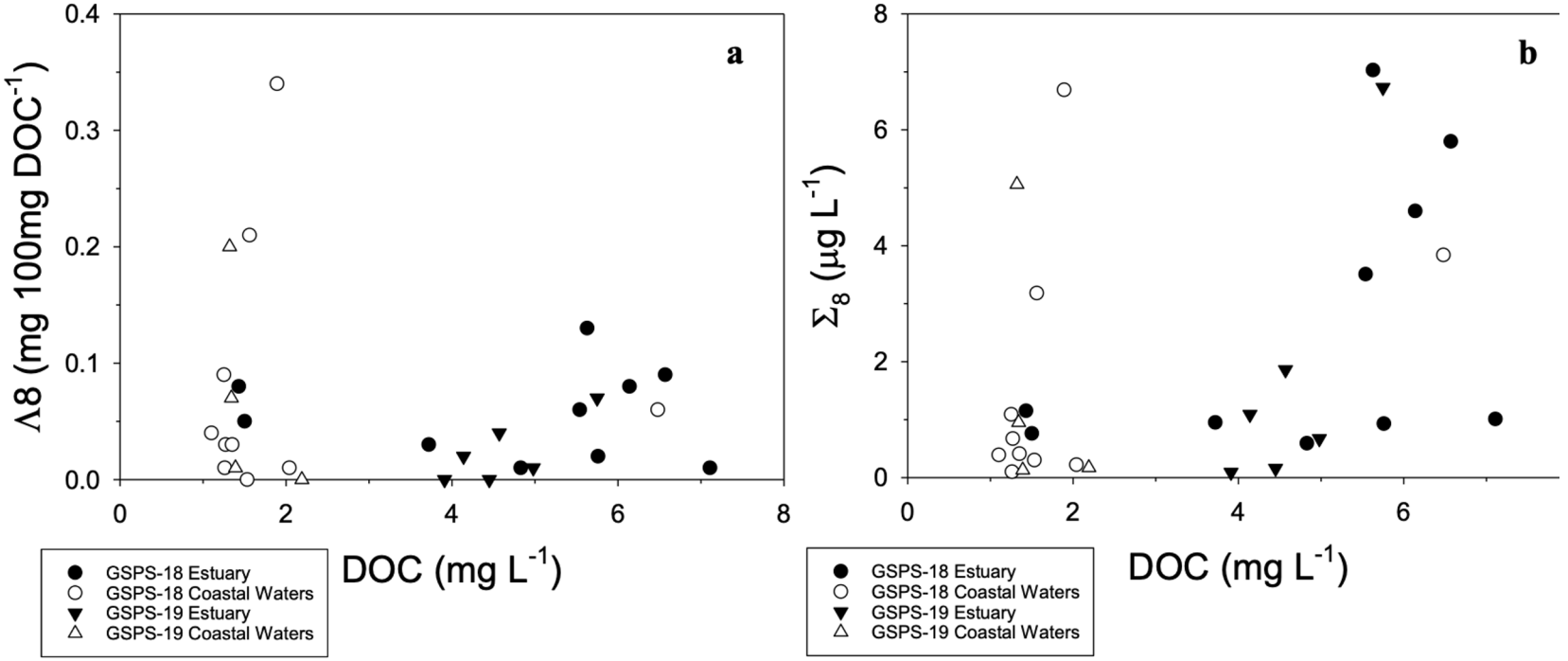

Figure A–4: DOC (mg L^{-1}) versus sum of total phenols in terms of a. Lambda–8, Λ_8, sum of total phenols in terms of (mg 100mg DOC^{-1}), b. Sigma – 8, Σ_8, sum of total phenols in terms of phenol yield ($\mu g\ L^{-1}$).

Table A–1: Retention time (min), molecular ion and qualifier ions for each lignin monomer. Retention time varies with each injection depending on mixed standard age and column usage.

Monomer ID	Retention time (min):	Molecular ion:	Qualifier ions (Q_n; n=1 – 3):
VAL	2.27	194	209, 193, 224
VON	2.08	223	193, 208, 238
VAD	3.63	297	267, 312, 223
SAL	1.95	224	239, 254, 223
SON	2.53	238	223, 253, 268
SAD	1.58	327	312, 297, 342
CAD	2.33	293	219, 249, 308
FAD	1.46	338	323, 308, 249
EVAL	2.55	167	195, 238, 179

Table A–2: Comparison of this study and Louchouarn et al. (2010) including total lignin and interclass ratios.

	Louchouarn et al., 2010 (mg g^{-1})	This Study (mg L^{-1})
VAL	0.32 ± 0.03	$2.85e^{-2}$ ± 0.00
VON	0.10 ± 0.01	$2.21e^{-2}$ ± 0.01
VAD	0.11 ± 0.01	$5.61e^{-2}$ ± 0.01
SAL	0.19 ± 0.02	$0.65e^{-2}$ ± 0.00
SON	0.07 ± 0.01	$0.85e^{-2}$ ± 0.00
SAD	0.07 ± 0.01	$2.22e^{-2}$ ± 0.01
CAD	0.05 ± 0.00	$0.81e^{-2}$ ± 0.00
FAD	0.04 ± 0.00	$0.80e^{-2}$ ± 0.00
Σ_8	0.97 ± 0.04	0.16 ± 0.01
Λ_8	2.20 ± 0.10	0.42 ± 0.02
S/V	0.61 ± 0.03	0.35 ± 0.08
C/V	0.16 ± 0.01	0.15 ± 0.06
$[Ad/Al]_V$	0.34 ± 0.04	1.97 ± 0.19
$[Ad/Al]_S$	0.33 ± 0.03	3.43 ± 0.40

Table A–3: Yield for each monomer for each sampling station for GSPS–18 and GSPS–19 all yields are expressed in terms of (μg L^{-1}). n.q. stands for not quantifiable based on instrument detection limits and n.d. stands for not detected.

Station ID	VAL	VON	VAD	SAL	SON	SAD	CAD	FAD
GSPS–18 Station 1	0.530	1.268	0.895	0.055	*n.q.*	0.792	0.578	0.483
GSPS–18 Station 2	0.037	0.339	0.057	0.019	*n.q.*	0.055	0.121	0.030
GSPS–18 Station 3	0.202	*n.d.*	0.867	0.229	0.726	0.706	0.994	3.309
GSPS–18 Station 4	0.203	0.756	1.043	1.108	0.109	0.137	0.083	0.163
GSPS–18 Station 5	0.091	0.274	0.196	0.204	*n.q.*	0.058	0.051	0.076
GSPS–18 Station 6	*n.d.*	*n.d.*	0.102	0.282	0.046	0.160	0.443	0.163
GSPS–18 Station 7	0.011	*n.d.*	0.057	0.671	0.008	0.039	*n.d.*	*n.d.*
GSPS–18 Station 8	0.364	*n.d.*	0.383	0.119	*n.q.*	0.146	*n.d.*	0.451
GSPS–18 Station 9	0.061	2.839	2.681	0.139	0.024	0.306	0.640	0.296
GSPS–18 Station 10	*n.d.*	*n.d.*	*n.q.*	*n.d.*	0.219	0.162	*n.q.*	*n.q.*
GSPS–18 Station 11	0.059	0.090	0.025	*n.d.*	0.028	0.014	0.017	*n.q.*
GSPS–18 Station 12	*n.d.*	*n.d.*	0.050	0.009	*n.d.*	*n.q.*	*n.d.*	*n.q.*
GSPS–18 Station 13	*n.q.*	*n.d.*	0.074	0.133	*n.q.*	*n.q.*	*n.d.*	*n.q.*
GSPS–18 Station 14	*n.d.*	0.156	0.124	0.119	0.167	0.010	*n.d.*	*n.d.*
GSPS–18 Station 50	*n.d.*	*n.d.*	*n.q.*	0.164	0.103	*n.d.*	*n.d.*	*n.d.*
GSPS–18 Station 51	0.166	*n.q.*	0.603	*n.q.*	0.233	0.575	*n.q.*	1.139
GSPS–18 Station 52	*n.q.*	*n.q.*	1.251	0.127	0.055	2.093	0.834	2.014
GSPS–18 Station 53	*n.d.*	0.042	0.257	0.134	*n.d.*	*n.q.*	*n.q.*	*n.d.*
GSPS–18 Station 54	0.760	*n.d.*	*n.d.*	0.047	0.291	*n.d.*	*n.d.*	0.803
GSPS–18 Station 55	1.337	0.864	0.659	0.034	*n.q.*	0.578	0.378	0.334
GSPS–19 Station 100	0.197	*n.q.*	0.428	*n.q.*	*n.q.*	0.114	*n.q.*	*n.q.*
GSPS–19 Station 101	*n.q.*	*n.q.*	0.694	0.298	*n.q.*	1.656	*n.q.*	*n.q.*
GSPS–19 Station 102	0.060	*n.d.*	0.059	*n.q.*	*n.q.*	*n.q.*	*n.d.*	*n.q.*
GSPS–19 Station 104	0.066	*n.d.*	0.022	*n.q.*	*n.q.*	*n.q.*	*n.d.*	*n.d.*
GSPS–19 Station 105	*n.q.*	*n.d.*	*n.q.*	*n.q.*	*n.q.*	0.019	*n.q.*	*n.q.*
GSPS–19 Station 106	0.151	*n.q.*	0.242	0.069	*n.q.*	0.146	*n.q.*	*n.q.*
GSPS–19 Station 107	0.025	*n.d.*	0.380	0.051	*n.q.*	0.369	*n.q.*	*n.q.*
GSPS–19 Station 108	*n.q.*	*n.d.*	0.097	*n.q.*	*n.q.*	*n.d.*	*n.d.*	*n.d.*
GSPS–19 Station 109	*n.q.*	*n.d.*	*n.q.*	*n.q.*	*n.d.*	0.117	*n.q.*	*n.q.*
GSPS–19 Station 110	0.627	*n.q.*	1.385	0.686	*n.q.*	0.552	*n.q.*	*n.q.*

Equation A–1: Simple equation for oxygenic photosynthesis.

$$6CO_2 + 12H_2O \xrightarrow{\text{sunlight}} C_6H_{12}O_6 + 6H_2O + 6O_2 + \text{energy}$$

Equation A–2: Simple equation for anoxygenic photosynthesis, commonly done by bacteria.
**H_2A = H_2O, H_2S, H_2 or other electron donor*

$$CO_2 + 2H_2A^* \xrightarrow{\text{sunlight}} CH_2O + H_2O + 2A^* + \text{energy}$$

Equation A–3: Quantification calculation for phenol yield concentration.

$$[\text{phen}]\ (\mu g\ L^{-1}) = \left(\text{phenol area} \times \frac{\text{resolution factor}}{\text{EVAL area}}\right) \times \left(\frac{\text{EVAL } (\mu L)}{\text{sample vol. (L)}}\right)$$